Kandidat:

# ŽIGA LIKAR

## VPLIV NAPETOSTNIH POTI IN ZRNAVOSTNE SESTAVE NA MEHANSKO OBNAŠANJE DROBLJIVEGA AGREGATA

Diplomska naloga št.: 3262/KS

## EFFECTS OF STRESS PATH AND GRAIN SIZE DISTRIBUTION ON THE MECHANICAL BEHAVIOUR OF CRUSHABLE GRANULAR MATERIAL

Graduation thesis No.: 3262/KS

**Mentor:**
izr. prof. dr. Janko Logar

**Predsednik komisije:**
doc. dr. Tomo Cerovšek

**Somentorica:**
dr. Francesca Casini

**Član komisije:**
izr. prof. dr. Vlatko Bosiljkov

Ljubljana, 16. 11. 2012

# Errata

| Page | Line | Error | Correction |
|------|------|-------|------------|

**IZJAVE**

Podpisani **Žiga Likar** izjavljam, da sem avtor diplomske naloge z naslovom »**Vpliv napetostnih poti in zrnavostne sestave na mehansko obnašanje drobljivega agregata**«.

Izjavljam, da je elektronska različica v vsem enaka tiskani različici.

Izjavljam, da dovoljujem objavo elektronske različice v repozitoriju UL FGG.

I, the undersigned **Žiga Likar**, hereby declare that I am the author of the diploma thesis titled »**Effects of stress path and grain size distribution on the mechanical behaviour of a crushable granular material.**«

I declare that electronic version of this thesis is identical to the hard copy.

I declare that I permit the publishment of the electronic version of this thesis in the digital repository of the Faculty of Civil and Geodetic Engineering, University of Ljubljana.


Ljubljana, 7. 11. 2012                                                                                          Žiga Likar

## BIBLIOGRAFSKO-DOKUMENTACIJSKA STRAN IN IZVLEČEK

**Izvleček**

V diplomski nalogi je obravnavan vpliv napetostne poti in začetne zrnavostne sestave na drobljenje agregata v peščenem materialu. Diplomska naloga je sestavljena iz dveh delov. V prvem delu so analizirani rezultati laboratorijskih testov in sicer izotropnih obremenitev vzorca, edometrskih testov, triosnih strižnih preiskav pri konstantnem celičnem tlaku ter triosnih strižnih preiskav pri konstantni srednji vrednosti efektivne napetosti. Za namene raziskave je uporabljen drobljen umeten material znan pod imenom LECA. Na podlagi ugotovitev analize je bil pripravljen računski model, s katerim je mogoče predvideti razvoj drobljenja pri različnih napetostnih poteh. V drugem delu diplomske naloge so bili analizirani različni načini modeliranja drobljenja v numerični simulaciji. Dva najbolj primerna načina sta bila na kratko preskušena, nato pa se je za najbolj primernega pripravil celoten model skupaj s potrebnimi meritvami za spremljavo obnašanja vzorca med simulacijo. Izkazalo se je da je uporaba vzporednih vezi, ki zahtevajo veliko bralno-pisalnega pomnilnika, nepotrebna. Zaradi drobljenja načina drobljenja agregata, pri katerem ne prihaja do drobljenja celotnih zrn temveč le do strižne porušitve na kontaktih, bi namreč povsem ustrezala uporaba kontaktnih vezi, ki so računsko mnogo bolj učinkovite. Prav tako se je priprava vzorca s povečevanjem osnovnih elementov ocenila kot manj primerna, saj jo je težko nadzorovati. Primernejši je način utrjevanja po plasteh. Kot se je izkazalo je priprava ustreznega modela zahtevna naloga, predvsem zaradi potrebe po zmogljivih računalnikih za izvedbo verodostojne simulacije.

**BIBLIOGRAPHIC-DOCUMENTALISTIC INFORMATION AND ABSTRACT**

**Abstract**

The effect of the stress path and the initial grain size distribution on grain crushing was investigated on artificial material of a sand grain size. The thesis consists of two parts. In the first part isotropic compression test, oedometer test, conventional triaxial test (at constant cell pressure) and triaxial compresion test with constant mean effective stress are analysed. For the purpose of the research described in this part of thesis crushed artificial material known under commercial name Light Expanded Clay Aggregate was used. Based on findings gained from the analysis a model describing grain crushing and changing of internal friction angle was prepared. In second part of the research different ways of crushing modelling were analysed. Two ways were then briefly tested. For the approach that showed to be better describing grain crushing a complete model was prepared together with all the measurements needed to track the sample behaviour during simulation. At the end the model was tested. It turned out that the application of parallel bonds in modelling grain crushing is unnecessary. The main reason for parallel bond application in the model was good description of tensile grain failure. Due to the high coordination numbers the tensile grain splitting is unlikely to occur. Instead, shear grain failure at contact is the most common grain failure. Therefore, contact bonds, which are much more computationally efficient, should be used instead. The sample preparation procedure with application of elementary particle expansion method turned out to be unsuitable. Since for different grain size distributions with the same initial porosity, the stresses induced with this procedure can vary significantly. Compaction of the sample layer by layer would much better serve this task.

**ACKNOWLEDGEMENT**

## ZAHVALA

**TABLE OF CONTENTS**

## LIST OF TABLES

## LIST OF FIGURES

# 1    INTRODUCTION

## 1.1    Motivation

Coarse grained material has a broad range of application in the engineering practice due to its permeability, friction and stiffness properties. Stress conditions for standard engineering applications are such that no drastic changes occur in the material grading. With the development of geotechnical knowledge more and more demanding geotechnical structures were constructed forcing the material to reach it limits. The construction of large earth fill dams (Marsal, 1967), new techniques in building foundations such as pile driving (Lobo-Guerrero, Vallejo, 2007) induce limiting stress conditions that cause a change of grading and consequently the reduction of permeability, increase of settlements and change of friction angle. However, it is not just the geotechnical structures, but also natural phenomena like landslides (Gerolymos, 2007) induce grain crushing.

Normally, the material we deal with in geotechnics has a rather high grain strength so the grains only start to undergo crushing under extreme conditions. In geotechnics, materials with rather low strength such as pyroclastic rocks, calcarenites, decomposed granite, etc. can be encountered and for these even the stresses at normal geotechnical application cause a critical condition for crushing. All of these materials are of natural origin while in this research artificial material known as LECA (Light Expanded Clay Aggregate) was used.

Some would question the application of crushable materials in construction of road embankments, quay extensions, etc. because of its unpredictable grading changes. But, materials like LECA and pyroclastic rocks have a great advantage that convinces many researchers to investigate such materials in order to broaden its application and that is its lightweight coupled with very high internal friction angle. Therefore, to design safe structures and deepen our understanding of natural phenomena, grain crushing needs to be investigated from its roots.

## 1.2    Critical State

In modern geotechnics the essence of soil mechanics is the critical state, at which there is a unique relationship between the shear stress, the normal stress and the voids ratio (Atkinson, 1993). It is typical for the critical state that for a given mean effective stress at large shear strains soil reaches a shear strength, at which the soil neither compresses nor dilates. At this constant state the void ratio for drained conditions is material and mean effective stress dependent. In other words, it is independent of a loading history. The behaviour of soil before reaching the critical state is dependent on the initial state of a soil. All of the initial states of soil can be divided into two distinct groups. The first group consists of samples that are normally consolidated or lightly over consolidated, which means that at a given confining pressure the soil void ratio is greater than the critical void ratio at this same confining pressure. In order to reach the constant state soils in this group must compress during shearing. Since

the void ratio in these soils is greater than at critical state, they can be specified as soils on the wet side of the critical state. Because there are only two distinct groups and since the opposite of wet is dry, soils in the second group can be characterized as soils on the dry site of the critical state. In the past these soils have undergone a process that resulted in a denser state than the critical state. Soil can reach the state on the dry site of the critical state either by successive loading and unloading or by its vibration into denser state. In order to overcome each other, grains must dilate since the void ratio is lower than at critical state. Because of this dilation, soil experiences a peak strength prior to reaching the critical state. Regardless of whether the sample is initially on the wet or the dry site at large deformations the sample approaches the same critical void ratio.
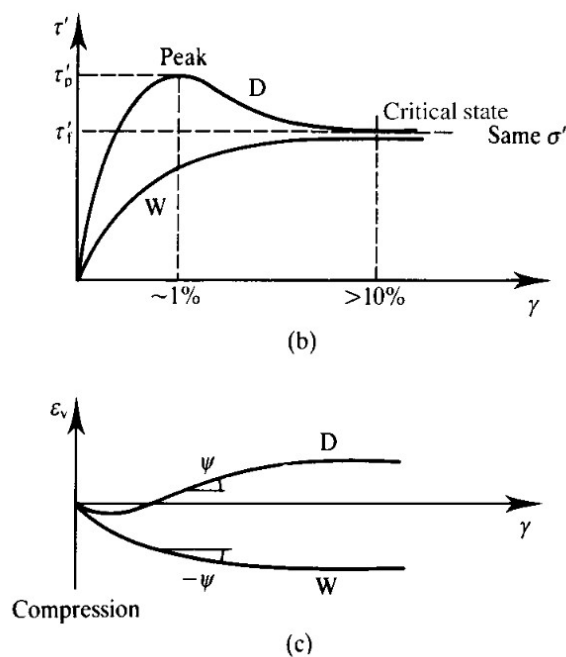


**Slika 1.1: Značilno obnašanje glin v dreniranem strižnem preizkusu (Atkinson, 1993)**

**Figure 1.1: Typical behaviour of clays in drained shear test (Atkinson, 1993)**

For soils tested in triaxial apparatus the critical state line can be defined as:

$$q'_c = M' \cdot p'_c \qquad\qquad (1\text{-}1)$$

Where $q'_c$ is a critical deviatoric stress for a given mean effective stress $(p'_c)$ and $M'$ is a material-dependent parameter denoting the critical $\frac{q'}{p'}$ ratio.
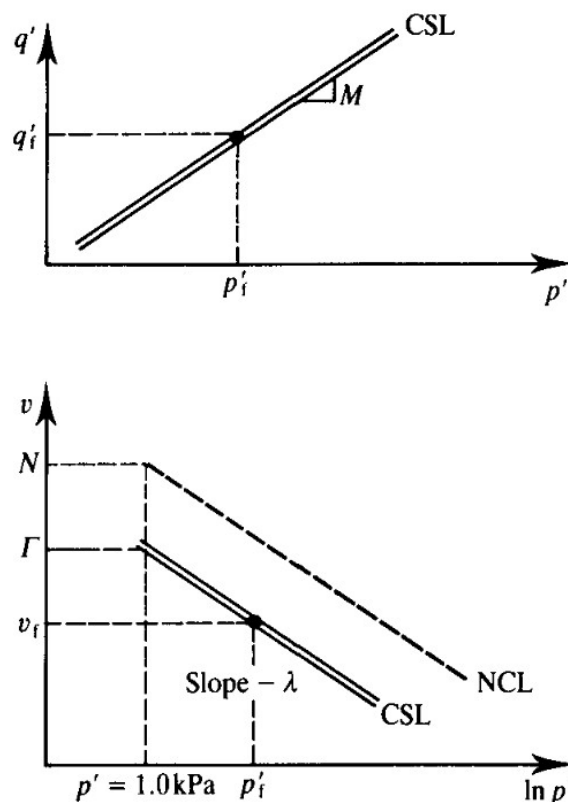
**Slika 1.2: Linja kritičnega stanja za triosni preskus (Atkinson. 1993)**

**Figure 1.2: Critical state line for triaxial apparatus (Atkinson, 1993)**

The critical state soil model is based on the behaviour of clays, whereas the behaviour of sands can only be described reasonably well if grain strength is high so the grains are not subjected to crushing. At higher pressures the grain rearrangement is in sands accompanied by grain crushing. When a normally consolidated sand with low grain strength at normal pressures or sand with high grain strength at high pressures reaches its peak shear strength, the gradient of volume changes is non-zero and is anticipated to stabilize at zero only at very large strains, too large for triaxial testing apparatus.

The fact that sand does not reach critical state at high pressures suggests that there are some changes in the sample grading due to the crushing.
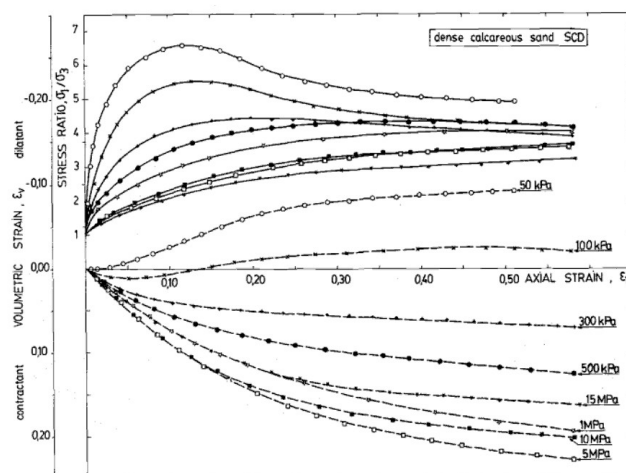
**Slika 1.3: Obnašanje peskov pri visokih tlakih (Colliat-Dangus, 1988)**

**Figure 1.3: Behaviour of sands at high pressure (Colliat-Dangus, 1988)**

## 1.3   Thesis composition

In this thesis it is tried to understand what in particular causes grading changes and how do these changes affect the soil behaviour. Is it possible to reach the so-called critical state also for sands at very high pressures relatively to the grain strength? Grain crushing is a micro scale phenomenon affecting the macro scale behaviour of a soil. For this reason this research consists of two parts.

The first part of the research was performed in laboratory where several different tests were performed on granular material with low grain strength. Each type of a test was performed on several samples with different initial uniformities. Because this thesis is part of the extended research at ETH IGT tests were performed by different students. Below the types of tests are specified while the students performing the tests are specified in the brackets:

- Isotropic compression (Leu, Low, Zimmermann)
- Oedometric compression (Wanninger, Pascal)
- Conventional triaxial test (Leu, Low, Zimmermann)
- Isotropically consolidated constant mean effective stress compression test (Likar)

Performing these tests samples were subjected to different stress paths. During the analysis the soil characteristics that are affected by grain crushing were singled out and analysed how they are affected by grain size distribution changing.

Second part of the research was performed in the computer program PFC3D based on the distinct element method (DEM). During this part different approaches of modelling grain crushing were studied. For the approach best describing the grain crushing behaviour a model was developed

together with measurements necessary to track changes of the parameters. At the end the program was tested and some improvements of the model were suggested for further research.

## 2    LABORATORY

### 2.1   Scope of research

While it is obvious that degradation plays an important role in sand behaviour, it is not that self-evident what causes grain crushing. Do all grains, regardless of their size, crush evenly or is the subjection to crushing dependent on the grain size? Since a grain size distribution (GSD) changes because of grain crushing, it is logical that some of the sand properties will change due to these grading changes. For sands at low pressures the friction angle is usually not constant due to the fact that it experiences dilation. This variation is rather small so the internal friction angle can be approximated with a secant friction angle. This way the shear strength of sand at low pressures is defined by the point of origin and the secant friction angle. For sand with low grain strength the change of a friction angle at higher pressures is not expected to be negligible, so the failure criterion should be defined by a nonlinear function. The question appropriate at this stage is, what are the effective parameters and how can the failure criterion for a crushable soil be defined.

In order to understand the causes of grain crushing and the effect of GSD changing on mechanical properties a series of tests with various stress paths and initial grading distributions were performed in an oedometer and a triaxial cell. Instead of using sand with high grain strength and a high pressure testing apparatus, alternative material with much lower grain strength was used. Therefore, a medium pressure oedometer ($\sigma_1 \leq 2\,MPa$) and a low pressure ($\sigma_c \leq 1\,MPa$, $\sigma_c$ - cell pressure) triaxial apparatus could be used.

Based on the knowledge gained through this extended research, a model defining the failure criterion for crushable sand was derived. It is presented at the end of section 2 together with its derivation and physical background.

### 2.2   Material used in the research

For the purpose of the research described in this thesis material known under its commercial name LECA (Light Expanded Clay Aggregate) was used. The main advantage of this material is its low apparent unit weight that is a result of a unique production cycle. Why the expression apparent has been used will be described later in this thesis.

### 2.2.1    Production of LECA material

First, clay material is excavated from shallow mines and then exposed to weathering effects. After several months the material is transported to a plant where its defragmentation is continued by grinding machines. A very uniform composition of a powder is achieved through this process. The next stage of the production takes place in the rotary kiln where the powder is heated close to the

melting point (T≈1200°C). During this heating procedure, the organic material within the powder is combusted and consequently a porous material is formed. Due to the constant rotation of the kiln, round shaped pellets are produced. The heating of the powder close to the melting point is a process called sintering, during which a normal diffusion of atoms is sped up. The atoms move towards the surface in order to achieve minimum surface at a maximum volume. Therefore, a strong solid crust is formed while the inside remains very porous. In this way the strength of a pellet is improved and a low specific weight is achieved. This specific weight is apparent since a high percentage of pores remains within each pellet.

### 2.2.2    Double porosity

Low bulk density is an evident characteristic of the material, which is a consequence of a double porosity. The two types of porosity are a) intragranular (pores that are closed within each grain) and b) intergranular porosity. Intragranular porosity is the reason that another type of specific gravity has to be used. The actual specific gravity of the material can be measured in a picnometer after grains have been broken down to a pore-free material. For material like LECA it can be assumed that grains of a diameter smaller than 0.063 mm contain no pores. The apparent specific gravity is measured on grains containing the internal pores. An obvious observation is that true and apparent specific density for grains of a diameter smaller than 0.063 mm are identical. In the following figure a comparison between typical aggregate and lightweight aggregate such as LECA is shown:



Normal agregate                              Lightweight aggregate (LWA)
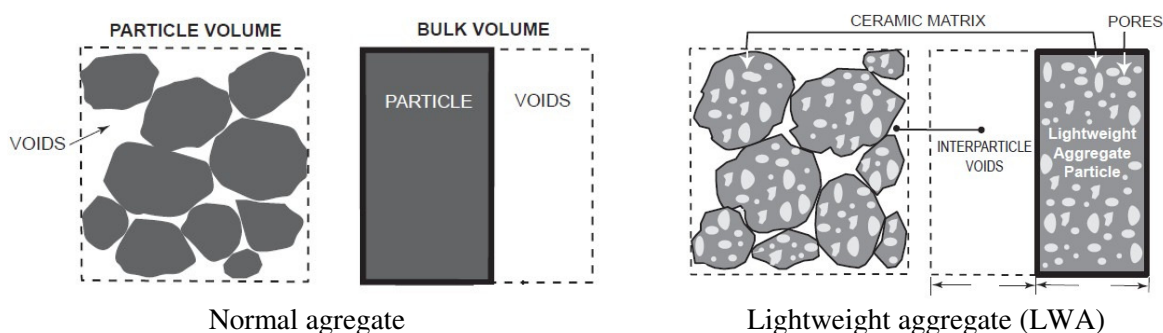
**Slika 2.1: Primerjava med običajnim agregatom in agregatom z nizko specifično težo (Casini and Viggiani, 2011)**

**Figure 2.1: A comparison between typical and lightweight aggregate (Casini and Viggiani, 2011)**

The structure of LWA can be further dissected into inter grain voids, ceramic matrix and intragranular pores as displayed by the next figure:
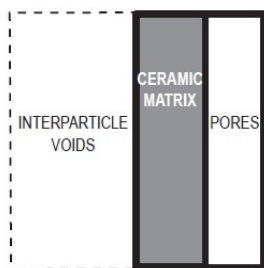
**Slika 2.2: Pore med zrni in znotraj zrn (Geotech)**

**Figure 2.2: Inter/intragranular pores (Geotech)**

Because pores within the grain are scattered all over each grain, some of intragranular pores are on the outer shell of the grain, therefore, if the grain is submerged in water for a short period of time, these pores will be filled with water. As time progresses more and more intragranular pores are saturated with water. Such process can be sped up by increasing the vacuum during the saturation.
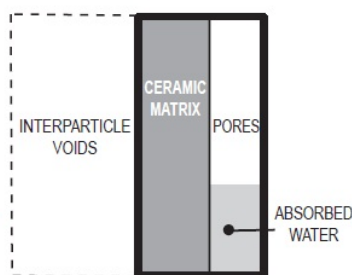


**Slika 2.3: Del por znotraj zrn je zapolnjenih z vodo (Geotech)**

**Figure 2.3: Part of intragranular pores filled with water (Geotech)**

### 2.2.3    Low specific density

In section 2.2.1 the production cycle of LECA material is described. The result of this process is high intragranular porosity. Because the amount of internal pores decreases with reducing grain size, apparent specific weight increases for smaller grains. Wanninger (2010) has analyzed images made with the scanning electron microscope (SEM) in image manipulation program by first turning pictures into black (pores) and white (matrix) images and then by counting the pixels determining the size of pores. In the Figure 2.4 SEM, where images of different grain size fractions are showed, it is possible to see how high the percent of intragranular pores is in LECA material.

| 2 - 4 mm (mag.: 30 x) | 1 - 2 mm (mag.: 50 x) | 0.5 – 1.0 mm (mag.: 50x) |
| 0.25 – 0.5 mm (mag.: 100 x) | 0.125 – 0.25 mm (mag.: 100 x) | 0.063 – 0.125 mm (mag.: 100 x) |
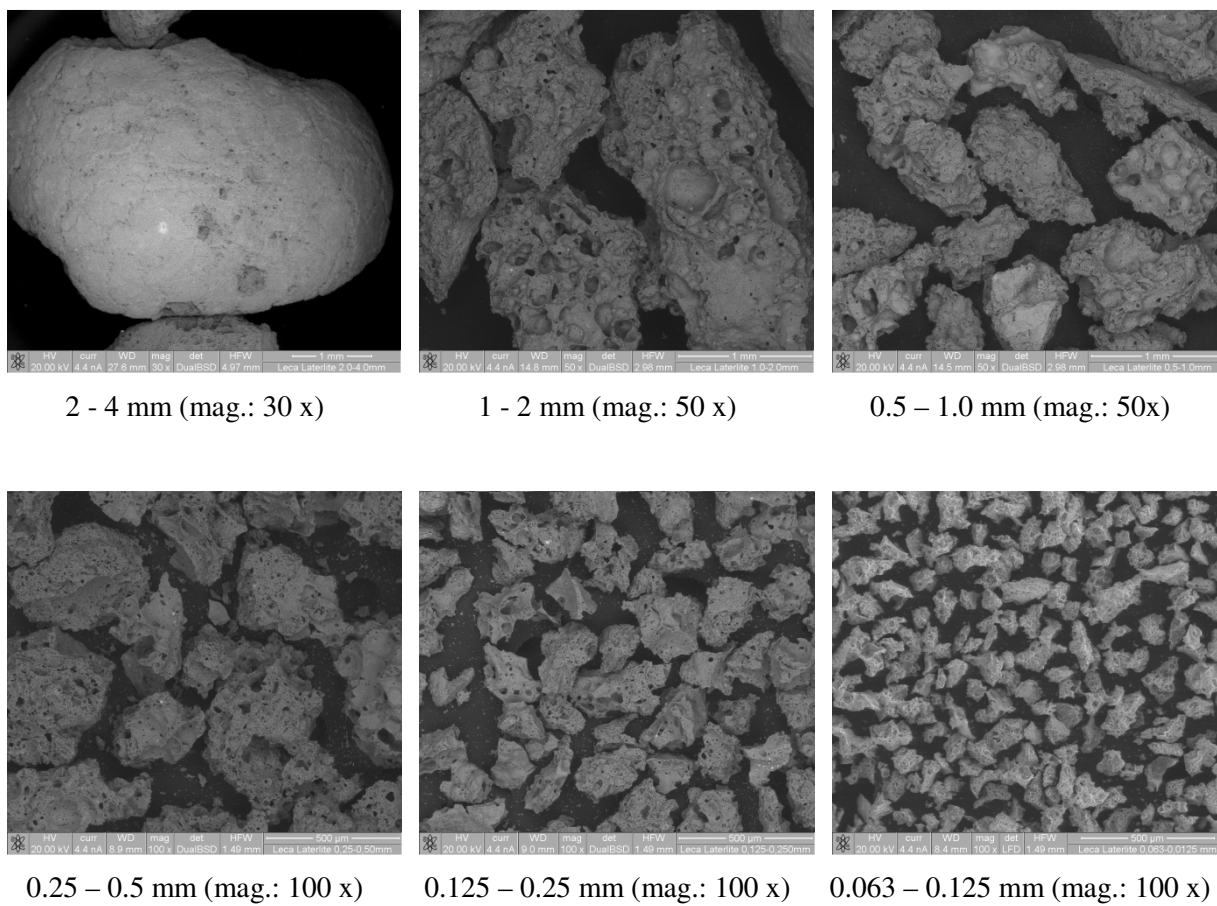
**Slika 2.4: Fotografije zrn različnih velikosti narejene z vrstičnim elektronskim mikroskopom**

**Figure 2.4: Images made with SEM for different grain size fractions**

**Preglednica 2.1: Poroznost zrn po frakcijah (Wanninger, 2010)**

**Table 2.1: Intragranular porosity by fraction (Wanninger, 2010)**

| Fraction | Pore volume | Clay volume |
|----------|-------------|-------------|
| 0.125-0.25 | 67.83 % | 32.17 % |
| 0.25-0.5 | 73.23 % | 23.77 % |
| 0.5-1 | 80.77 % | 19.23 % |
| 1-2 | 75.99 % | 24.01 % |
| 2-4 | 85.66 % | 14.34 % |

Since the apparent specific weight is not constant, it is important to distinguish between the cumulative function of grain size distribution by weight and by volume. The relation between the two is defined with a function of apparent specific weight. The specific weight of the clay matrix without pores has been determined with tests and is equal to 26.5 kN/m$^3$. For bigger grains the apparent specific weight decreases exponentially and can be written as:

$$\gamma_s = a \cdot d^{-b} = 12.64 \cdot d^{-0.268} \text{ for } d \geq 0.063 \text{ mm} \tag{2-1}$$

$\gamma_s$ – apparent specific weight [kN/m$^3$]

$a, b$ – curve fitting parameters

$d$ – diameter of a grain [mm]
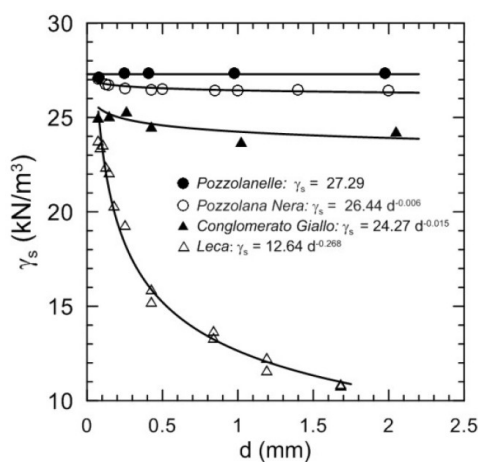


**Slika 2.5: Primerjava navidezne specifične teže LECA-e z drugimi materiali (Casini & Viggiani, 2011)**

**Figure 2.5: A comparison of apparent specific weight for LECA with different materials (Casini & Viggiani, 2011)**

## 2.3  Grain crushing

### 2.3.1    Parameters affecting grain crushing

As mentioned in the introduction it is known that grain crushing takes place in sands at high pressures relative to the grain strength. But, there is still a lack of understanding to what extent and under what conditions do the influential parameters induce grain crushing. Hardin (1985) proposed several parameters such as grain size distribution, grain shape, void ratio, state of effective stress, effective stress path, and grain strength. As these parameters vary, the relation between the energy needed for grains to rearrange without crushing and the energy needed for grains to crush in order to overcome one another changes. For example, for poorly graded soil with angular shape of grains, low void ratio, and at high effective stress state it is very difficult for grains to overcome one another, therefore in such a sample crushing is expected to be considerable.

### 2.3.2    Ultimate grain size distribution

As the grains crush during loading the grading evolves and here another question arises, an ultimate grading that samples approach as the load is increased exists. The ultimate grading depends on the proneness of the grains to crush. Since parameters like coordination number, in other words the number of contacts with neighbouring grains, and number of the defects change with grain size, it is logical to expect that crushing will not be evenly distributed among all grain sizes. Nowadays, it is

widely accepted that the two aforementioned parameters have a contrary effect on a grain crushing. A number of defects increases with grain size, therefore decreasing the grain strength. On the contrary, the coordination number that also increases with grain size reduces the liability to crushing since it reduces the tensile stresses. It is now important to determine which of the two parameters has a bigger influence on grading changes in order to back up certain theory of ultimate grading. Below, two completely different theories for the ultimate distribution are presented.

(i)    Hardin's theory

Hardin assumed that potential for grain crushing increases with grain size since normal contact forces and the amount of defects both increase with grain size. The latter assumption is quite logical and easy to imagine since the defects cause material weakening, and therefore, represent the location of cracks. On the contrary, the assumption that crushing increases with the number of contact points conflicts with a growing understanding that bigger grains get cushioned by smaller grains (Figure 2.6). Higher coordination number of a grain means more uniform stress distribution within a grain, therefore larger grains are less prone to crushing.

With an assumption that bigger grains have a bigger potential to crush the only logical definition of an ultimate distribution is clay. Hardin presumed that grains under silt size don't crush, in other words, he proposed a comminution limit of a silt size ($d = 0.074$ mm). Bearing in mind that the effect of imperfections stabilizes with increasing grain size he proposed next equation for determining the potential of crushing for a given grain size:

$$b_p = \log_{10}\left[\frac{d}{0.074}\right] \text{ for } d \geq 0.074 \text{ mm} \qquad (2\text{-}2)$$

$d$ – grain diameter in mm

Crushing potential of entire sample is determined by:

$$B_p = \int_0^1 b_p \, \mathrm{d}f \qquad (2\text{-}3)$$

$f$ – portion of a sample passing the sieve of a size $d$

The total crushing caused by loading is determined by:

$$B_t = \int_0^1 \left(b_{p0} - b_{pl}\right) \mathrm{d}f \qquad (2\text{-}4)$$

$b_{p0}$ – original value of crushing potential

$b_{pl}$ – value of crushing potential after loading

Relative crushing is determined by:

$$B_r = \frac{B_t}{B_p}$$    (2-5)

### (ii)    Fractal distribution

In recent times much more attention than Hardin's theory has drawn a theory saying that bigger grains get cushioned by smaller grains and, therefore, do not crush when the load is applied. For structural materials, such as concrete, it is known that any kind of internal voids reduce the material strength, therefore, researchers (Nazari, 2010) are adding nano particles in order to fill even the smallest voids (defects). Determining the ultimate distribution for a crushable soil the same thinking is applied. The most non-uniformly loaded grains crush under the loading and fill in the voids, in this way they increase the coordination number of larger grains. While larger grains get cushioned by smaller grains, the latter can get trapped between only two larger grains. When grains are diametrically loaded, the tensile stresses arise perpendicular to the line connecting the contact points. Because rock and ceramics do not tolerate much tension, the grains crush. As this procedure is continuously repeated with smaller and smaller grains, the grain size distribution is naturally trying to reach the best grading (the one with the least defects/intergrain voids). Researchers have showed that the distribution that is able to completely fill the space is self-similar or fractal. For a particular case a definition of a fractal dimension is given by the relationship between the number of objects and an object size. The number of objects with characteristic linear dimension greater than $\Delta$ is given by (Casini and Viggiani, 2011):

$$N(d > \Delta) = C \cdot \Delta^{-\alpha}$$    (2-6)

$d$ – grain size

$\alpha$ – fractal dimension

$C$ – constant

$N$ – number of grains with size greater than $\Delta$
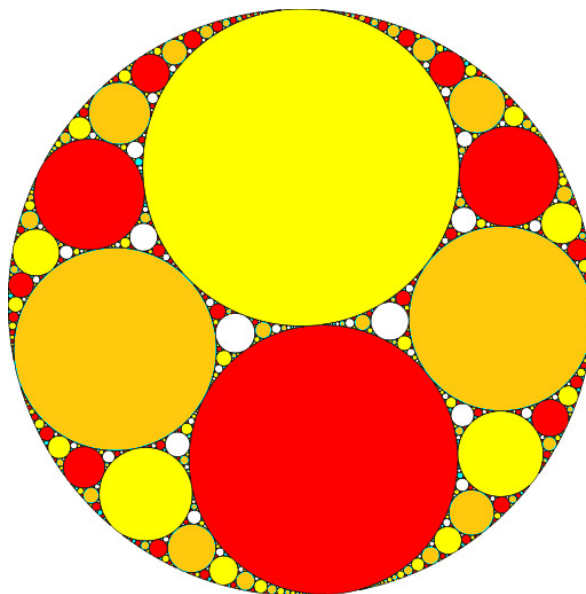
**Slika 2.6: Primer fraktalne distribucije (Wikipedia)**

**Figure 2.6: Example of fractal distribution (Wikipedia)**

If a function of a cumulative fractal distribution is drawn in log-log plot it will appear as a straight line where $\alpha$ represents the slope of the line, and $C$ the $y$–value for $x = 1$.
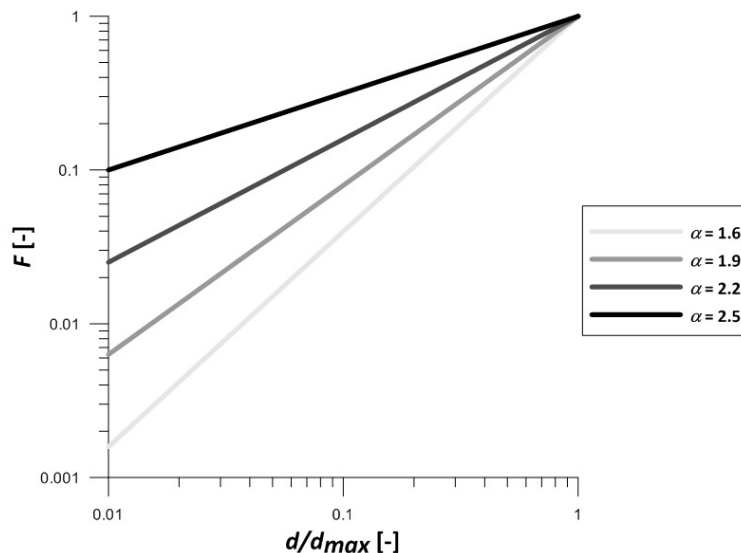


**Slika 2.7: Kumulativna funkcija fraktalne distribucije na grafu z obema osema v logaritemskem merilu**

**Figure 2.7: Cumulative function for fractal distribution in log-log plot**

Very interesting research was performed by Schoutens (1979), which is in favour of fractal final distribution. A sieving analysis was performed on a soil that was removed from the ground after an underground bomb explosion. During the explosion soil was exposed to extremely high pressure. It can be expected that this loading produced an ultimate distribution. The results of sieving analysis

performed after such test were in favour of fractal hypothesis. Even more, it has been shown that function describing such a grain size distribution had a fractal dimension of 2.5.

Since the ultimate grading distribution is still debatable, in this research the most uniformly graded distribution achieved during the tests is considered as an ultimate one. As presented in the section 2.6, where the test results are discussed, the fractal dimension of the grading that was chosen as an ultimate one is 2.39. It is important to emphasise that this is the fractal dimension of the cumulative grain size distribution by volume.

### 2.3.3    Tracking of grain crushing

In order to be able to model the effects of grading changes due to grain crushing on a mechanical behaviour of a soil there are three requirements (Wood, Maeda – 2008):

- a grading state index that can be used to describe the current grading changes of the soil needs to be defined;
- an evolution law needs to be able to describe the way in which this grading state index changes with compression or shearing;
- some rules are required describing the influence of a grading state index on the mechanical properties of the soil.

In the past, several different such indexes measuring the amount of crushing have been proposed. Leslie (1975) based the crushing measurement on the increase of a percent passing the sieve on which originally 90 % of soil remained. Lee and Farhoomand (1967) compared the size of the $d_{15}$ before and after the test. This way of crushing determination is suitable for the design of earth-fill dam since the filter requirements are commonly based on this grain size. But, when interested in complete crushing behaviour of a soil, such crushing evaluation is inadequate since it only measures the change of a grain size distribution curve in a single point.

Hardin, on the other hand, proposed a single digit evaluation of crushing by comparing the area between the initial GSD line and the final GSD line. Like mentioned before, he also proposed a comminution line at $d = 0.074$ mm and defined a crushing potential as an area between initial GSD line and a vertical line at $d = 0.074$ mm. For easier comparison of crushing for grain size distributions with different initial crushing potentials, he has also proposed a relative crushing index as defined in (2-5).

Later, different variations of this approach have been proposed by Einav (2007), Wood and Maeda (2008). Instead of a comminution limit at $d = 0.074$ mm, Einav has used a fractal final distribution, but he did not determine the final fractal dimension. Wood made a step further and defined initial GSD line relatively to final distribution and a single grain size distribution. In this way he proposed a

grading index suitable both for crushing, where the amount of fine grain fractions increases, and the seepage, where fine grain fractions are flushed away. Since this research primarily focuses on grain crushing Einav's approach is used.
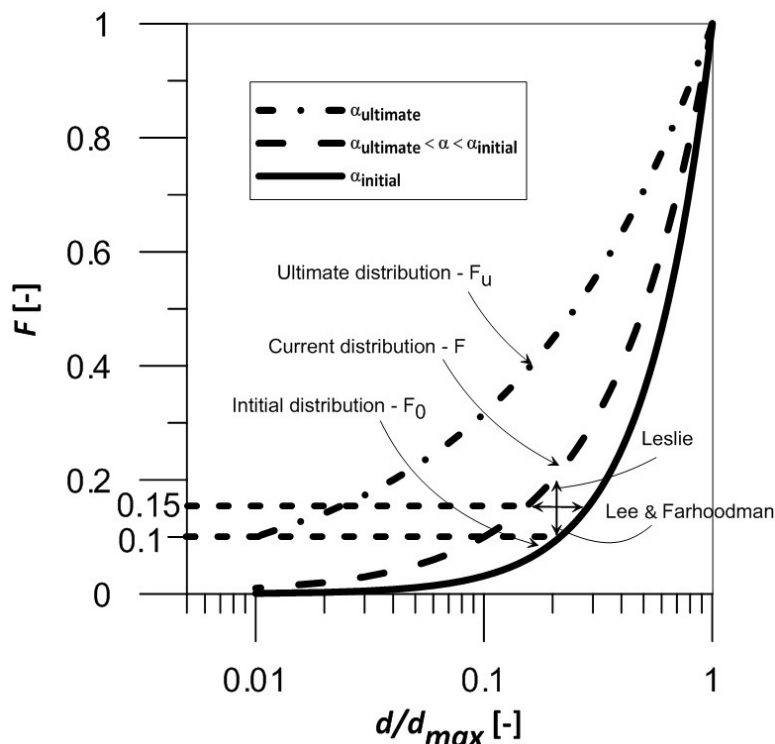


**Slika 2.8: Primeri vrednotenja sprememb zrnavostne sestave**

**Figure 2.8: Different evaluations of grading changes**

Although the initial and intermediate cumulative grain size distributions are not self-similar/fractal, they can be fitted reasonably well with an equation like (2-11). Plus, the loading required to shift the initial distribution to self-similar would be rather small (Casini and Viggiani, 2011). Assuming that it is possible to write a cumulative grain size distribution at every stage as a fractal distribution, which is described with the equations (2-9) or (2-11), the number of grains that have a dimension $d$ greater than $\Delta$ can be determined with the equation (2-6).

From this equation it is possible to derive an equation for number of grains in a certain grain size fraction (Casini and Viggiani, 2011):

$$dN(\Delta) = \alpha \cdot C \cdot d^{-\alpha-1}$$

(2-7)

Knowing the number of grains for each grain size fraction, a cumulative grain size distribution by weight can be written as:

$$F_W(d) = \frac{W(d < \Delta)}{W_T} = \frac{\int_0^d s \cdot \gamma_s(\Delta) \cdot \Delta^3 \cdot dN(\Delta)}{\int_0^{d_{max}} s \cdot \gamma_s(\Delta) \cdot \Delta^3 \cdot dN(\Delta)} \tag{2-8}$$

$\gamma_s$ – apparent unit weight of a grain

$s$ – shape factor of a grain

$d_{max}$ – maximal grain size

If $\gamma_s(\Delta)$ is substituted with the equation (2-1), determining the specific weight depending on the grain size, $dN(\Delta)$ with the equation (2-7) and integrate the function this expression simplifies into:

$$F_W(d) = \left(\frac{d}{d_{max}}\right)^{3-\alpha-b} \quad \text{or} \quad F_W(d) = \left(\frac{d}{d_{max}}\right)^{\beta_W} \tag{2-9}$$

A similar process follows in the case of cumulative grain size distribution by volume:

$$F_V(d) = \frac{V(d < \Delta)}{V_T} = \frac{\int_0^d s \cdot \Delta^3 \cdot dN(\Delta)}{\int_0^{d_{max}} s \cdot \Delta^3 \cdot dN(\Delta)} \tag{2-10}$$

This can be simplified into:

$$F_V(d) = \left(\frac{d}{d_{max}}\right)^{3-\alpha} \quad \text{or} \quad F_V(d) = \left(\frac{d}{d_{max}}\right)^{\beta_V} \tag{2-11}$$

It follows that:

$$\beta_V = \beta_W + b \tag{2-12}$$

Following Einav's calculation method the crushing potential can be calculated as follows:

$$B_p = \int_{d_{min}}^{d_{max}} \left(F_{Wu}(d) - F_{W0}(d)\right) \, d(\log d) \tag{2-13}$$
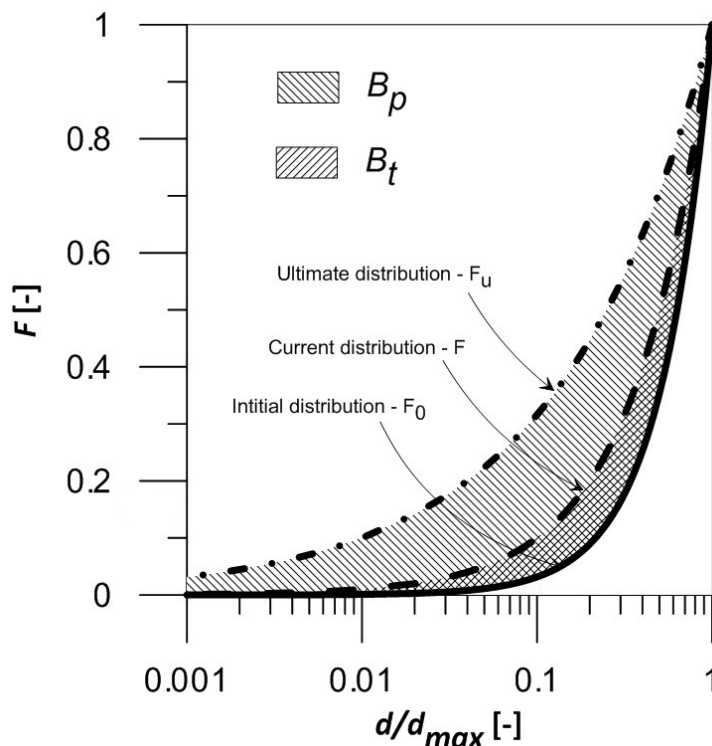
**Slika 2.9: Definicija potenciala drobljenja ($B_p$) in celotnega drobljenja ($B_t$)**

**Figure 2.9: Definition of crushing potential ($B_p$) and total crushing ($B_t$))**

In this study it is that assumed there is no comminution limit, therefore $d_{min} = 0$. By substituting $F_W(d)$ with the equation (2-9) and integrating the expression crushing potential can be written as:

$$B_p = 0.434 \cdot \left( \frac{1}{\beta_u} - \frac{1}{\beta_0} \right) \qquad \text{(2-14)}$$

$\beta_u$ – exponent value for ultimate distribution

$\beta_0$ – exponent value for initial distribution

Analogically, it is also possible evaluate the total amount of crushing as an area between the initial and final distribution:

$$B_t = 0.434 \cdot \left( \frac{1}{\beta} - \frac{1}{\beta_0} \right) \qquad \text{(2-15)}$$

$\beta$ – exponent value for current distribution

The ratio of these two values presents relative crushing:

$$B_r = \frac{B_t}{B_p} \qquad \text{(2-16)}$$

## 2.4  Laboratory testing

In laboratory a series of isotropically consolidated constant mean effective stress compression tests (TXP) were performed on LECA material, of which properties are described in the section 2.2. Using this material, testing could be performed on the normal triaxial apparatus and still being able to encompass complete sand behaviour including grain crushing.

### 2.4.1    Apparatus

Figure 2.10 shows the triaxial apparatus that was used for this research and it is schematically presented in Figure 2.11. It was designed at ETH IGT and has the following properties. The top and bottom cap have a diameter of 56.4 mm which corresponds to a surface area of 25 cm$^2$. The height of the sample is conditioned by the height of split mould (128.5 mm), therefore the initial height to diameter ratio is slightly higher than the minimal requested value of 2. The total range of a load cell is 5 kN. The axial loading is induced by an external motor underneath the triaxial cell and is transferred via the loading frame that is situated within the cell. For this reason the cell volume change needs to be corrected as the steel rods move in or out of the cell. Where the still rods exit the cell through the bottom plate the cell is hermetically sealed. In order to avoid frictional load losses, the cell measuring the axial load is placed between the sample and the loading frame. The sample has two drainages, one on the top and the other one on the bottom of the sample. The two drainages reduce the consolidation time and enable a special way of sample preparation, which is described in section 2.4.2, used in this research. The sample and cell drainages are connected to the two loading pilons outside the triaxial cell that have been used for inducing the load as well as for measurement of the volume change. One of the loading pilons was used for regulating the pore water pressure and the other one for regulating the cell pressure. The medium used for inducing the cell load was water. The apparatus is designed in a way so that both strain controlled and stress regulated tests can be performed. The capabilities of the apparatus are specified in Table 2.2.

**Table 2.2: Triaxial apparatus specification**

**Preglednica 2.2: Specifikacije triosnega aparata**

|  | Measurement range | Resolution |
|---|---|---|
| Load cell | 5 kN | 0.2 N |
| Pore water pressure | 1 MPa | 0.03 kPa |
| Cell pressure | 1 MPa | 0.03 kPa |
| Internal LVDT | 50 mm | 0.003 mm |

**Slika 2.10: Triosni aparat uporabljen v raziskavi**
**Figure 2.10: Triaxial apparatus used for the research**
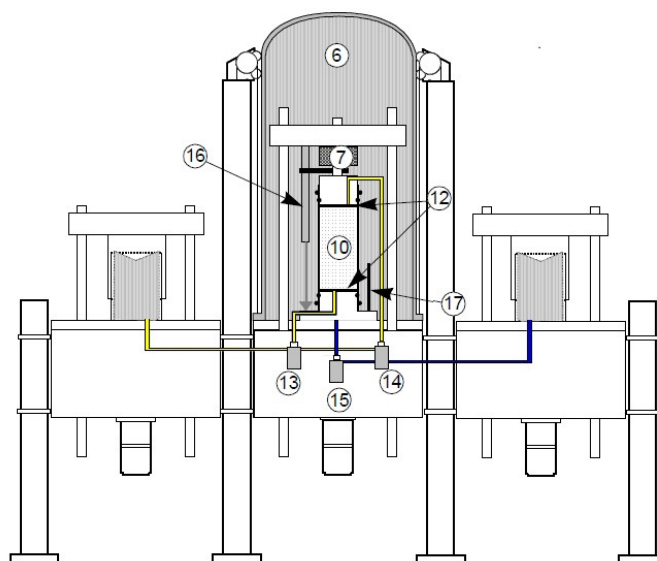
**Slika 2.11: Shema triosnega aparata (po Arensonu, 2003)**
**Figure 2.11: Apparatus scheme (after Arenson, 2003)**

The triaxial cell is made of 2 cm thick steel and is tightened to the bottom plate by 12 bolts of M24. This way the cell itself was not the limit for maximum loading.

## 2.4.2     Sample preparation

For material like LECA it is very hard to achieve a satisfying saturation using the desiccator, especially because bigger grains have specific weight lower than water, which means that they float in water. For this reason a different method called the *Dry setting method* was chosen. In this method a sample is prepared dry and stabilized with slight vacuum. Later on, by setting different pressures at the top and bottom drainage a hydraulic gradient is induced in the sample and, therefore, water flows through the sample. This procedure is presented step by step bellow.

### 2.4.2.1  Sample preparation

1.  The latex membrane is put over the bottom cap. Between the membrane and the bottom cap a small amount of water is put and all the bubbles removed. Next, the membrane is tightened with two O-rings.
2.  A split mould is put around the membrane, which is carefully rolled over the edge of the mould. The membrane is put in the correct position with a vacuum pump and straightened so there are no membrane wrinkles.
3.  The well mixed/homogenized soil sample is pluviated inside the membrane using a funnel. By maintaining a constant drop of 1 cm and a radial movement of a funnel a uniform sample as well as maximum void ratio is achieved.

4.  When the mould is full it is moved inside the triaxial cell and centred. It is important to be very careful in this step, not to cause any unwanted settlement of the sample.

5.  The bottom cap is screwed to the bottom plate of the cell.

6.  The top of the sample is carefully flattened taking care that the sample is not compressed. Following, the surface is checked using the spirit level and is corrected if needed.

7.  The top cap is carefully fitted to the top of the sample. Contact between the top can and a sample is achieved manually by looking at the deviator graph. When the deviator changes, contact between the top cap and sample is achieved.

8.  Next, the membrane is carefully put over the top cap and sealed with two O-rings.

9.  The internal LVDT is set, making sure that it is able to measure the displacement equal to the 30 percent of the initial sample height.

10. Slight vacuum is set to the sample to stabilize it.

11. The split mould is removed.

12. The specimen's height is measured 3 times. The diameter is measured 3 times at the top, middle and the bottom.

13. The triaxial cell is closed and tightened with 12 bolts.

14. The water tank is raised above the highest point of the cell and the valve is opened in order to fill the cell with water.

15. When the cell is full the valve is closed and the sample is set for the saturation.

### 2.4.2.2 Sample saturation

After the sample is prepared as described in last section it is ready for saturation. For this purpose a specific connection of water tanks has been prepared like shown in Figure 2.12. Prior to the sample preparation the following steps are made.

1.  The top water tank is filled close to the top and is connected through the bottom to the cell drainage. The water tank in the middle is also filled close to the top and is connected through the bottom to the bottom sample drainage. The bottom water tank emptied entirely and connected to the top sample drainage. The connection tubes between the top two water tanks and the triaxial apparatus are filled with water while the tube connecting the bottom tank with the triaxial apparatus is emptied.

2.  All three tanks are connected to the vacuum pump through the valve at the top of each tank. There is also a safety tank between the pump and the tanks, so that, in case some water escapes through the top of a tank, it does not ruin the vacuum pump.
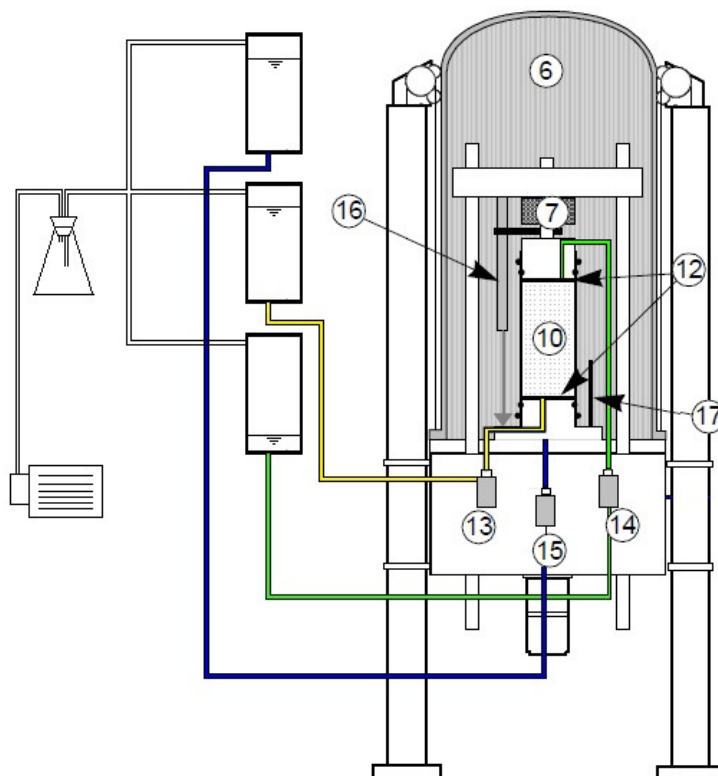
**Slika 2.12: Shematičen prikaz vodnih celic, ki so bile uporabljene za pripravo vzorca**

**Figure 2.12: Scheme of the water tanks used for the sample preparation**

With this type of connection of the water tanks and by opening and closing the correct valve sample stability is achieved at all times during the saturation. Below the steps that follow, after the sample is prepared, are listed.

3. The top sample drainage is already open, because a slight vacuum has already been applied to the sample. The cell drainage is opened.

4. Using the pump, vacuum is slowly increased to as close to 1Bar as possible. The maximal vacuum that is achieved depends on the capabilities of the vacuum pump (in our case it was 86kPa). It is important to increase the vacuum as high as possible. The air expands when vacuum is applied and so a higher amount of air is replaced by water.

5. When the vacuum reaches its maximum the bottom sample drainage is opened. Because of the hydraulic gradient that is induced by the water tank setting described in first step, water flows through the sample and replaces the air.

6. Water is left to flow through the sample for 2 to 3 hours.

7. Because at high vacuum water starts to boil at room temperature, there is also vapour circulation through the sample. If the vacuum is reduced in a short time, the vapour will not turn in to water fast enough and vapour bubble would be left in the drainage. Because of that, the initial volume change measurement would not be correct. For this reason, the vacuum is

reduced to 65kPa so the water stops boiling and the water is left to flow through the sample for another 30 minutes.

8. The top drainage is then closed and vacuum is slowly reduced to 0. Because the pressure adjustment in the cell takes longer than in the sample special, care need to be taken in order to maintain the sample stability (The cell pressure must be higher than pore water pressure at all times). For this reason the vacuum needs to be reduced slowly.

9. After vacuum is reduced to zero, the drainages are reconnected to the loading pilons. The top and bottom sample drainages are connected to the same pore water pilon.

10. In order to get as close to 100 percent saturation as possible a back pressure of 200kPa is imposed. To do this the pore water pressure and the cell pressure are increased simultaneously to 200kPa and 210kPa, respectively.

11. The sample is left over night so that the air that is still in the sample can dissolve in water.

### 2.4.3    Skempton's B-value

To be able to measure the correct volume changes, it is important to assure that the sample is fully saturated. In other words, it is important to replace all the air within the sample before the test. Because, if the air bubble escapes from the sample during the test and it is replaced by water, this would be recorded as a volume change, although the actual volume would not change. The procedure of assuring the maximal sample saturation is described in section 2.4.2. Here the evaluation of sample saturation is presented. The evaluation is performed using Skempton's B-value. When the sample undergoes a stress increment, the relation between the water pressure and the stress increment can be written as:

$$\Delta u = B \cdot (\Delta\sigma_3 + A \cdot (\Delta\sigma_1 - \Delta\sigma_3)) \qquad\qquad (2\text{-}17)$$

$\Delta u$ – increment of water pore pressure

$\Delta\sigma_1$ – increment of axial stress

$\Delta\sigma_3$ – increment of radial stress

$A, B$ – Skempton's pore pressure parameters

The term $A \cdot (\Delta\sigma_1 - \Delta\sigma_3)$ stands for the contribution of dilatancy to the increase of the pore pressure. In order to determine Skempton's $B$ parameter, the sample needs to be loaded isotropically with closed drainages. Doing so, the second term in equation (2-17) is eliminated and Skempton's equation simplifies into:

$$B = \frac{\Delta u}{\Delta \sigma_3}$$

(2-18)

To determine the $B$-value, the cell pressure is increased and the pore pressure that arises, because the water cannot escape the sample, is measured. To achieve satisfactory saturation, $B$-values of 0.95 or higher need to be achieved. The extent of saturation is evaluated by Skempton's $B$-value in place of the degree of saturation, $S_r$, because the $B$-value is a more sensitive index when a specimen is near the complete saturation (Towhata, 2008).
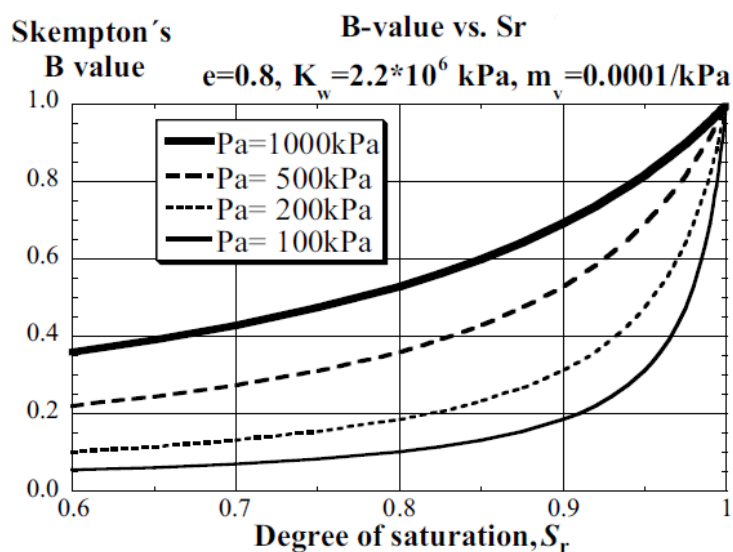


**Slika 2.13: Primer zveze med Skemptonovim parametrom $B$ in stopnjo zasičenosti za zemljino z $e = 0,8$ in $m_v = 10^{-4}/kPa$ (stisljivost zrn) (Towhata, 2008)**

**Figure 2.13: Example of relation between the Skempton's $B$-value and the degree of saturation for soil with $e = 0.8$ and $m_v = 10^{-4}/kPa$ (compressibility of a skeleton) (Towhata, 2008)**

## 2.4.4    Sieving

LECA material can be obtained from a producer in different size ranges. For the purpose of this research a crushed material with grain sizes ranging from 0 mm to 2 mm was used. The shape (angularity) and porosity of every grain size fraction can be seen in Figure 2.4. The material was sieved into 8 subfractions so that different grain size distributions could be prepared. The following sieve sizes were used: 2 mm, 1.4 mm, 1.0 mm, 0.71 mm, 0.5 mm, 0.25 mm, 0.125 mm, 0.063 mm.

The amount of crushing that the sample has undergone during the test was determined comparing the GSD before and after the test. Before the test sample was prepared according to the pre-defined GSD, while after the test the GSD was determined by sieving analysis. During sieving the procedure outlined in CEN ISO/TS 17892-4:2004 was followed, which is schematically presented in Figure 2.14.
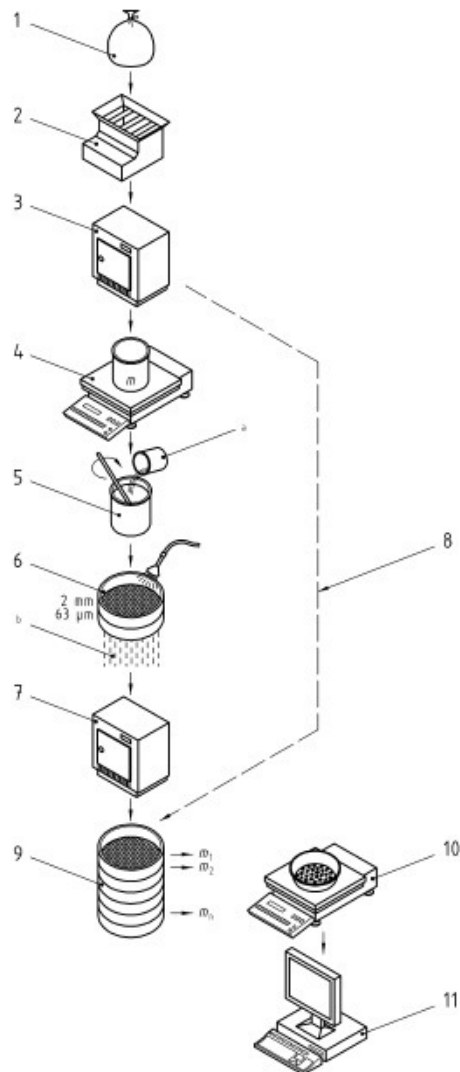
1. Sample
2. Riffling or quartering – this step was skipped because samples were small enough.
3. Drying
4. Weighing
5. Stirring
6. Wet sieving (10 minutes) – this step is used to separate grain of sizes smaller than 0.063 mm, which tend to stick to bigger grains, from the rest of the sample
7. Drying
9. Dry sieving(10 minutes)
10. Weighing
11. Analysing

**Slika 2.14: Sejanje vzorca (CEN ISO/TS 17892-4:2004)**

**Figure 2.14: Sample sieving procedure (CEN ISO/TS 17892-4:2004)**

Because LECA material has low grain strength, care needed to be taken during sieving procedure so that grains would not additionally crush. To prevent grains from crushing during sieving the amplitude of the shaking table needed to be adjusted. This was performed by sieving the pre-prepared sample and comparing the masses, which remained on each sieve with the input masses. The duration of the sieving was constant (10 minutes) while the amplitude varied until the error on all the sieves was smaller than 1 percent. The amplitude that was used for sample sieving after the triaxial test was set to 1.0 mm.

## 2.5 Samples and stress paths

This study is part of extended research on crushable material performed at ETH IGT [1]. The aim of this thesis is to investigate the behaviour of crushable soil under different stress paths and with different initial grain size distributions. Therefore, the test results obtained by other students are also included in the analysis. Wanninger and Pascal performed a series of oedometer tests (OED) while Leu, Low and Zimmermann have investigated the effect of isotropic compression (ISO) and triaxial compression tests (TXC) on grain crushing. To extend this research a set of isotropically consolidated constant mean effective stress compression tests (TXP) were performed by the author of this analysis.

### 2.5.1     Samples

All of the above mentioned tests were performed on samples with three different coefficients of uniformity ($U_W$ = 3.5, 14, 28), while the mean grain size of the cumulative distribution by weight ($d_{50,W}$) was constant and equal to 0.5 mm. On samples with initial coefficient of uniformity equal to 7 and mean grain size of 0.5 mm only OED and TXP tests were performed. The samples were prepared as fractal distributions according to the equation (2-9), therefore, the two parameters ($\beta_W$ and $d_{max,W}$) needed to be evaluated from $U_W$ and $d_{50,W}$ by using the following equations:

$$F\big(d_{50,W}\big) = \left(\frac{d_{50,W}}{d_{max,W}}\right)^{\beta_W} = 0.5 \qquad \rightarrow \qquad \boxed{d_{max,W} = \frac{d_{50,W}}{0.5^{\wedge}\left(\frac{1}{\beta_W}\right)}} \qquad (2\text{-}19)$$

$$F\big(d_{60,W}\big) = \left(\frac{d_{60,W}}{d_{max,W}}\right)^{\beta_W} = 0.6 \ \ \text{and} \ \ F\big(d_{10,W}\big) = \left(\frac{d_{10,W}}{d_{max,W}}\right)^{\beta_W} = 0.1 \qquad (2\text{-}20)$$

$$\frac{F\big(d_{60,W}\big)}{F\big(d_{10,W}\big)} = \left(\frac{d_{60,W}}{d_{10,W}}\right)^{\beta_W} = U_W^{\wedge}\beta_W = 6 \qquad \rightarrow \qquad \boxed{\beta_W = \log_{U_W} 6} \qquad (2\text{-}21)$$

Parameters $\beta_W$ and $d_{max,W}$ are important for sample preparation, because each grain size fraction is added with specified weight ratio of the total weight of the sample. But, for the behaviour of the sample its volumetric distribution plays a crucial role. For a material with a constant specific weight, the grain size distributions by weight and by volume coincide. But, if the specific weight depends on the grain size (apparent specific weight), the two distributions differ from one another. Therefore, in the Table 2.3 a comparison between the parameters of grain size distribution by weight and by volume is listed.

---

[1] ETH IGT – Swiss Federal Institute of Technology Zurich - Institute for Geotechnical Engineering

**Table 2.3: Parameters for determination of initial grain size distributions**

**Preglednica 2.3: Parametri za določitev izhodiščnih zrnavostnih krivulj**

| $U_W$ | $d_{50,W}$ [mm] | $\beta_W$ | $d_{max,W}$ [mm] | $\beta_V$ | $d_{max,V}$ [mm] | $U_V$ | $d_{50,V}$ [mm] | $B_{p,V}$ |
|-------|-----------------|-----------|-------------------|-----------|-------------------|-------|-----------------|-----------|
| 3.5 | 0.5 | 1.43 | 0.81 | 1.69 | 0.81 | 2.89 | 0.54 | 0.45 |
| 7 | 0.5 | 0.92 | 1.06 | 1.16 | 1.06 | 4.7 | 0.58 | 0.34 |
| 14 | 0.5 | 0.68 | 1.39 | 0.89 | 1.39 | 7.48 | 0.64 | 0.22 |
| 28 | 0.5 | 0.54 | 1.81 | 0.75 | 1.81 | 10.9 | 0.72 | 0.13 |

$\beta_V$ can be calculated from $\beta_W$ using the equation (2-11) where, for LECA, the value of $b$ is 0.268. But, the values calculated with this equation differ from the values listed in the Table 2.3. Parameters $U_V$ and $d_{50,V}$, specified in the Table 2.3, were determined by fitting the curve to the actual grain size distribution by volume. The reason for this error is that the apparent specific weight is not exponential for particles smaller than 0.063 mm. For grains with a diameter smaller than 0.063 mm apparent specific weight is constant as stated in equation (2-16) (Casini, Viggiani, 2011).
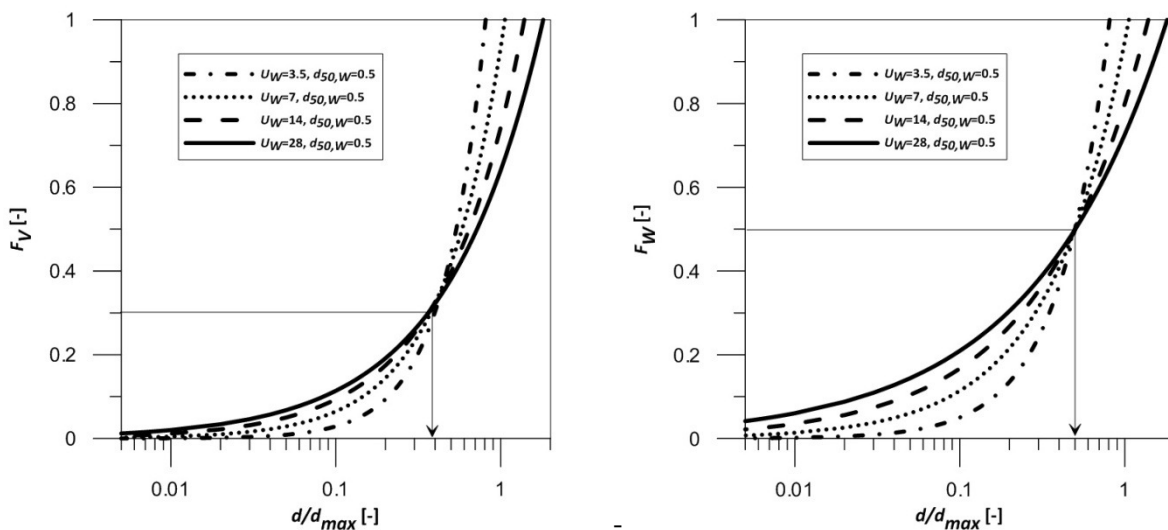


**Slika 2.15: Primerjava volumske in masne zrnavostne sestave**

**Figure 2.15: A comparison of grain size distribution by volume and by weight**

In Figure 2.15 a comparison between the two distributions, by volume and by weight, is presented. While for GSD by weight all samples have in common the grain size $d_{50}$, for GSD by volume samples have a common grain size $d_{35}$. The behaviour of non-cohesive soil mainly depends on the size and shape of grains while the role of the specific weight has a negligible effect. In the rest of the thesis the term grain size distribution will refer to grain size distribution by volume, unless stated otherwise. In reality the specific weight is an important parameter since the weight of upper layers represents the load on the lower layers, but in the tests performed the external pressures are much higher than the pressures due to the self-weight.

## 2.5.2    Stress paths

As mentioned at the beginning of section 2.5, the goal of this research is to investigate the effect of different stress paths on evolution of GSD and the effect of crushing on mechanical properties of the soil. For this reason samples were exposed to different stress paths (ISO, OED, TXC and TXP) and different final mean effective stresses (175 kPa, 350 kPa and 700 kPa). In Figure 2.16 a stress path program for every sample, described in section 2.5.1, is presented.
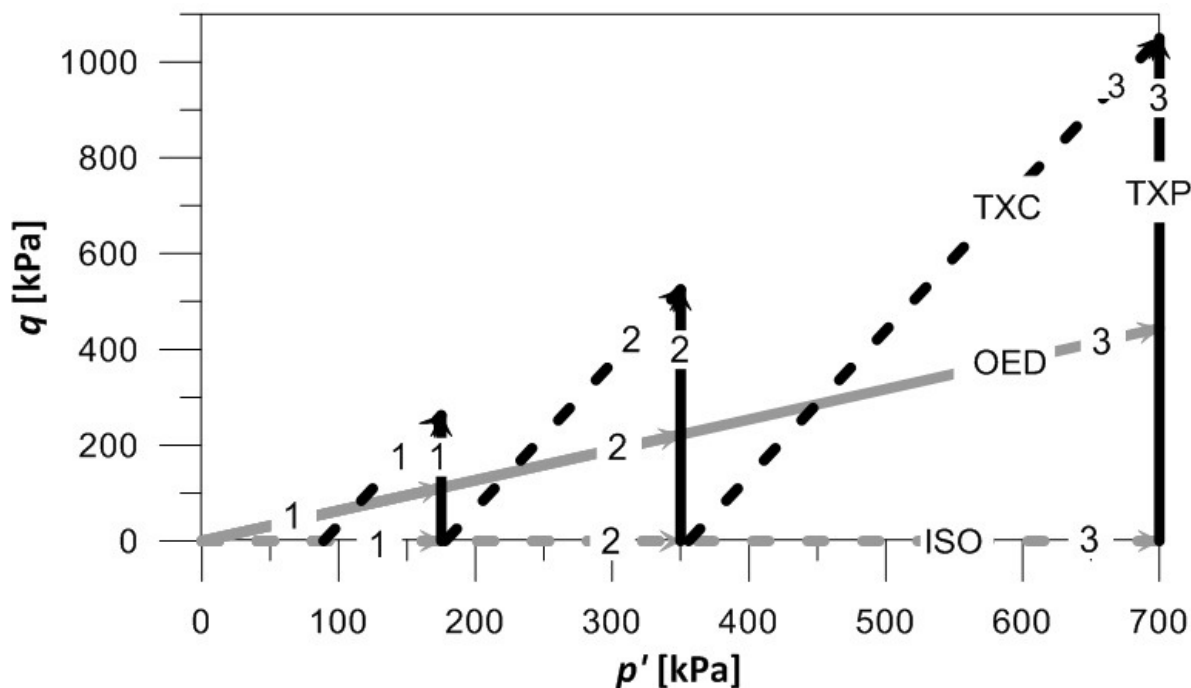


**Slika 2.16: Program napetostnih poti**

**Figure 2.16: Stress path program**

Where the numbers on each stress path denote the following final mean effective stress:

- 1 – 175 kPa
- 2 – 350 kPa
- 3 – 700 kPa

Each of the stress paths showed in Figure 2.16 induce different boundary condition to the sample. These boundary conditions are shortly presented bellow
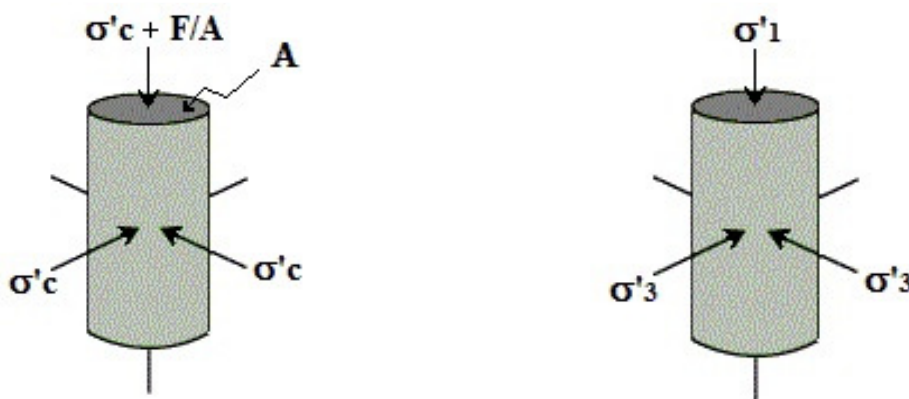
**Slika 2.17: Napetosti, ki delujejo na vzorec**

**Figure 2.17: Stresses acting on sample**

i)      Isotropic loading

During isotropic compression, stresses in all directions are equal:

$$\sigma_1' = \sigma_3' \tag{2-22}$$

$$p' = \frac{\sigma_1' + 2 \cdot \sigma_3'}{3} = \frac{3 \cdot \sigma_1'}{3} = \sigma_1' \quad \text{and} \quad q = \sigma_1' - \sigma_3' = \sigma_1' - \sigma_1' = 0 \tag{2-23}$$

ii)     Oedometric loading

For the oedometric test only the vertical pressure is known while the radial pressure cannot be measured. In order to compare the results from this test with the rest of the tests lateral soil pressure ($\sigma_3'$) needs to be estimated. Knowing that lateral displacement is not allowed in oedometer, horizontal pressure can be estimated through the equation:

$$\sigma_3' = K_0 \cdot \sigma_1' \tag{2-24}$$

Where the coefficient of earth pressure at rest ($K_0$), for normally consolidated soils, can be evaluated with the Jaky's equation:

$$K_{0NC} = 1 - \sin \varphi' \tag{2-25}$$

To be able to perform this correlation an estimation of an internal friction angle is needed. Here the problem arises since the friction angle of the soil used in this research changes during the test. Since it is not possible to track how the friction angle changes during the test, only a rough estimation can be made. A good approximate of the internal friction angle for sands is the angle of repose.
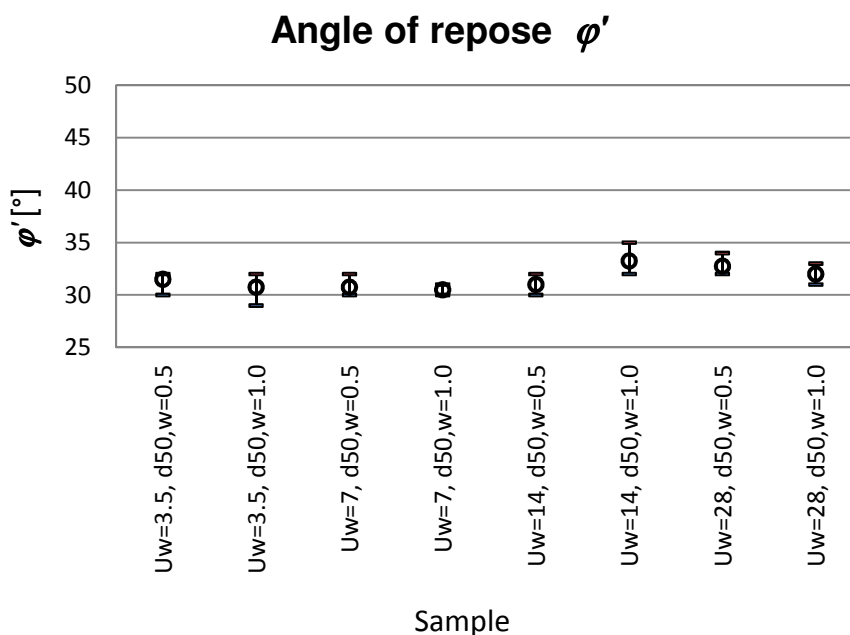
**Slika 2.18: Nasipni kot za vzorce z različnimi začetnimi vrednostmi koeficienta enakomernosti in d₅₀ pri masni zrnavostni strukturi (Wanninger, 2010)**

**Figure 2.18: Angle of repose for samples with different uniformities and values of d₅₀ for GSD by mass (Wanninger, 2010)**

The mean value of the angle of repose is $31°$ and therefore the value of $K_0$ is 0.48. From this the value $M'$ can be determined:

$$q = \sigma_1' - \sigma_3' = \sigma_1' - \sigma_1' \cdot K_0 = \sigma_1' \cdot (1 - K_0) \tag{2-26}$$

$$p' = \frac{\sigma_1' + 2 \cdot \sigma_3'}{3} = \frac{\sigma_1' + 2 \cdot \sigma_1' \cdot K_0}{3} = \frac{\sigma_1' \cdot (1 + 2 \cdot K_0)}{3} \tag{2-27}$$

$$\eta = const. = \frac{q}{p'} = \frac{(1 - K_0) \cdot 3}{(1 + 2 \cdot K_0)} = \frac{(1 - 0.48) \cdot 3}{(1 + 2 \cdot 0.48)} = 0.79 \tag{2-28}$$

**Table 2.4: Calculation of mean effective stress and deviatoric stress for oedometer tests**

**Preglednica 2.4: Račun srednjih efektivnih napetosti in deviatoričnih napetosti za oedometrski test**

| $\sigma_1'$ | $K_0$ | $\sigma_3'$ | $p'$ | $q$ |
|---|---|---|---|---|
| [kPa] | [-] | [kPa] | [kPa] | [kPa] |
| 250 | 0.48 | 120 | 163 | 130 |
| 500 | 0.48 | 240 | 327 | 260 |
| 1000 | 0.48 | 480 | 653 | 520 |

iii)      Triaxial compression test

During this test the cell pressure is held constant while vertical stress is increased. Because of this, both deviatoric and mean effective stress change.

$$\sigma_1' = \sigma_c' + \frac{F}{A} \quad \text{and} \quad \sigma_3' = \sigma_c' \tag{2-29}$$

$$q = \sigma_1' - \sigma_3' = \sigma_c' + \frac{F}{A} - \sigma_c' = \frac{F}{A} \tag{2-30}$$

$$p' = \frac{\sigma_1' + 2 \cdot \sigma_3'}{3} = \frac{\sigma_c' + \frac{F}{A} + 2 \cdot \sigma_c'}{3} = \sigma_c' + \frac{q}{3} \tag{2-31}$$

Although the cell pressure remains constant, it follows from the equation (2-31) that mean effective stress increases together with deviatoric stress.

iv)      Isotropically consolidated constant mean effective stress compression tests

As emphasised in its name, for this test the mean effective stress remains constant. Therefore, as it follows from the equation (2-31):

$$\sigma_c' = p' - \frac{q}{3} \tag{2-32}$$

The cell pressure needs to be reduced during the test.

## 2.6 Results

### 2.6.1      Isotropic compression tests (ISO)

A characteristic feature of soil under isotropic compression is the specific volume ($v = 1 + e$) in relation to hydrostatic pressure which is in the $q : p'$ plane equal to the mean effective stress ($p'$).
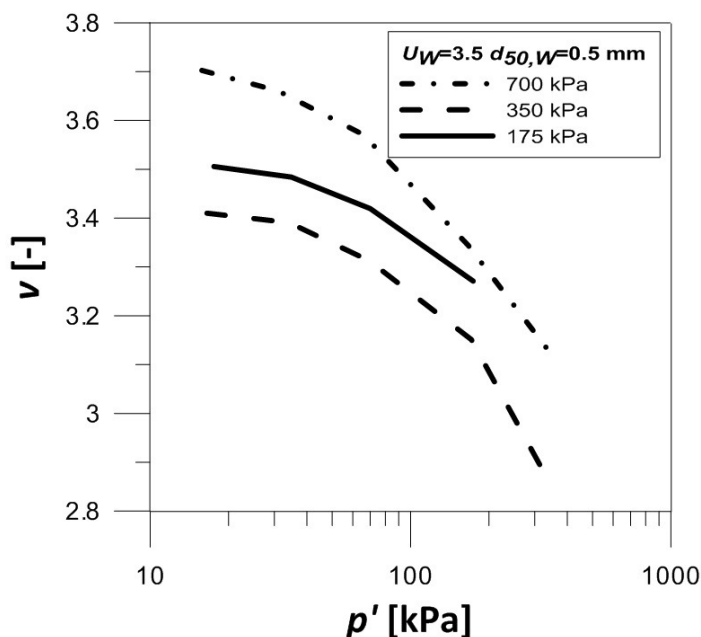


**Slika 2.19: Izotropna tlačna obremenitev ($d_{50,W} = 0,5$ mm, $U_W = 3,5$) (Leu, 2011)**

**Figure 2.19: Isotropic compression ($d_{50,W} = 0.5$ mm, $U = 3.5$) (Leu, 2011)**

As seen in the upper graph, LECA for isotropic compression behaves like sand with high grain strength. Because tests were performed on loose reconstituted samples, there is an initial nonlinearity even in $v - \log(p')$ plane. The curve of the sample loaded up to $p' = 700$ kPa already starts to approach the linear line that is typical for sands with high grain strength and can be described as:

$$v = N - C_c \cdot \log_{10} p' \tag{2-33}$$

$N$ – specific volume for $p' = 1$ kPa

$C_c$ – Compressibility index

In Figure 2.20 equations for primary compression are shown for different initial coefficients of uniformity. It is possible to note that well graded samples are much stiffer than more uniformly graded samples. In well graded samples the smaller grains fill in the voids between bigger grains. Such soil has higher modulus of compressibility and, therefore, lower void changes with an increase in isotropic pressure.
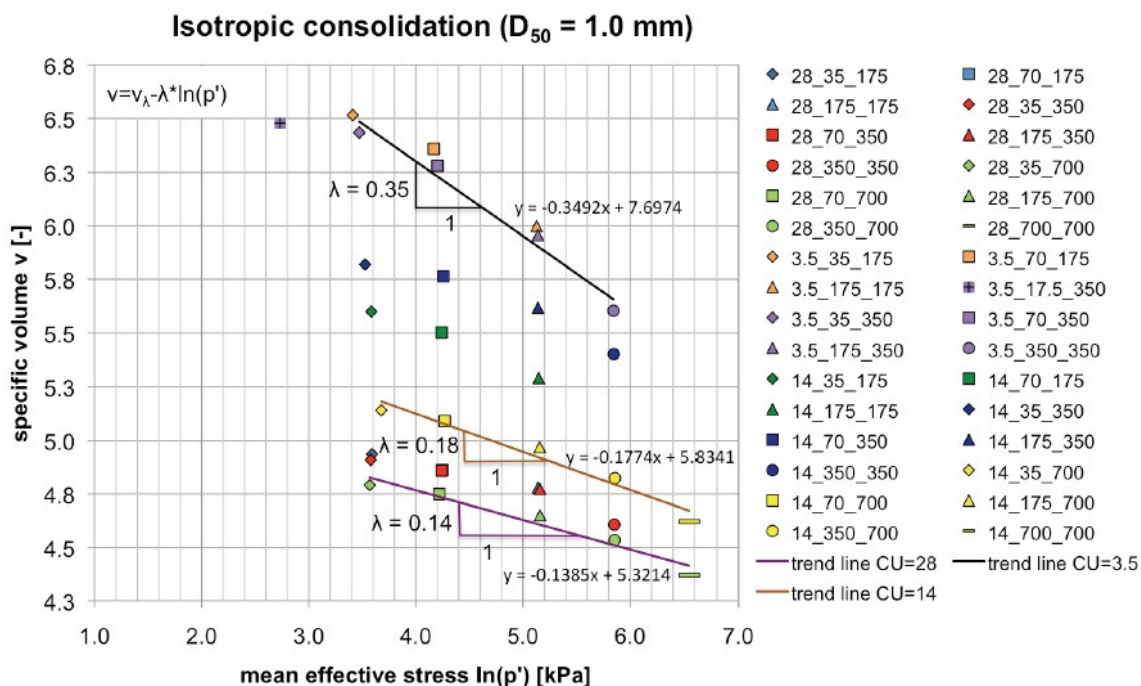
**Slika 2.20: Enačbe stisljivostne krivulje za različne koeficiente enakomernosti in $d_{50,W} = 1.0$ mm (Leu, 2011)**

**Figure 2.20: Equations of the compression lines for different coefficients of uniformity and $d_{50,W} = 1.0$ mm (Leu, 2011)**

The behaviour of sand with low strength for isotropic compression can be well described with parameters that are normally used for sand. The reason for this is shown in Figure 2.21.
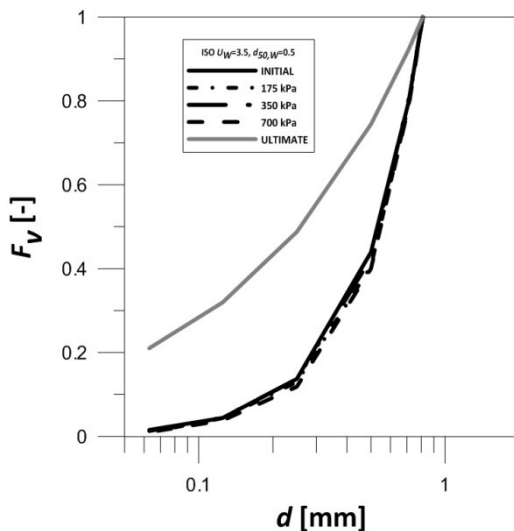


**Slika 2.21: Volumska zrnavostna sestava po izotropni tlačni obremenitvi za vzorec z $d_{50,W} = 0,5$ mm $U_W = 3,5$ (Leu, 2011)**

**Figure 2.21: Volumetric GSD after isotropic compression test for sample with $d_{50,W} = 0.5$ mm $U_W = 3.5$ (Leu, 2011)**

In Figure 2.21, the GSD by volume of the sample with initial coefficient of uniformity by weight of 3.5 is shown. Such initial distribution is most uniformly graded and considering the assumption that

the final distribution has a fractal dimension of approx. 2.39 it means it has the highest crushing potential. For the same stress path the sample with higher crushing potential is expected to experience higher value of total crushing. From this graph it is evident that isotropic compression does not affect the grain size distribution at least not at pressures at which the tests were performed. Therefore, most of the volumetric changes that occur during the tests are due to local grain reorganization.

Some of the grading curves in Figure 2.21 are actually below the initial grain size distribution curve. This is not physically possible since the grains cannot merge back together. The reason for this is that when dismantling a sample and during sieving analysis a small percent of material is lost and this results in unnatural changes of GSD curve.

### 2.6.2 Oedometric compression tests (OED)

During the oedometric compression interesting behaviour was observed (Figure 2.22). Surprisingly, the most uniformly graded distribution ($U_W = 28$) has, at low pressures, the lowest compression modulus. At higher pressures, when the sample approaches minimal void ratio, it shows much stiffer behaviour then the rest of the samples. In contrast, the most poorly graded sample shows the stiffest behaviour at the beginning, but later its modulus of compression increases less than for the rest of the samples. A possible explanation for this behaviour is that the poorly graded sample shows the high initial stiffness due to the interlocking of grains since they are of an even size. Once the pressure is high enough, the edges start to crush and the grains rearrange. Because of high void ratio the grains easily rearrange so the compression modulus only slightly increases. For the well graded sample, because of the presence of a whole spectrum of grain sizes, the interlocking of grains has a smaller effect. Each GSD has a minimal void ratio and when the actual void ratio starts to approach its minimal value the compression modulus drastically increases. It is obvious that the difference between the $e_{max}$ and $e_{min}$ for more uniform distributions is higher than for poorly graded distribution and, therefore, the compression modulus does not increase as fast as in uniformly distributed samples.
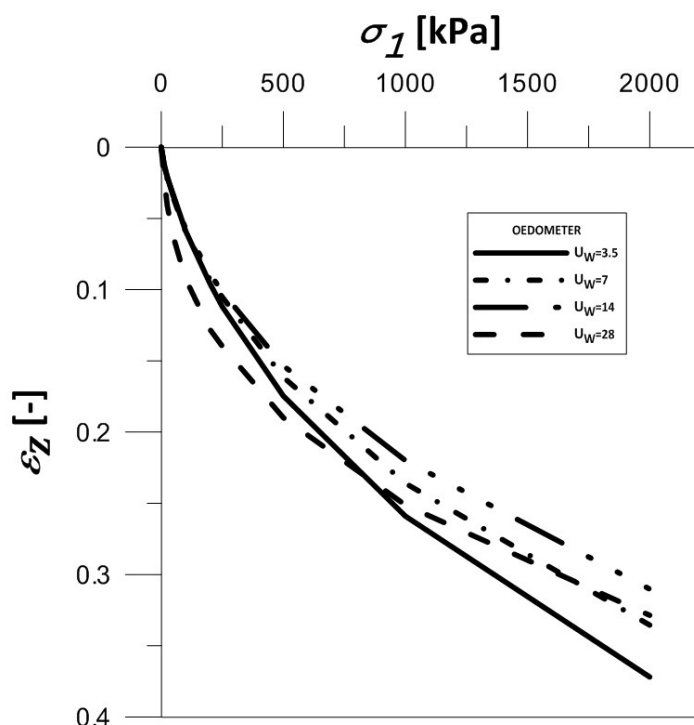
**Slika 2.22: Diagram napetosti in deformacij za vzorce z različnimi začetnimi vrednostmi koeficienta enakomernosti in konstantni vrednosti $d_{50,W}$ (Wanninger, 2010)**

**Figure 2.22: Stress-strain relation for different uniformities and constant values of $d_{50,W}$ (Wanninger, 2010)**

### 2.6.3      Isotropically consolidated conventional triaxial compression tests (TXC)

For conventional triaxial test it is characteristic that during shearing the cell pressure remains constant. Therefore, by increasing the vertical loading $(\sigma'_1)$ mean effective stress $(p')$ increases as well.

Two of the important parameters that influence crushing are the state of the effective stress and the void ratio during shearing. The test is very similar to the TXP test as the axial loading is increased until the sample fails. The difference is presented in equations (2-29), (2-30) and (2-31). As the axial load is increased, unlike for the TXP test where $p'$ is constant, the mean effective stress also increases Therefore, the void ratio change has two parts: one due to the isotropic compression and the other due to the grain reorganization due to shearing. It was mentioned that tests were planned in such a way that the final mean effective stress was the same for all the tests. Since for the TXC test the initial mean effective stress is lower than for TXP test, the void ratio at the beginning of the test is higher and the grains are not as interlocked. Because of that they can rearrange easier and experience less crushing.
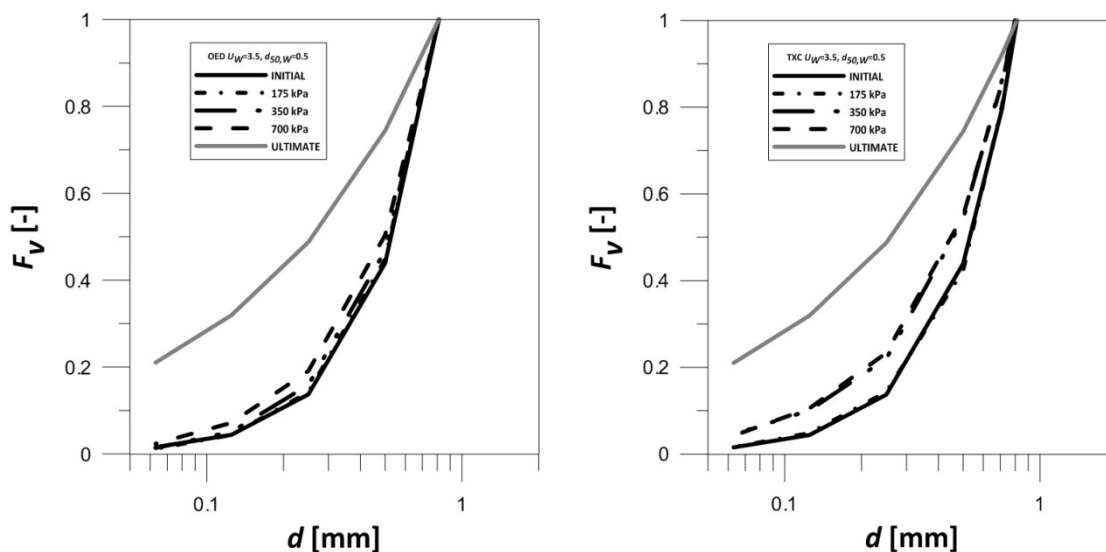
**Slika 2.23: Zrnavostna krivulja po oedometerskem in triosnem strižnem preskusu**

**Figure 2.23: Grading curves after the OED and TXC tests**

From Figure 2.23 it is possible to see that, even though a high value of deviatoric stresses was reached, the amount of crushing is only slightly higher than in the oedometric test. Anyways, by comparing the results from the OED and the TXC tests with ISO tests it is evident that deviatoric stresses play an important role in grain crushing.

As mentioned in section 2.3, many researchers dealing with grain crushing are trying to determine the ultimate grain size distribution. Several different suggestions have been proposed. In recent times the theory of final fractal distribution attracted great interest. The consequence of theory of final fractal distribution is that bigger grains have a greater coordination number which causes more uniform stress distribution within the grain and, therefore, smaller tensile stresses. In other words larger grains, because of their size, cannot get trapped between only two other grains, which represent the worst loading condition. Rather, they are surrounded (cushioned) by a number of smaller grains. Therefore, they are not subjected to crushing while smaller grains can get trapped between only two grains, which results in a non-uniform stress distribution and are more likely to crush. Such behaviour can also be observed in the results of tests performed in this research, where the maximal grain size remains constant while the grading approaches the ultimate grading by only rotating around the tip of the graph defined by:

$$F_V(d_{max}) = 1.0 \hspace{5cm} (2\text{-}34)$$

### 2.6.4      Isotropically consolidated constant mean effective stress compression test (TXP)

In this section the results obtained from the triaxial tests at a constant mean effective stress will be presented. Although these are results of sand with very weak grains similar behaviour can be expected for sand with high grain strength at very large pressures.

#### 2.6.4.1 Dependence of crushing on initial GSD

The changing of grain size distribution mainly consists of a rotation around the point defined by $F_V(d_{max}) = 1.0$, where $d_{max}$ represents the maximal grain size in the initial grading. But, the amount of this rotation greatly depends on the initial grading. In more uniform grading grains have on average a lower coordination number, consequently higher potential and, therefore, exhibit more crushing.
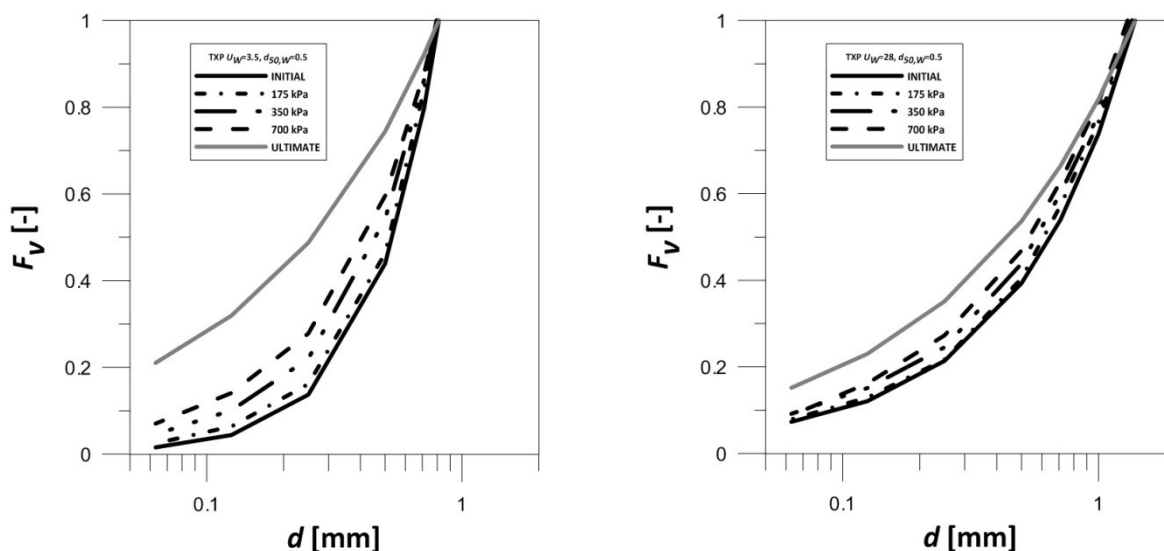


Slika 2.24: Primerjava zrnavosti po končanem triosnem strigu za vzorca z $U_W = 3,5$ in $U_W = 28$

Figure 2.24: A comparison of grading after triaxial sheering for distributions with $U_W = 3.5$ and $U_W = 28$

The results of the present study have more or less confirmed the two assumptions stated at the beginning of this chapter (constant $d_{max}$, fractal ultimate distribution). Although, for samples with more uniform distribution the maximal grain size starts to slightly reduce. This suggests two phases of grain crushing. During first phase, the change of the grain size distribution can be described as a rotation of the GSD around the point defined as $F_V(d_{max}) = 1.0$. This means that during this phase the maximal grain size does not change, while smaller grains crush in such a way that the curve of GSD approaches the ultimate fractal distribution. As it is shown in Table 2.5, in this research 2.39 is assumed as the fractal dimension of ultimate grading.
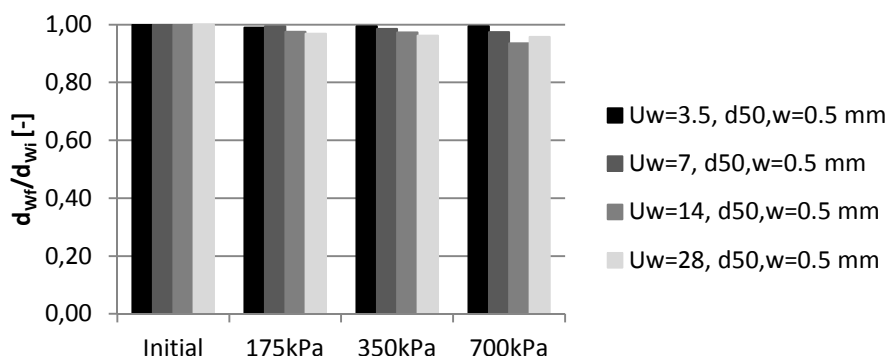
**Slika 2.25: Zmanjševanje velikosti maksimalnega zrna s povečevanjem srednje vrednosti efektivne napetosti**

**Figure 2.25: Reduction of maximal grain size with increasing mean effective stress**

The second phase starts when GSD reaches the ultimate fractal grain size distribution and all of the grain sizes are equally loaded. Because of higher amount of imperfections in bigger grains they have lower grain strength. Therefore, in such uniform sample bigger grains become the weakest link in the chain so their size begins to reduce.

The fractal dimension of sample grading changes during the test. At first sight it is rather surprising that the sample grading can be described with a fractal dimension at all times. Casini and Viggiani (2011) highlight that although the initial cumulative grain size distribution may not be self similar (fractal), in most cases, the cumulative grain size distribution would be reasonably fitted by equation (2-11). The loading required to reduce the initial distribution to a self similar distribution would be rather small. To support this assumption Table 2.5 provides final fractal dimension which are fitted with least squares method. In the right column the values of the coefficient of determination $R^2$ are given.

**Table 2.5: Fractal dimensions and $R^2$-values**

**Preglednica 2.5: Fraktalne dimenzije in $R^2$ vrednosti**

| Sample | $\alpha_V$ | $R^2$ | | Sample | $\alpha_V$ | $R^2$ |
|---|---|---|---|---|---|---|
| TXP $p' = 175$ kPa $U_W = 3.5$ | 1.70 | 0.9986 | | TXP $p' = 175$ kPa $U_W = 14$ | 2.12 | 1.0000 |
| TXP $p' = 350$ kPa $U_W = 3.5$ | 1.72 | 0.9990 | | TXP $p' = 350$ kPa $U_W = 14$ | 2.19 | 0.9986 |
| TXP $p' = 700$ kPa $U_W = 3.5$ | 1.91 | 0.9994 | | TXP $p' = 700$ kPa $U_W = 14$ | 2.28 | 0.9994 |
| TXP $p' = 175$ kPa $U_W = 7$ | 1.08 | 0.9990 | | TXP $p' = 175$ kPa $U_W = 28$ | 2.29 | 0.9977 |
| TXP $p' = 350$ kPa $U_W = 7$ | 2.05 | 0.9992 | | TXP $p' = 350$ kPa $U_W = 28$ | 2.32 | 0.9917 |
| TXP $p' = 700$ kPa $U_W = 7$ | 2.20 | 0.9992 | | TXP $p' = 700$ kPa $U_W = 28$ | 2.39 | 0.9990 |

As it is mentioned in section 2.3.2 grain crushing can be described in several different ways. In this study two ways of quantifying crushing are used. The first one is an absolute change of area under the

grain size distribution graph called total crushing, while the second one is the relative crushing that has also been introduced in section 2.3.3. As the name suggests, relative crushing indicates how much crushing the sample has undergone relative to the crushing potential. As shown in Figure 2.9 the crushing potential is represented with the area between the initial and final grain size distribution graph.
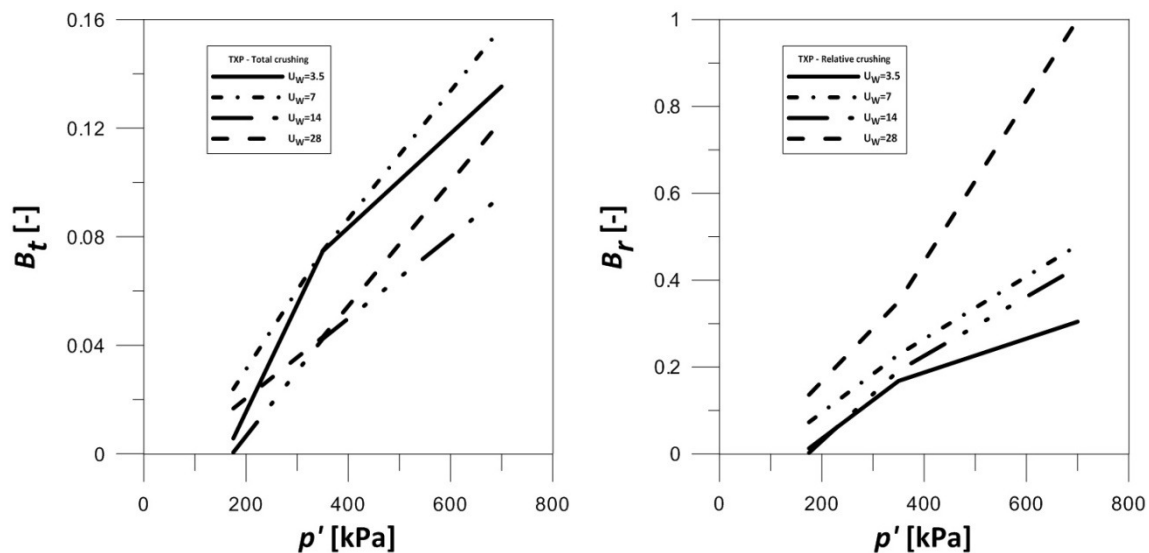


**Slika 2.26: Celotno ($B_t$) in relativno drobljenje ($B_r$)**

**Figure 2.26: Total ($B_t$) and relative crushing ($B_r$)**

For samples with different initial grain size distributions it is expected that the crushing is not going to be the same for all of them. Instead, the poorly graded samples should undergo more crushing due to their high crushing potential. In Figure 2.26 the two above-mentioned indexes are shown. At first sight the graph with absolute change of an area looks very odd since it shows that the sample with initial uniformity of 7 is more prone to crushing than the one with initial uniformity of 3.5. But, it needs to be mentioned that the sample with coefficient of uniformity equal to 3.5 for the confining pressure of 700 kPa did not reach its peak strength because the internal LVDT went out of range prior to sample failure and consequently the test stopped. Just by measuring the GSD before and after the test it is not possible to tell how much crushing the sample undergoes in the last part of the test. During the triaxial shearing of the normally consolidated soil, the sample compresses and the coordination number increases, while with increasing deviatoric stresses the non-uniformity of grain loading also increases. The two parameters have contrary effects and, therefore, the reason for this deviation can only be assumed based on the theory that shear stresses overrule the increase of the coordination number and, therefore, cause more crushing. But, this can be checked in the numerically simulated test where the GSD can be extracted any time during the test. Another anomaly is the sample with initial uniformity of 28 at the confining pressure of 700 kPa, where the unexpectedly high amount of total crushing has been observed. Similar behaviour has been observed for the tests performed by Hardin, but so far no

logical explanation has been found. Although, it is possible the this behaviour is a consequence of a reduction of maximal grain size for more uniform distributions, presented in Figure 2.25.
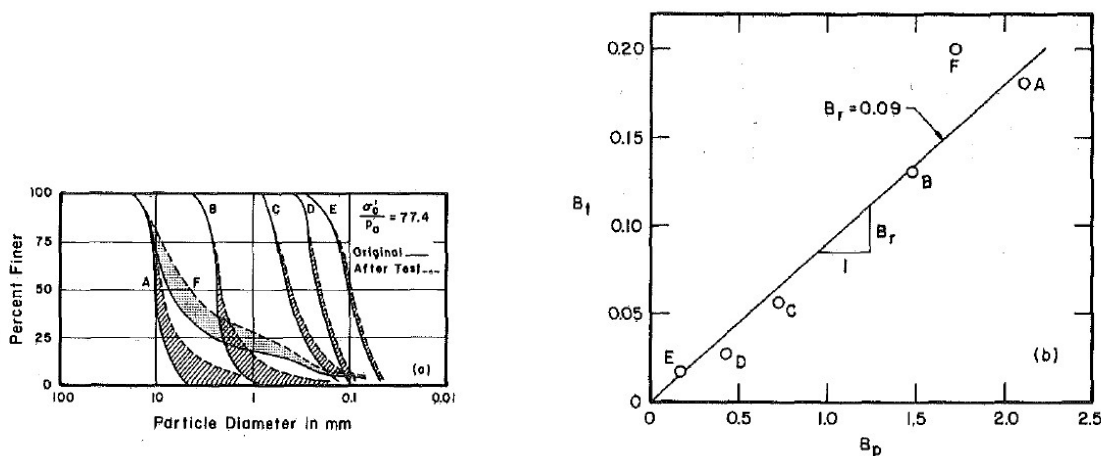


**Slika 2.27: Visoka vrednost absolutnega drobljenja za vzorec z visokim koeficientom enakomernosti (Hardin, 1985)**

**Figure 2.27: High value of total crushing observed for samples with high uniformity (Hardin, 1985)**

The right graph in Figure 2.26 shows that the amount of crushing is actually quite consistent. The parallelism of the graphs shows that the amount of total crushing greatly depends on the crushing potential. That means that grains in samples with more uniformly graded distribution have a greater average coordination number, which prevents grains from crushing. The two anomalies ($U_W = 28$, $p' = 700$ kPa; $U_W = 3.5$, $p' = 700$ kPa) mentioned at the end of previous paragraph were excluded from further analysis.

## 2.6.4.2 Volumetric changes

In critical state soil mechanics, which is based on clay behaviour, one of the fundamentals is that at critical state there is no volumetric changes. Sands need to experience very large strains to reach the critical state, too large for triaxial testing apparatus. So when the shear srength is reached is still experiences volumetric changes. In this section the volumetric changes for different initial gradings and different confining pressures are compared. From the graph in Figure 2.28 two observations can be made. The first one is that the volumetric deformations decrease with increasing coefficient of uniformity of the grading distribution. The second one is that at failure still crushable soil in a non-uniformly graded sample experiences volumetric changes. This specific behaviour seems to be another consequence of crushing since at failure a gradient of volumetric changes is larger for the samples that experienced more crushing.
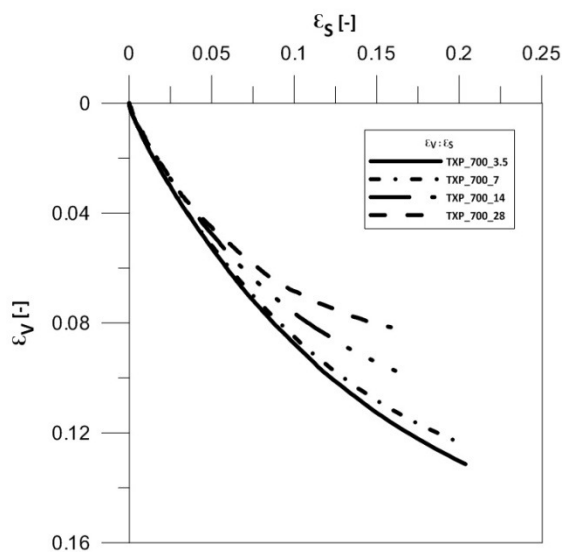
**Slika 2.28: Volumske deformacije v odvisnosti od strižnih deformacij**

**Figure 2.28: Volumetric strain with respect to the shear strain**

Although the peak value of the deviatoric stress is reached the volumetric deformations still have gradient different than 0. In section 1.2 the behaviour of clay is presented and briefly explained. For clays on the wet side of the critical state line the peak value and zero gradient of volumetric deformations are reached at the same time.

**Table 2.6: Gradients of volumetric changes at the end of the test**

**Preglednica 2.6: Gradienti volumskih sprememb na koncu testa**

| $d_{50,W}$ [mm] | $U_W$ [-] | 175 kPa | 350 kPa | 700 kPa |
|---|---|---|---|---|
| 0.5 | 3.5 | 0.224 | 0.212 | 0.358 |
| 0.5 | 7 | 0.132 | 0.179 | 0.331 |
| 0.5 | 14 | 0.123 | 0.130 | 0.283 |
| 0.5 | 28 | 0.024 | 0.123 | 0.185 |

In the Table 2.6 the final gradients of volumetric deformations are listed and the trend is quite obvious. For more uniform initial gradings and higher confining pressures the final gradient is higher, which means that the sample has undergone more crushing. The results in the table suggest that the volumetric changes stabilize when final distribution is reached as, for example, in sample $U_W = 28, d_{50,W} = 0.5$ at 175 kPa where almost no crushing takes place and the distribution is already final. From the gradient of volumetric changes it is expected that the sample will experience more crushing even after reaching its shear strength. From different gradients for the same confining pressure and different initial gradings it is expected that final distribution (at very large deformations) will be approximately the same. However, this cannot be expected for the same distribution and the different

confining pressure. Samples at lower confining pressure have smaller gradients and smaller shear strains at sample failure. This suggests that the grading even at very large stresses will not be the same as for samples at higher confining pressure. Nevertheless, even samples with very uniform grading at low confining pressures are not expected to crush at all. Solely based on this results it is not possible to be certain how the grading will change with increasing shear deformations. Therefore, it should be checked, with additional strain controlled tests, where the post peak behaviour can be observed, what type of grading the sample approaches at high strains. Nevertheless, these results point out another basic parameter that cause crushing. Besides the low coordination number, that results in higher tensile stresses at lower pressures and the confining pressure that increases the grain interlocking, shear strains are crucial for the inducement of particle crushing.

### 2.6.4.3 Failure line

After the initial linear behaviour, which is typical for non-crushable soils, the $M'$-value starts to decrease due to the grading changes. Interestingly, the grading that was initially closest to the ultimate grading has the highest internal friction angle. During crushing the maximal grain size remains more or less constant while the grading curve rotates around the point $F_V(d_{max}) = 1.0$. Since the internal friction angle reduces with crushing this suggests that the most uniform grading at the same maximal grain size would have the lowest internal friction angle. In case of this research the most uniformly graded sample has on the contrary the highest internal friction angle. This shows the influence of maximal grain size on the internal friction angle. By increasing the size of the maximal grain the whole distribution shifts to the right the graph in Figure 6.12 b) where an angle of repose is shown by fraction size. Based on this results it is possible to assume that the angularity of grains increases with fraction size
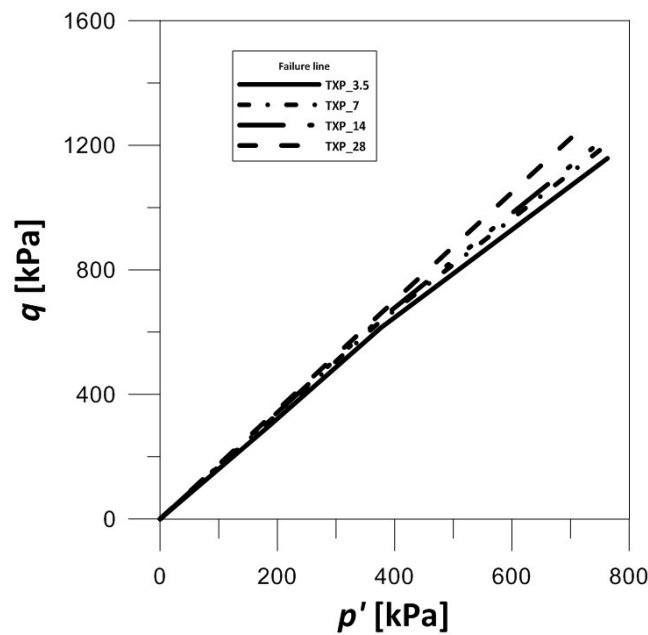
**Slika 2.29: Porušna ovojnica za TXP**

**Figure 2.29: Failure line for TXP**



a)                                          b)
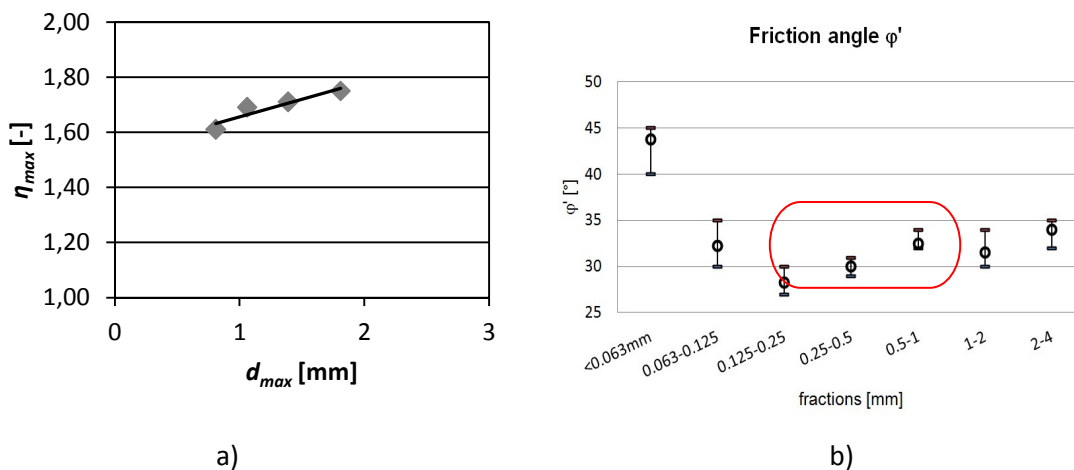
**Slika 2.30: a) $\eta_{max}$ kot funkcija velikosti maksimalnega zrnja, b) Nasipni kot po frakcijah (Wanninger, 2010)**

**Figure 2.30: a) $\eta_{max}$ as a function of maximal grain size, b) Friction angle by fractions (Wanninger, 2010)**

The failure line should consist of three parts. The first part would represent the friction angle that depends on the initial grading and would represent the failure line below the pressure at which the soil starts to crush. The last part of the failure line would again be linear and it's steepness should be defined by internal friction angle of ultimate grading with fractal dimension of around 2.39. While the middle section should be represented by a nonlinear function that would depend on the relative crushing index. Since the crushing potential diminishes with increasing crushing, the rate of changing the friction angle should be somehow logarithmic. A rough estimation would be to say that the reduction of friction angle changes in the same way as the relative crushing. In other words, the changing of friction angle would be described with the same function as the relative crushing, but the

values of the function should be for the pressures between the $p'_{br\_start}$ and $p'_{\mathrm{br\_stop}}$ between 0 and 1. $p'_{br\_start}$ is the minimal mean effective stress that causes particle crushing and $p'_{\mathrm{br\_stop}}$ the mean effective stress at which the ultimate grading is reached during loading.

## 2.7  Result comparison

In previous section the characteristic features of each stress path and its results were presented. Already such results have shown some interesting facts about sand crushing and its mechanical behaviour. But in order to have a more complete picture of how stress path influences crushing a comparison between the results from different tests is required. The results of such complete analysis are described in this section. First the analysis is strictly concentrated on grain crushing and later on the mechanical behaviour of crushable soil.

### 2.7.1    Grain crushing

#### 2.7.1.1  Determination of effective parameters:

Grain crushing, in other words, changing of GSD greatly influences the behaviour of crushable soil. For this reason a complete understanding of crushing is crucial before someone tries to understand its influence on mechanical behaviour. Therefore, here the parameters that appear to influence grain crushing will be highlighted.

In the previous section it was already shown that isotropic compression does not cause crushing, while samples exposed to the axial compression with constant mean effective stress experienced a great amount of crushing. In order to see how the stress path or the ratio $q/p'$ affects the crushing, the results for different tests are compared at this stage. The basic behaviour of crushing can easily be shown by comparing the cumulative grain size distribution before and after the test for different stress paths and different initial coefficients of uniformity.
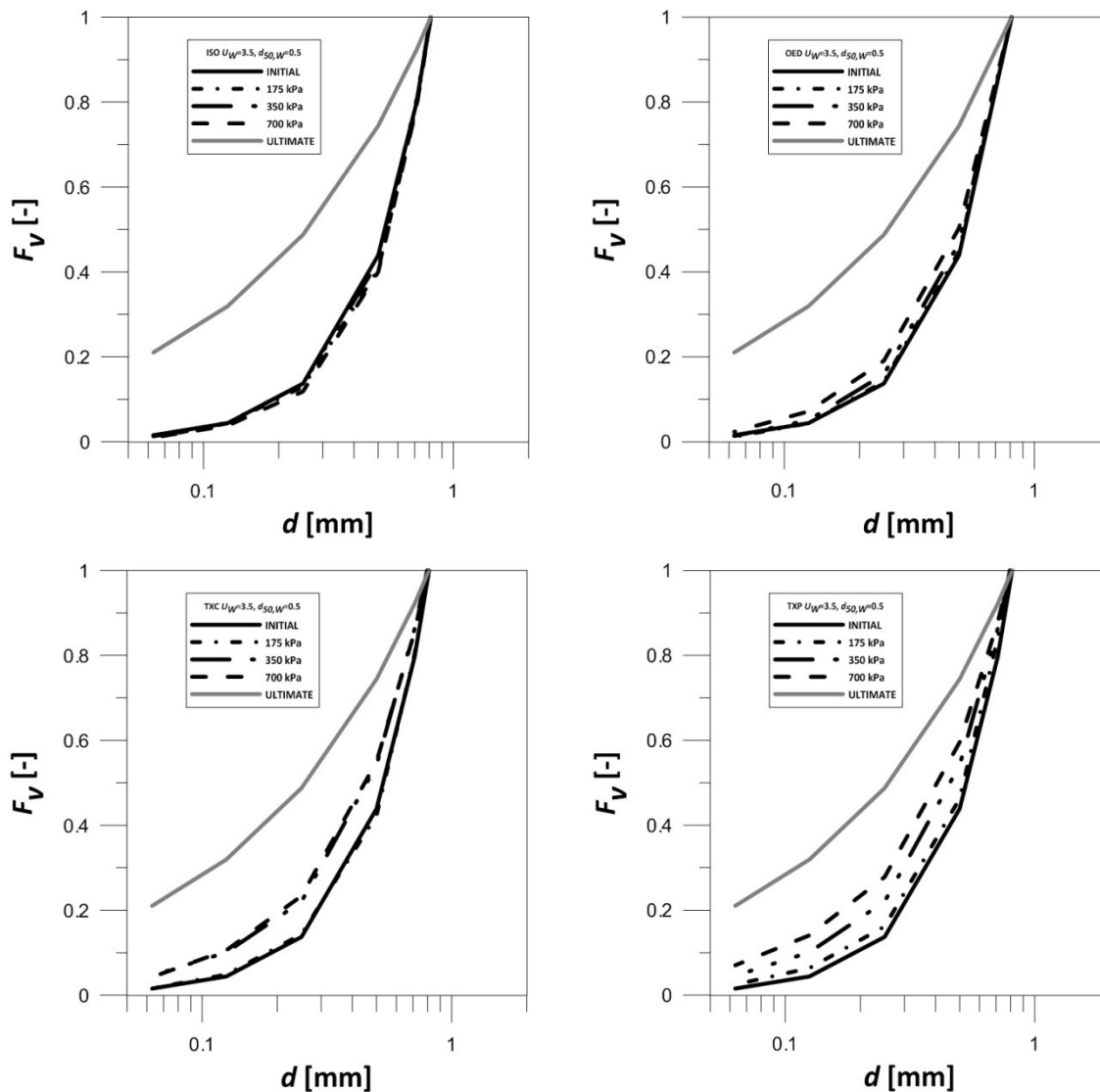
**Slika 2.31: Zrnavostne krivulje vzorcev po opravljenih testih**

**Figure 2.31: Grain size distributions after the tests**

The tests were planned in such a way that final confining pressures would be approximately the same for all types of tests. This way the influence of the deviatoric stress can be distinguished. The fact that at isotropic stress state the samples experience no crushing while for the oedometric and the triaxial compression tests (TXC,TXP) the samples undergo a certain amount of crushing shows that the deviatoric stresses and shear strains play important role in grain crushing. But, indeed the mean effective stress is of great importance as well since it represents a sort of a potential for grain crushing. Even though during the isotropic compression there is no crushing, mean effective stress plays an important role since it increases the energy needed for grains to overcome each other. But, since for low strength aggregate it is easier to crush than to overcome another grain, at high confining pressure such sand experiences more crushing. In order to simplify the comparison for different stress paths at the same mean effective stress the obliquity $\eta = q/p'$, defined as the ratio between the deviatoric

stress and the mean effective stress, was introduced. The values of $\eta$ at sample failure are very similar for the TXC and TXP tests (Figure 2.32) yet, still the amount of crushing is considerably higher for the test with constant mean effective stress. This points to the fact that it is not only final ratio of $q/p'$ affects the total amount of crushing but also the way this maximal ratio is reached.
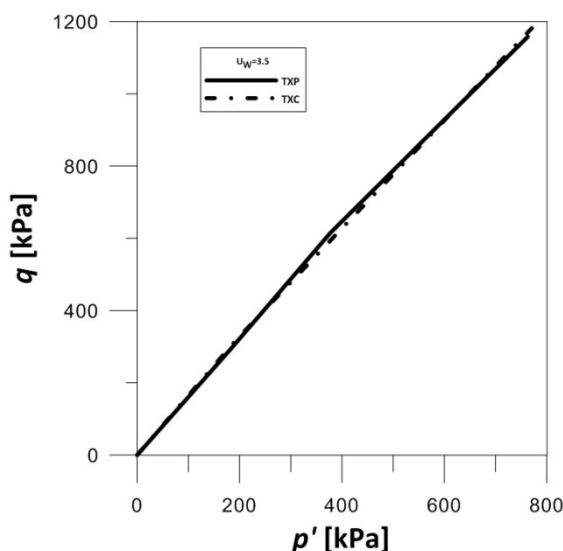


**Slika 2.32: Primerjava porušne ovojnice za testa TXP in TXC**

**Figure 2.32: A comparison of the TXP and the TXC failure line**

The three parameters that affect crushing:

- deviatoric stresses,
- coordination number,
- confining pressure

need to all act at once. For example, the void ratio during the isotropic compression is higher than during the axial compression with constant mean effective stress which means that the coordination number is lower than during the shearing (TXP). But, there are no shear strains, therefore grain crushing is negligible. Also if grain size distribution is very close to the ultimate grading (high coordination number) during shearing at high mean effective stress, the grading will not change drastically.

From Hardin's list of the effective parameters only stress path, the void ratio and the grain size distribution differ for the two (TXC, TXP) tests. Unlike for overconsolidated soils the void ratio directly depends on the stresspath in samples that are loosely reconstituted. For grain crushing it is widely accepted that it depends on the coordination number and grain stress distribution. Since both the void ratio and grain size distribution either directly or indirectly depend on the stress path, it is possible to single out the one main parameter that leads the behaviour of crushable soil. A parameter

defining a stress path should, therefore, be used for modeling the relation between the crushing and the expected loading of soil.

### 2.7.1.2  Influence of crushing potential (initial coefficient of uniformity):

In the last section the influence of the stress path is compared for samples with constant initial grading, while in this section the influence of parameter $U$ is studied for different stress paths. The research discussed in this thesis is based on the assumption of fractal ultimate grading. Crushing potential is defined as an area between the inital grading and the ultimate fractal grading.

Comparing the relative crushing for samples with different crushing potentials, the theory stating that samples with a higher crushing potential will experience more crushing is proven. Grains in samples with more uniformly graded distribution are more uniformly loaded than grains in single grain size distribution and, therefore, subjected to less crushing. Below, the results of the different tests are shown comparing the crushing for different inital $U$-values:
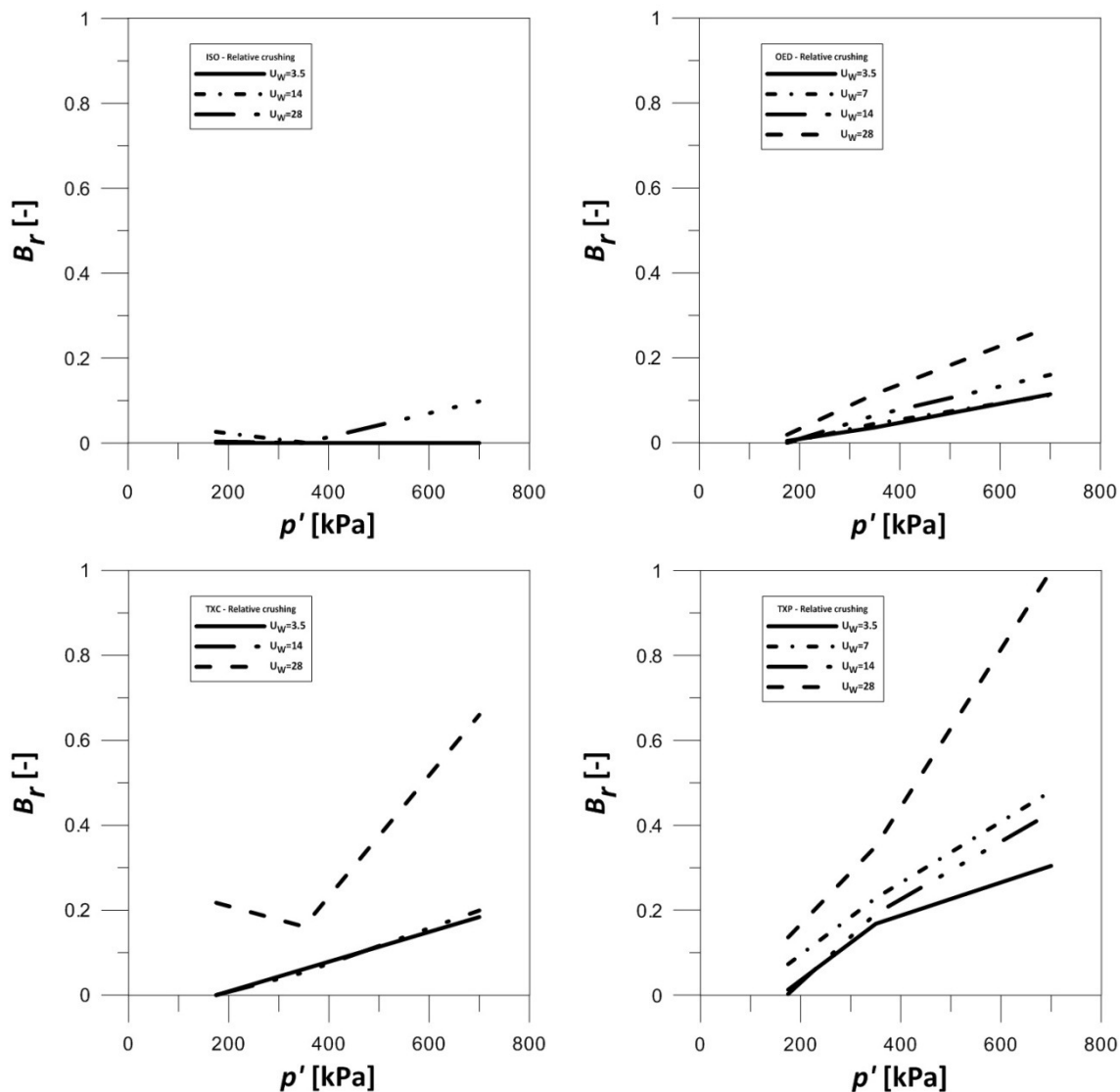
**Slika 2.33: Zrnavostne strukture po končanem preskusu za različne napetostne poti**

**Figure 2.33: Grain size distributions after the test for different stress paths**

If the results for distribution with $U_W$=28 are neglected, it is possible to see that crushing is indeed influenced by the initial crushing potential. For each stress path an average value is evaluated at each mean effective stress. The result of this averaging are the graphs showed in the Figure 2.34.
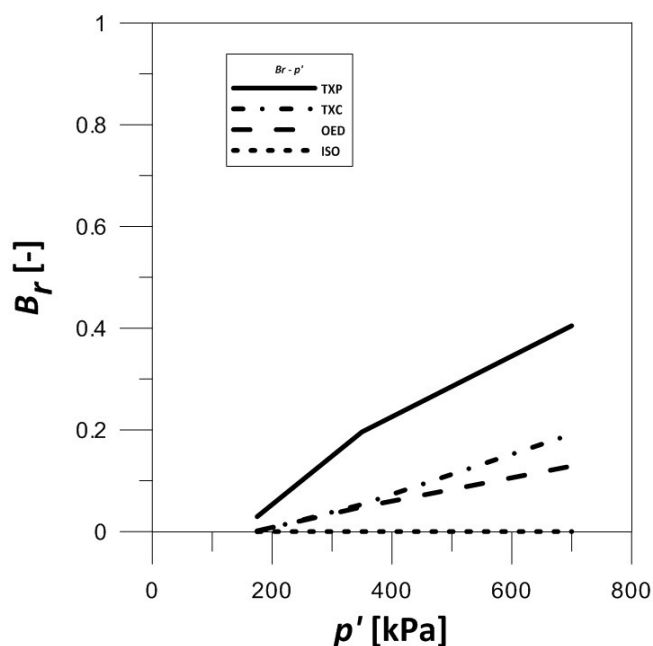
**Slika 2.34: Primerjava relativnega drobljenja kot funkcija napetostne poti in končne srednje efektivne napetosti**

**Figure 2.34: Comparison of relative crushing as a function of stress path and the final mean effective stress**

The graph shows a nice correlation between the stress path and the relative crushing, except that the trends of increasing crushing are very similar for the TXC and OED tests. The explanation lies in sample shape. For the oedometer the ratio between the surface and the volume is twice as high as for the triaxial cell due to its low height compared to the diameter.

**Table 2.7: Comparison of surface to volume ratio of the sample for oedometer and triaxial cell**

**Preglednica 2.7: Primerjava razmerja med površino in prostornino vzorca za oedometer in triosno celico**

| Apparatus | H [cm] | D [cm] | V [cm$^3$] | S [cm$^2$] | S/V [1/cm] | Ratio [OED/TXC] |
|---|---|---|---|---|---|---|
| Triaxial cell | 11.28 | 5.64 | 281.81 | 249.83 | 0.89 | 1.95 |
| Oedometer | 1.72 | 7.14 | 68.67 | 118.48 | 1.73 | |

The problem is that the outer grains of the sample next to the boundary have much lower coordination number due to the presence of the wall on one side. Marketos (2010) has stated that the region adjacent to the boundaries, non-representative of far-field material behaviour, will affect the behaviour of a granular sample in the DEM or laboratory tests. With local porosity differences leading to a change in the transport properties of the sample, and force distribution changes leading to a bias in the location of grain cracking or crushing events for sufficiently high stress levels.

Likar, Ž. 2012. Effects of stress path and grain size distribution on mechanical behaviour of crushable granular material
Grad. Th. – University Studies. Ljubljana, UL FGG, Department of Civil Eng.

49
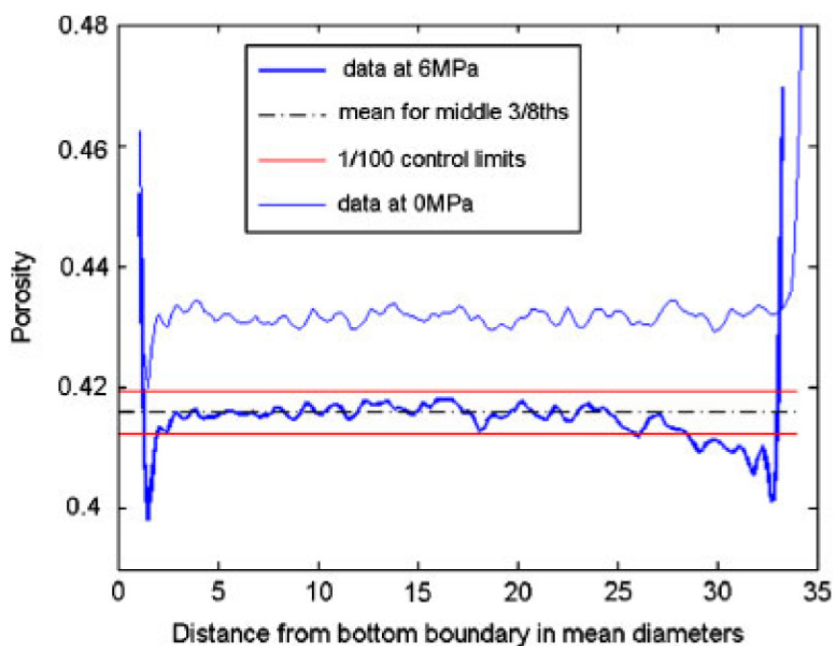
**Slika 2.35: Količnik por za 10 vodoravnih prerezov v odvisnosti od oddaljenosti od spodnjega roba pri srednji efektivni napetosti 6 MPa (Marketos, 2010)**

**Figure 2.35: The mean porosity for 10 horizontal slices versus height above the bottom boundary at 6 MPa (Marketos, 2010)**

### 2.7.2 Failure line

The previous section concentrated on the effect of stress path on grain crushing and in Figure 2.34 its affect can be seen. In this section the failure line will be checked for different stress paths. In Figure 2.32 the failure lines for the TXC and TXP tests with initial coefficient of uniformity of 3.5 are very close together. Similar behaviour can be observed for other initial distributions.
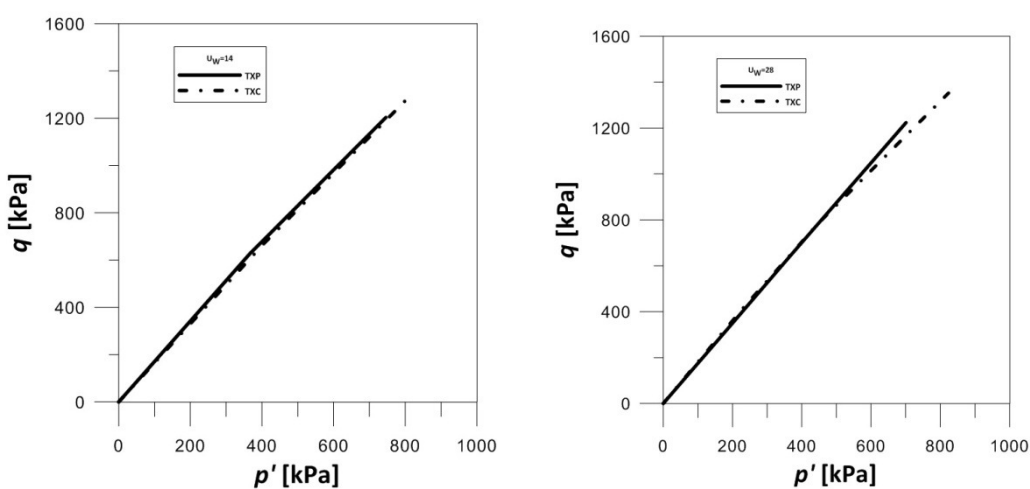


**Slika 2.36: Primerjava porušnih linij testa TXP in TXC pri vzorcih s koeficientom enakomernosti $U_W = 14$ in $U_W = 28$**

**Figure 2.36: Comparison of failure line for tests TXP and TXC for samples with uniformities of $U_W = 14$ and $U_W = 28$**

From all the tests it is possible to distinguish that the friction angle reduces with increasing confining pressure. The surprising fact is that the failure lines of TXC tests are in most cases below the TXP failure line. Table 2.8 presents the values of relative crushing, which show that they are lower for the TXC test. Therefore, the comparison of failure lines for these two different stress paths is even more surprising.

**Table 2.8: A comparison of relative crushing $(B_p)$ for the TXP and TXC tests**

**Preglednica 2.8: Primerjava indeksa relativnega drobljenja $(B_p)$ za preskusa TXP in TXC**

|  | 175,00 | | 350,00 | | 700,00 | |
|---|---|---|---|---|---|---|
|  | TXP | TXC | TXP | TXC | TXP | TXC |
| $U_W = 3.5, \ d_{50,W} = 0.5$ | 0,01 | 0,00 | 0,17 | / | 0,30 | 0,18 |
| $U_W = 7, \ d_{50,W} = 0.5$ | 0,07 | / | 0,23 | / | 0,48 | / |
| $U_W = 14, \ d_{50,W} = 0.5$ | 0,00 | 0,00 | 0,19 | 0,05 | 0,43 | 0,20 |
| $U_W = 28, \ d_{50,W} = 0.5$ | 0,14 | 0,22 | 0,35 | 0,16 | 1,00 | 0,66 |

One possible explanation would be that the friction angle increases for smaller grain size fractions of LECA material and therefore the friction angle of a sample does not reduce with increasing crushing but this would be in contradiction with the reduction of $M'$ value for higher confining pressures where samples experience more crushing. At this stage it is important to note that the $M'$-values previously related to the term *at failure* are maximal values and further changes are expected with increasing shear strains until reaching the actual critical state due to the fact showed in section 2.6.4.2

## 2.8  Failure model

Sand and gravel are often used in engineering structures such as dams, road tampon, railway ballast. Also the interaction between sand material and engineering structures is considered on daily basis, for example driven piles in sandy soil, compacted backfill behind the retaining walls. In order to be able to predict the behaviour of these structures the behaviour of soils used in these structures needs to be thoroughly investigated. Detailed understanding of such behaviour and its effects are crucial for prediction of the behaviour of such structures. But in order to apply the knowledge learned during the research to the design of engineering structures a model describing the behaviour of material used is needed.

In this research sand grain crushing was taken under consideration. In the previous section it has been analysed how the grading changes for different stress paths, confining pressures, initial grain size distributions affect the failure criterion. All of the new knowledge gained through the investigation has been used in the derivation of a simple model describing the grading changes and a stress ratio $q/p'$ at failure depending on the stress path and initial grain size distribution. The main aim of the model is to be able to determine the stress ratio at failure and to predict the grading at failure. It was also endeavoured to be set in a way that would also describe the physical reasons behind the grading changes and the changes of the stress ratio at failure.

On the following few pages, the assumptions that represent the basis of the model and the genesis of the model itself are shortly described.

### 2.8.1     Crushing

#### 2.8.1.1  Initial grading and confining pressure

Section 2.7.1.2 shows that the amount of crushing that sample undergoes greatly depends on the initial grading. The more uniformly the sample is graded the more crushing it undergoes. Nevertheless, it has also been shown that this amount of crushing is directly related to the crushing potential. The closer the initial grading is to the ultimate distribution the slower the sample grading changes. The parallelism of the curves for different intial grading describing the crushing relativelly to confining pressure in Figure 2.33 suggests that a unique function describing the grading changes can be implemented into the model under construction.

The relative crushing index is defined as:

$$B_r = \frac{A - A_0}{A_u - A_0} \tag{2-35}$$

Where the denominator represents the crushing potential and the numerator the total crushing that the sample has undergone. This index was used to quantify the amount of crushing from initial stress

conditions until sample failure (TXC, TXP) or until a certain mean effective stress has been reached. But it can also be used to determine the amount of crushing between any two points on the loading path. Table 2.5 also shows that the ultimate distribution by volume tends to be fractal with the fractal dimension of 2.39. As the sample undergoes grain crushing the area under the graph increases while the area under the graph of the ultimate grading remains constant. Therefore the crushing potential diminishes as the grading changes. From the fact that the rate of crushing diminishes by decreasing the crushing potential because the cushioning effect increases it can be infered that crushing index obeys a function whose gradient diminishes with increasing value on the abscissa. The values of this function should vary from 0 to 1 as the pressure increases from the pressure at which the crushing starts towards the pressure at which the ultimate grading is reached at the sample failure. One of such functions is logarithmic function and it can be described as:

$$y = k \cdot \ln x + n \qquad\qquad (2\text{-}36)$$

Where k indicates the rate at which the value of the function increases with the increasing variable $x$, and $n$ determines the value of $x$ at which the $y$ values start to cover the values greater or equal to zero.

- Variable $x$ will depend on the final mean effective stress and it will define how the amount of crushing will change with increasing mean effective stress at the end of the test;
- parameter $k$ will incorporate the inclination of a stress path into the equation;
- while paramter $n$ will defined by the mean effective stress ($p'_{br\_start}$) at which the grain crushing will begin to take place.
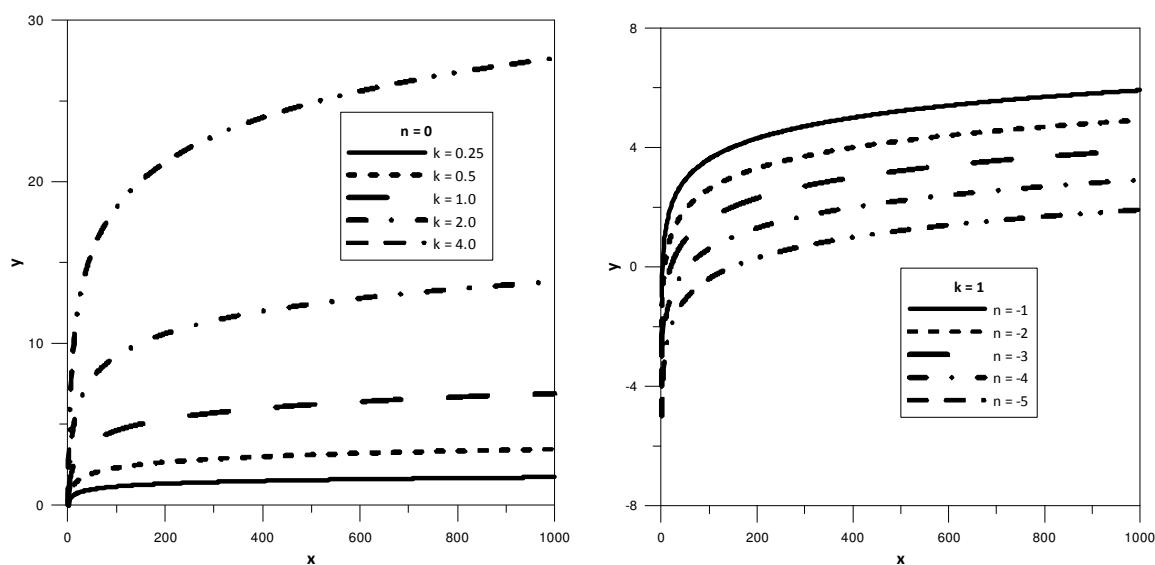


**Slika 2.37: Vpliv parametrov $k$ in $n$ v enačbi (2-36)**

**Figure 2.37: Effect of the $k$ and $n$ parameter in the equation (2-36)**

### 2.8.2    Stress path

The analysis performed on the results of test performed on crushable soil showed that the stress path greatly influences the crushing. Samples loaded with isotropic pressure experience almost no crushing since all of the grains are uniformly loaded and no tensile stresses arise within the grains. In contrast, with increasing deviatoric stress the crushing increases fast. But, the deviatoric stresses showed not to be a single parameter causing crushing since it was showed that it is indeed important the way this deviatoric stress has been reached. For example, the mean effective stress changes during the test, in most cases, and the way this stress changes greatly influences the sample void ratio and also the grain interlocking. Therefore, the parameters considering the complete stress path need to be introduced. One of the parameters is defenitely the final confining pressure since as shown in section 2.6.4.2 it represents a sort of crushing potential. For lower stresses, the grading will never reach the ultimate grading with fractal distribution of 2.39.  Another parameter needs to take into consideration the effect of different stress paths on the rate of crushing. Such parameter should consider complete stress path not only the final stress conditions.
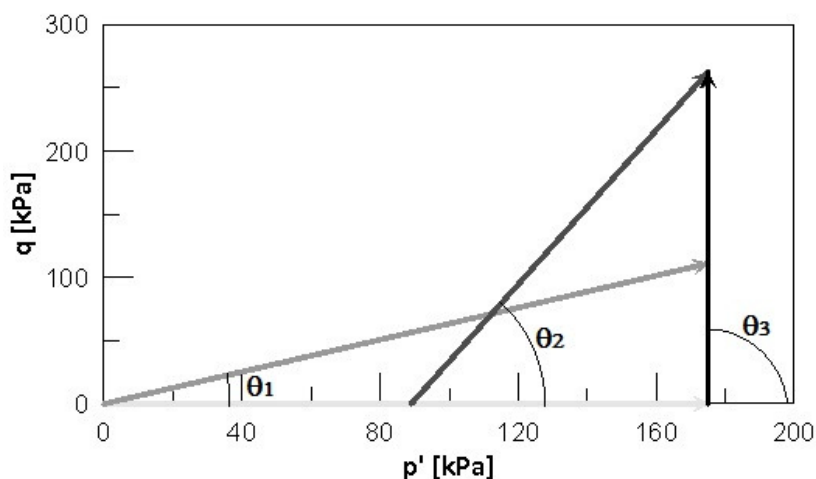


**Slika 2.38: Definicija naklona napetostne poti $\theta$**

**Figure 2.38: The definition of inclination of a stress path $\theta$**

Since all of the stress paths chosen for this research circumscribe linear function in the $q:p'$ plane, an inclination of a stress path ($\theta$) at which the deviator increases with increasing mean effective stress has been chosen as a parameter. This parameter is not suitable for stress paths such as the undrained conventional triaxial test, where the stress path is a non-linear function. Nevertheless, each stress path can be approximated with a linear function.
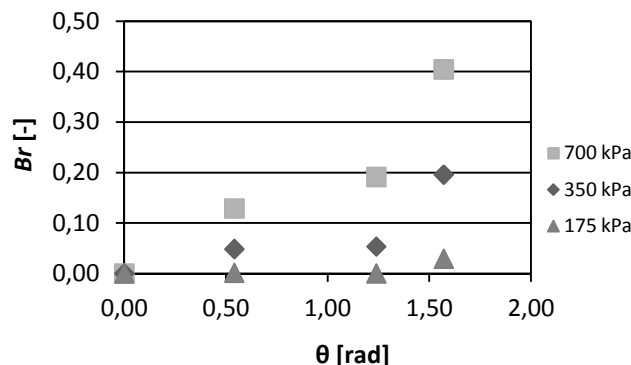
**Slika 2.39: Relativno drobljenje kot funkcija naklona napetostne poti v ravnini $q$: $p'$**

**Figure 2.39: Relative crushing as a function of stress path inclination in $q$: $p'$ plane**

The inclination of stress path determines the rate at which the crushing increases, so its influence should be incorporated in the parameter $k$ in the equation (2-36), while the parameter $n$ is determined based on the stress at which the grains start to crush.

$$B_r = k(\theta) \cdot \ln[f(p')] + n(p'_{br\_start}) \tag{2-37}$$

### 2.8.2.1 Coefficients $k$ and $n$

Since the angle of the stress path does not directly define the rate of increasing crushing it needs to be corrected in order to better fit the behaviour. By trial and error it was found that the equation best describes the behaviour of relative crushing function when the angle of the stress path is divided with the angle describing the full circle, that is $2\pi$. In order to assure that the equation will be dimensionally correct the term within the natural logarithm needs to be divided by $p' = 1 kPa$.

$$k = \frac{\theta}{2\pi} \tag{2-38}$$

The parameter $n$ is determined so that the equation satisfies the boundary condition which is that at pressure $p'_{br\_start}$ the crushing is equal to zero:

$$n = B_r(p'_{br\_start}) - \frac{\theta}{2\pi} \cdot \ln \frac{p'_{br\_start}}{1kPa}; \quad B_r(p'_{br\_start}) = 0 \tag{2-39}$$

$$n = -\frac{\theta}{2\pi} \cdot \ln \frac{p'_{br\_start}}{1kPa} \tag{2-40}$$

### 2.8.2.2 $p'_{br\_start}$

In order to completely determine the grain crushing a determination of $p'_{br\_start}$ is needed. $p'_{br\_start}$ is the lowest pressure at the end of stress path (Figure 2.40) at which grains in sample start to crush. It

is obvious that this pressure depends on grain strength since for harder grains higher pressure needs to be imposed for them to crush.
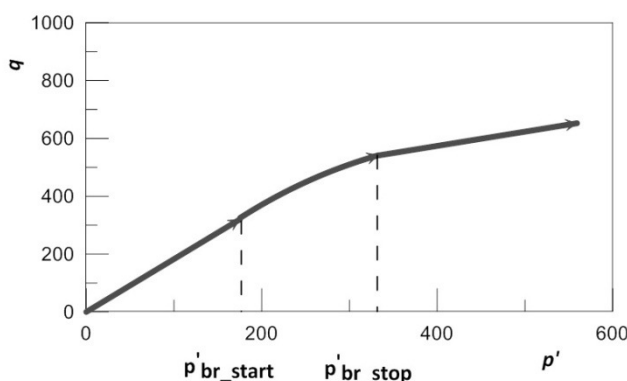


Slika 2.40: Definicija srednjega efektivnega tlaka p′$_{br\_start}$ in p′$_{br\_stop}$

Figure 2.40: Definition of mean effective pressure p′$_{br\_start}$ and p′$_{br\_stop}$

Analogically to the amount of crushing for different stress paths discussed in 2.7.1.2  it is logical to expect that $p'_{br\_start}$ will also differ for different stress paths. Therefore, the amount of crushing has been extrapolated for each stress path in order to determine the pressure at which the amount of crushing is zero. The pressures obtained with extrapolation are presented in the table below.

Table 2.9: $p'_{br\_start}$ for LECA for different stress paths

Preglednica 2.9: $p'_{br\_start}$ za različne napetostne poti pri uporabljenemu materialu (LECA)

| ISO | / |
|-----|-----|
| OED | 190,91 kPa |
| TXC | 192,49 kPa |
| TXP | 128,80 kPa |

Similarly as for higher pressures the pressure at which grains start to crush decreases for stress paths with higher deviatoric stresses. The reason for similar TXC and OED values has already been presented in section 2.7.1.2. A proper way of determining a $p'_{br\_start}$ would be to relate its calculation to the grain strength so it could be used for sand material with different strengths. However, such information was not available in this research and should be investigated in further research.

### 2.8.2.3  Different point of view of the influence of relative breakage index

Another and more physical way to look at the equation (2-37) would be, that for lower mean effective stress the crushing potential is reduced. At lower stresses, the final grading will never reach the ultimate distribution with fractal dimension of 2.39. Therefore, the crushing potential calculated with $A_u$ as an area under the grain size distribution of forementioned ultimate distribution shuld be reduced.

The function describing the crushing index is defined so that crushing index covers the values between 0 and 1. Now, there are two ways of calculating the crushing index:

$$B_r = \frac{A - A_0}{A_u - A_0}$$
(2-41)

A – Area under current grain size distribution graph

$A_0$ – Area under initial grain size distribution graph

$A_u$ – Area under ultimate grain size distribution graph

and

$$B_r = k(\theta) \cdot \ln[f(p')] + n(p'_{br\_start})$$
(2-42)

Since the latter function covers the values between 0 and 1 a crushing potential can be calculated as:

$$A_p = B_r \cdot (A_u - A_0) + A_0$$
(2-43)

If we look at this equation in such a way, the sample at failure will with certain pressure experience the amount of crushing so that the total crushing at failure will be equal to the crushing potential at the beginning of the test.
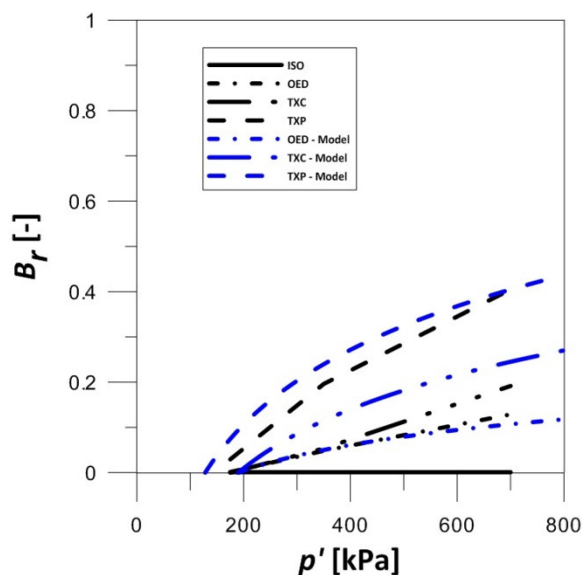


**Slika 2.41: Primerjava rezultatov laboratorijskih testov z modelom**

**Figure 2.41: Comparison of laboratory tests with model results**

## 2.8.3    Failure criterion

An essence of critical state soil mechanics is that the critical state does not depend on the loading history but it is rather a material parameter. This means that for the same type of material the critical state line depends solely on the soil grading. For soils with high grain strength the grading does not change when loaded. Therefore, the critical state can be described with a linear function that has the only parameter the mean effective stress. When a crushable soil is considered it is reasonable to expect that the critical state will not be defined with a linear function since the grading changes when the soil is exposed to certain loading. Still, its behaviour at critical state and in case of normally consolidated soils also at failure is assumed to depend solely on the grading. At first sight it seems odd to distinguish between the failure and the critical state for normally consolidated soils, but as shown in section 2.6.4.2 there are still volumetric changes for crushable sand at failure. These volumetric changes suggest that the grading will further change with increasing shear deformations and so the deviatoric pressure will either increase or decrease depending on the angularity of different grain sizes.

In order to keep the model simple at this stage a presumption that the $q/p'$ ratio at failure changes according to the same function as the grain size distribution is applied. There are two boundary conditions that the criterion describing the failure line needs to fulfill:

- For low confining pressures where the grading does not change the ratio $\eta_{max} = q/p'$ at failure is constant.
- At high confining pressures the grading at failure reaches the ultimate grading and therefore the $\eta_{max}$ value is again constant for very high pressures.

An example of a function describing these characteristics is:

- $\eta_{max} = \eta^I_{max}$   $for$   $p' < p'_{br\_start}$
- $\eta_{max}(p', \theta) = \eta^I_{max} + (\eta^F_{max} - \eta^I_{max}) \cdot Br(p', \theta)$
  $\rightarrow$ $for$   $p'_{br_{start}} \leq p' \leq p'_{br_{stop}}$                                    (2-44)
- $\eta_{max} = \eta^I_{max}$   $for$   $p'_{br\_stop} < p'$

$\eta_{max}(p', \theta) - q/p'$ ratio at failure for $p'_{br\_start} < p' < p'_{br\_stop}$

$\eta^I_{max} - q/p'$ ratio at failure for $p' < p'_{br\_start}$

$\eta^F_{max} - q/p'$ ratio at failure for $p' > p'_{br\_stop}$

Figure 2.25 shows that for a uniformly distributed grading at high pressure the maximal grain size also decreases. Since this effect is very small for the pressures considered it was decided to not include this effect on the reduction of $\eta_{max}$.

## 3    COMPUTER MODELLING

In order to complete the puzzle of describing the material behaviour, scientists use a variety of different approaches. A certain approach helps you put together a certain part of that puzzle. Trying to increase the understanding of grain crushing and its effect on the soil behaviour in this research two different approaches have been incorporated.

The first part of the thesis presents the laboratory testings and the results are analysed in detail. A triaxial apparatus is an excellent device, allowing the performance of a broad variety of different tests. Being able to reproduce different stress states, stress paths, etc. and being able to record the parameters describing the soil response helps gain a deeper understanding of soil behaviour and its macro properties. In spite of its great capabilities mentioned above, it does not offer any information on the micro properties of soil, on the grain size distribution or the grain loading during the test whatsoever.

In cases like this, numerical methods are a very helpful tool. They allow the researcher to reproduce the tests performed in a laboratory and gain further understanding by being able to, theoretically, track the behaviour of every single grain in the sample at any stage of the test. Despite the many advantages numerical methods offer, they also have their disadvantages. The main disadvantage is that the sample reproduced in a computer program is still just a model that is simplified to lesser or greater extent. Therefore, great care must be taken while setting up the model to incorporate all the important physical parameters.

Trying to improve the understanding on grain crushing a model based on numerical methods, particularly the distinct element method (DEM) was incorporated in this research. In DEM material is modelled with large number of small spherical particles. Every calculation step a dynamic equation is solved for every single particle. These spherical particles interact with each other through the contacts, where based on the ovelaps the contact forces are calculated. To broaden the applicability of the method bonds at particle contact can also be applied. This way rock material can be modelled as well as different object shapes can be applied.

The samples were reproduced in a program known under the commercial name Particle Flow Code 3D (PFC3D). The capabilities of the program were studied and different approaches of modelling crushable soil analysed. Based on this analysis, the approach believed to be most suitable to describe grain crushing was chosen to prepare a model, which was developed together with algorithms for the measurement of different parameters.

## 3.1 The advantages and disadvantages of numerical modelling using PFC3D

Investigating natural phenomena it is always attempted to mathematically describe the phenomena in order to be able to reproduce the results and, especially in engineering practice, to foresee the behaviour of materials, machines and structures, etc.. Instead of constructing buildings by trial and error, structures can be designed and optimized before the actual construction. In this way the duration of the whole construction process and the cost of the project are reduced. A lot of phenomena can be described analytically so the behaviour can be precisely described. Nevertheless, models based on analytical equations are usually only able to describe simple behaviour and only include a small range of influential parameters. When trying to describe more complicated behaviour a wide variety of parameters needs to be included and analytical modelling becomes impossible. To overcome this issue scientist have tried to find numerical solutions that produce a limited number of outcome values. With a development of computer efficiency solutions to more and more complicated phenomena using numerical methods could be found.

When modelling behaviour of different materials, structures, machines… using such methods it is important to be aware of its capabilities and limitations. For the purpose of this research a program PFC3D was used. The main advantage of this program is that instead of a wide variety of predefined commands a programming language called FISH is integrated. Therefore, it is suitable for all the situations that users come across while the accuracy of the model depends on user's needs and knowledge. As most computer programs, it allows you to track the behaviour of your model at any time during the test and at any distinct element of your model. The user can predefine an algorithm that will carry out measurements of just about any physical quantity during the test. Unlike in the laboratory, where each measuring device with its stiffness to smaller or greater extent affects the stiffness and degrees of freedom of a sample, here an endless amount of parameters can be tracked during the test with no effect on the test results. The amount of measurements carried out during the calculation affect the calculation time. But, as it was observed for the PCF3D, if a good algorithm is prepared the measurements have a negligible effect on the increase of the calculation time.

Despite all the capabilities of such program, the calculation cycle is still quite computationally intensive and in order to achieve a reasonable calculation time the model needs to be truncated to a certain extent. Therefore, when preparing a model great care needs to be taken to include all of the parameters that influence the behaviour under investigation. It is equally important to be aware of the drawbacks of neglecting certain parameters. Another limitation is the accuracy of the input material properties modelled in a program. Although, the calculation of a material response that was incorporated in the model can be very precise, it is crucial to accurately determine this parameters in laboratory tests to be sure that the response of the model will describe the actual behaviour.

Assuming that the input parameters obtained from the laboratory tests are accurate the biggest limitation of model accuracy is the number of particles used. For the numerical model based on the distinct element method accuracy of the model increases with the number of particles that compose it. But, the efficiency of the computer limits the amount of particles integrated. To avoid this drawback different by-passes have been incorporated in models. For example, a periodic boundary reduces the number of particles needed to compose the model by modelling two linked boundaries. The particles at one boundary actually act on the particles on the second boundary as shown in Figure 3.1.
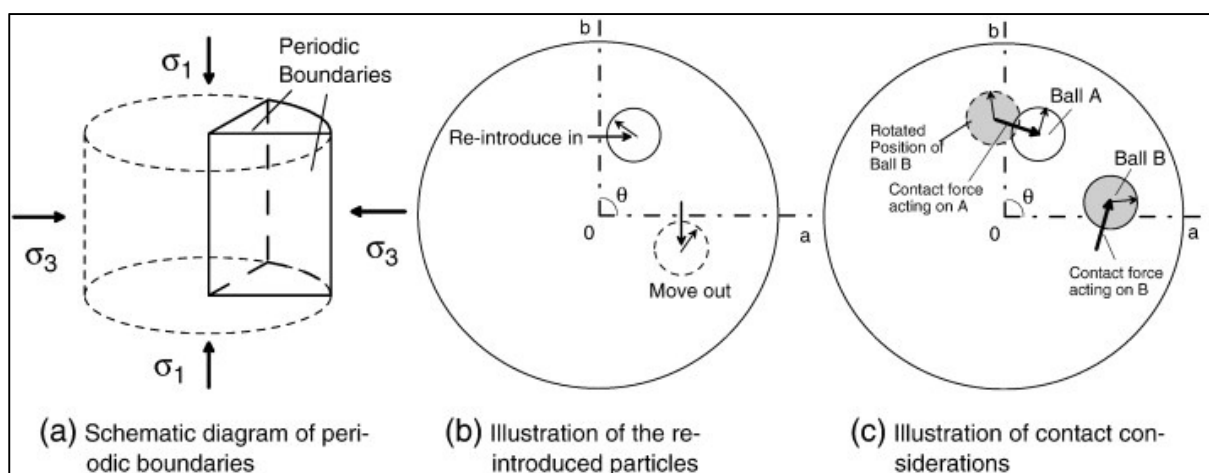


**Slika 3.1: Periodični robni pogoji (Cui, O'Sulivan, O'Neil, 2007)**

**Figure 3.1: Periodic boundary conditions (Cui, O'Sulivan, O'Neil, 2007)**

Nevertheless, such modelling is beyond the scope of this research and it was decided to limit the boundary model to a simple wall model described in section 3.5.1.

## 3.2  Scope of research for computer modelled tests

The first goal of this research is to analyse different types of modelling grain crushing and determine the advantages and disadvantages for each approach. Next, for the most appropriate approach to serve the task in this research a model was developed together with all the measurements. To distinguish the influential parameters affecting the sample behaviour simplified models were prepared and tested. With these simplified models the critical values of influential parameters were determined below which parameter values start to affect the test results. For the case where parameter values needed to be lower than critical ones, their effect on sample behaviour was determined. At the end, the model was tested, the results were shortly analysed and the possible improvements were established.

### 3.3 DEM in PFC3D

### 3.3.1     Basic Principles

The DEM is based on the interaction of distinct particles that can move independently of one another. The interaction of particles is treated as a dynamic process where Newton's second law of motion is satisfied at every calculation step. Before the law of motion equation is solved, the algorithm checks the external forces acting upon each particle. There are two types of forces that can act on each particle. The first types of force are gravitational forces that are constant at every step for a particular particle. The next group of forces are contact forces that are being calculated every step from the overlap of the two neighbouring particles using a force-displacement law. In other words, the DEM implemented in PFC3D uses a soft contact approach, in which a finite normal stiffness is taken to represent the measurable stiffness at each contact. Another important feature of this program is a time stepping algorithm that presumes a constant value for accelerations and velocities within each step. Since this is quite a harsh simplification, it is important to adjust the time step length so that the error due to this simplification is negligible. All of the main features listed above and their implementation within the program code are here explained in more detail.

**Fundamental assumptions**

- Particles are treated as rigid bodies.
- Contacts occur at a point. The calculation is done with contact forces rather than stresses.
- Contact behaviour uses the soft-contact approach (particles can overlap one another at contacts)
- All elementary particles are spherical (they can be connected into various shapes with bonds)
- Contact forces are calculated from the overlaps of the particles. Overlaps are small in relation to the particle sizes.

### 3.3.1.1 Calculation cycle

The calculation cycle implemented in PFC3D consist of four major steps:

(i)     At the beginning of each cycle the position of particles and walls is updated. Consequently the locations of contacts and the sizes of the overlaps are determined.

(ii)     Based on the overlaps, the contact forces are calculated from the force-displacement law.

(iii)     The contact forces are applied to each particle.

(iv)     Newton's law of motion is applied to each particle and the new velocity vector and position is calculated. At this stage the new wall location is calculated based on the user-defined wall velocity (Law of motion is not applied to walls).
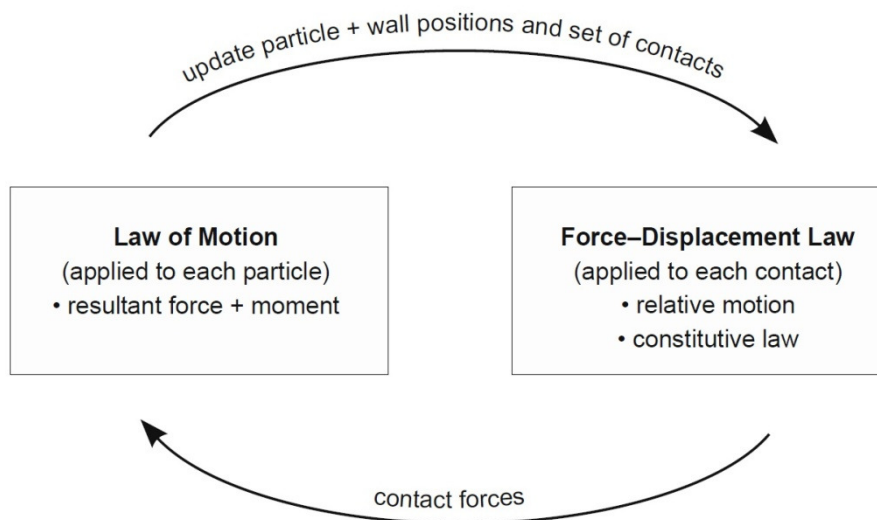
**Slika 3.2: Zaporedje računskih korakov (Itasca group, 2004)**

**Figure 3.2: Calculation cycle (Itasca group, 2004)**

### 3.3.1.2 Force-Displacement Law:

The contact model used for this simulation is rather simple. The contacts are modelled as a linear springs with contact stiffness $k_n$ (normal) and $k_s$ (shear). When the distance between two particles is smaller or equal to the sum of their radii, a contact is formed on the line connecting the particle centres. Because the overlapping of particles is allowed, the location of the contact point is defined in a way that the distances between the contact point and the centre points of the two particles in contact have the same ratio as the ball radii of the touching particles. When particles move closer together, the overlap in normal direction is calculated from the equation:

$$U^n = R^{[A]} + R^{[B]} - d \tag{3-1}$$

$$d = \sqrt{\left(x^{[B]} - x^{[A]}\right) \cdot \left(x^{[B]} - x^{[A]}\right)} \tag{3-2}$$

Where the $\boldsymbol{x}^{[A]}$ and $\boldsymbol{x}^{[B]}$ are the location vectors of the touching balls and the $R^{[A]}$ and $R^{[B]}$ are the ball radii. Analogically, the procedure is adopted to the ball-wall contact except that $d$ is the shortest distance between the ball centre and the wall. When the overlap is calculated the Force-Displacement Law is applied and the normal and shear contact forces are calculated:

$$\boldsymbol{F^n} = K^n \cdot U^n \cdot \boldsymbol{n} \tag{3-3}$$

$\boldsymbol{n}$ is the normal vector pointing from the ball in contact to the currently handled ball. $\boldsymbol{U^n}$ is a normal displacement vector. $K^n$ is a contact stiffness in normal direction that depends on the stiffness of both particles in contact (or particle and wall stiffness) and is calculated as:

$$K^{\vartheta} = \frac{k_{\vartheta}^{[A]} \cdot k_{\vartheta}^{[B]}}{k_{\vartheta}^{[A]} + k_{\vartheta}^{[B]}} \qquad (3\text{-}4)$$

Where $\vartheta$ is $n$ for normal stiffness and $s$ for shear stiffness.

While the calculation of overlapping in normal direction is trivial, the determination of relative motion in shear direction at the contact is not such. For the shear relative motion, first, the velocity of the contact point is calculated separately for each particle. Then, the relative velocity is calculated and a normal component of the velocity is subtracted. At the end, the shear velocity is multiplied with a time step to get a relative shear displacement for the two touching particles.

$$\boldsymbol{V} = \left(\dot{\boldsymbol{x}}^{[C]}\right)_{[B]} - \left(\dot{\boldsymbol{x}}^{[C]}\right)_{[A]} \qquad (3\text{-}5)$$

$$\boldsymbol{V}^s = \boldsymbol{V} - \boldsymbol{V}^n \qquad (3\text{-}6)$$

$$\Delta \boldsymbol{U}^s = \boldsymbol{V}^s \cdot \Delta t \qquad (3\text{-}7)$$

$\boldsymbol{V}$ – contact velocity vector

$\boldsymbol{V}^n, \boldsymbol{V}^s$ – normal and shear component of a contact velocity vector

$\dot{\boldsymbol{x}}^{[C]}$ – translational velocity of the entity (ball, wall)

$\Delta t$ – timestep

$\Delta \boldsymbol{U}^s$ – shear component of the contact displacement-increment vector

While the normal contact force only depends on the relative position of the two entities in contact, the shear normal force depends on the history of loading.

$$\Delta \boldsymbol{F}^s = k_s \cdot \Delta \boldsymbol{U}^s \qquad (3\text{-}8)$$

$$\boldsymbol{F}^s (t + dt) = \boldsymbol{F}^s (t) + \Delta \boldsymbol{F}^s \qquad (3\text{-}9)$$

$k_s$ – contact shear stiffness

$\Delta \boldsymbol{F}^s$ – force-increment vector

### 3.3.1.3 Law of motion:

After the external forces are determined Newton's second law of motion is applied to each particle:

$$\boldsymbol{F} = m \cdot (\ddot{\boldsymbol{x}} - \boldsymbol{g}) \qquad (3\text{-}10)$$

$$\boldsymbol{M} = I \cdot \dot{\boldsymbol{\omega}} \qquad (3\text{-}11)$$

$\ddot{x}, \dot{\omega}$ – longitudinal and angular accelerations at particle's centre of mass

$g$ – gravitational acceleration

$m, I$ – mass and moment of inertia

$F, M$ – resultant force and moment

The equations (3-10) and (3-11) are solved for $\ddot{x}$ and $\dot{\omega}$. From the assumption that the acceleration is constant within each timestep, the final velocity is determined. Analogically, the location vector is determined at the end of the timestep.

### 3.3.1.4 Time step Determination:

Because of the simplification in the dynamic equations, where a constant acceleration for a timestep is presumed, a time step must be determined in a way that assures a stable calculation. A critical time step is determined at the beginning of every cycle as the minimum eigenperiod of the system. For each ball and each degree of freedom a critical time step is determined with an equation:

$$t_{crit} = \sqrt{\frac{m}{k_{tran}}} \qquad (3\text{-}12)$$

$$t_{crit} = \sqrt{\frac{I}{k_{rot}}} \qquad (3\text{-}13)$$

$k_{tran}, k_{rot}$ – translational and rotational stiffness of a particle

The time step chosen for each calculation cycle is a fraction of the smallest critical time step.

### 3.3.1.5 Particle Stress determination:

Since in the PFC3D only contact forces and particle displacements are determined, it is not possible to directly determine the stress distribution within the particle. Therefore stresses need to be averaged over the particle volume. These average stress values within each particle can be determined with the following equation:

$$\bar{\sigma}_{ij} = -\frac{1}{V_p} \cdot \sum_{Nc} x^{(c)} \cdot F^{(c)} \qquad (3\text{-}14)$$

Where $V_p$ is a particle volume, $x^{(c)}$ a location of a contact relative to the centre of the particle, and the $F^{(c)}$ is the force acting at the contact $c$.

### 3.3.2    Contact models

### 3.3.2.1    Slip model

The slip model is, besides the stiffness model, the most fundamental contact model integrated in the program and its behaviour only depends on one parameter, a friction coefficient $\mu$. For this model contact shear strength depends on the magnitude of the stress acting perpendicular to the contact plane. Since for the PFC model contact is only modelled as a single point, another simplification is made where stresses are replaced by forces so that:

$$F_{max}^{s} = \mu \cdot F^{n}$$

(3-15)

When the maximum contact shear strength is reached a constant value of shear force equal to $F_{max}^{s}$ is imposed to the contact. The slip model is assigned to the contact automatically unless one of the following two bond models is assigned to the contact. When the bond strength is exceeded the bond is deleted and the slip model is automatically assigned to the contact again.

### 3.3.2.2  Contact bond model

The simplest of the two bond models is the contact bond model. A characteristic of this model is that two particles are bonded together in a single point (contact). The contact bond model is actually a simple stiffness model that has a defined tensile and shear strength. When the tensile strength is exceeded, the two previously bonded particles separate. When the shear strength of the bond is exceeded, the value of contact shear strength is reduced to the shear strength of a slip model. It is distinct for such model that it can only oppose translation while it has no resistance to rotation. The two parameters that define contact bond are normal and shear strength. The normal and shear stiffness of a contact are defined by the normal and shear stiffness of the two connected particles.
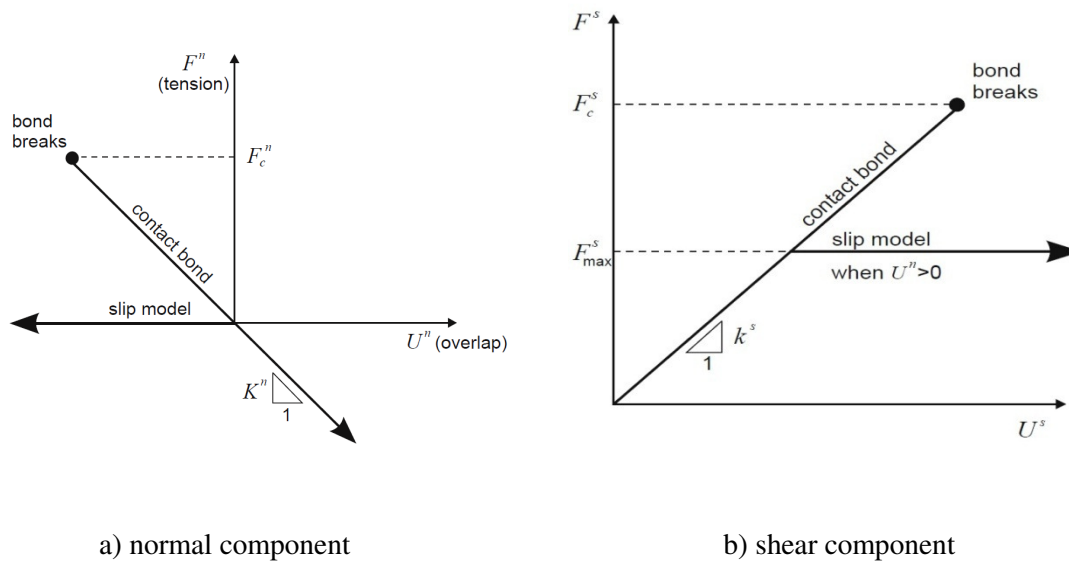
a) normal component                                          b) shear component

**Slika 3.3: Delovanje modela kontaktne vezi in trenjskega kontakta v a) normalni in b) strižni smeri (Itasca group, 2004)**

**Figure 3.3: Behaviour of contact bond and slip model: a) normal component, b) shear component (Itasca group, 2004)**

### 3.3.2.3 Parallel bond model

Unlike the contact bond that connects two particles in a single point, the parallel bond connects particles into a cylindrical shaped bond. That means that it can also resist bending, in other words, it represents a cement material binding of two particles. Due to its complex structure more parameters are needed to determine its behaviour:

- Normal and shear stiffness
- Normal and shear strength
- Bond radius

The parallel bond has its own stiffness that can differ from particle stiffness so the actual contact stiffness depends on both, a particle stiffness and a parallel bond stiffness.
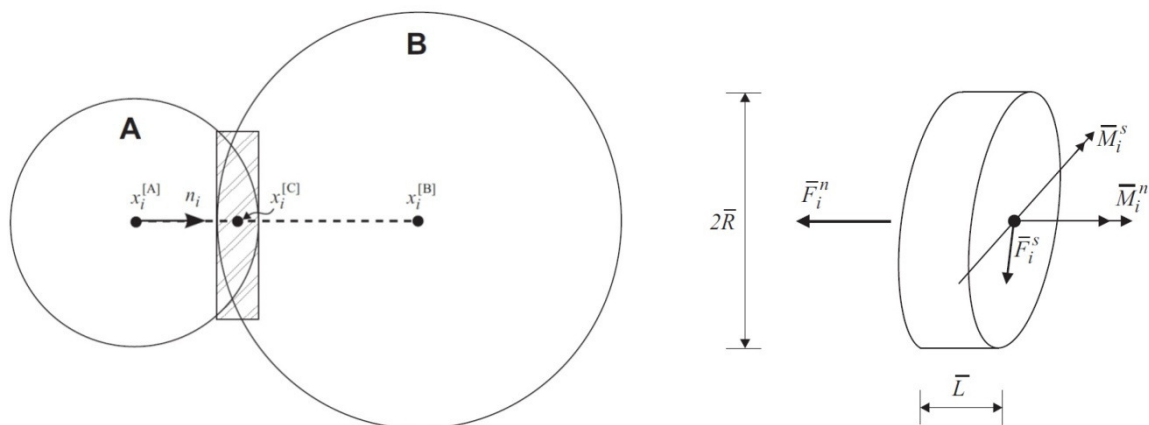
**Slika 3.4: Vzporedna vez in prostostne stopnje na katere vpliva (Itasca group, 2004)**

**Figure 3.4: Parallel bond (Itasca group, 2004)**

$$\sigma_{max} = \frac{-\left|F^n\right|}{A} + \frac{\left|M^s\right|}{I}\bar{R} \tag{3-16}$$

$$\tau_{max} = \frac{-\left|F^s\right|}{A} + \frac{\left|M^n\right|}{J}\bar{R} \tag{3-17}$$

Where $A$ is a parallel bond cross-section, $I$ moment of inertia around the axis perpendicular to the axis linking the particle central points, $J$ moment of inertia around the axis linking the particle central points and $\bar{R}$ parallel bond radius. Another difference between the contact bond and parallel bond is that the parallel bond, because it has its own stiffness, allows particles to separate while the contact bond does not.

Due to its simplicity contact bond does not use much computer memory and, therefore, its application to model does not drastically increase the calculation time. However, this does not apply to the parallel bond. In terms of calculation time the parallel bond can be imagined as another particle bonded to the two neighbouring particles with contact bond. For this *particle* a similar portion of computer memory is required as for the actual ball element and, therefore, drastically influences the computation time.

## 3.4  Breakage modelling types

### 3.4.1     Grain crushing modes and breakage criteria

The behaviour of every soil and its response to the load applied depends on the properties of its constituents. Angularity, texture, size, stiffness, strength are just some of the major grain characteristics that affect the behaviour of the soil constituted of these grains. While it is a common practice to consider the first four characteristics when setting up the model of a soil, the last one is usually neglected since in low stresses and for sands with high grain strength the stresses within each grain are much lower than its strength. When dealing with very high pressures or with low grain

strength this grain characteristic plays a crucial role in the behaviour of such soil. Therefore, the understanding of the conditions under which grain crushing or attrition takes place needs to be acquired prior to modelling such soil. There are three basic crushing modes: tensile splitting, shear failure and abrasion.

### 3.4.1.1  Tensile Splitting

Like the chain ceases to counteract the load when the weakest link fails, it is the same for other materials. For rocks it is known that the tensile strength is the weakest link in the chain when the coordination number is relatively low. The widely accepted testing apparatus for determining the tensile grain strength is the Brazilian test apparatus, where two loading platens impose a load on a single grain. Within the loaded grain in such a manner tensile stresses appear perpendicular to the line connecting the two contact points.



a)                                                                    b)
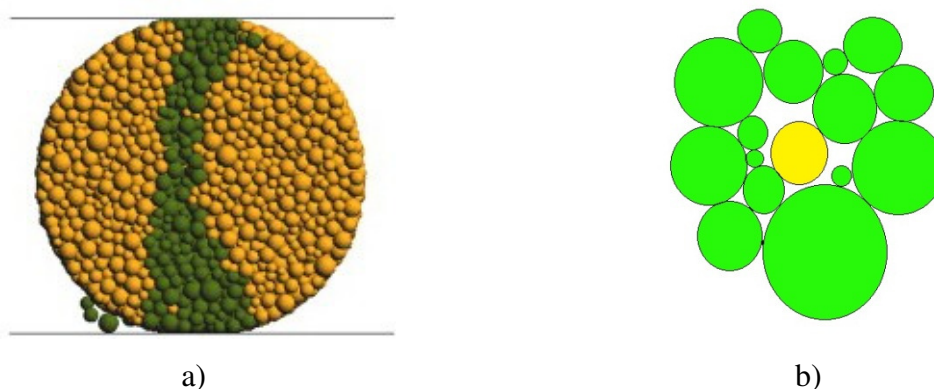
**Slika 3.5: a) Brazilski test; b) Primer podobne obremenitve v vzorcu: rumen delec ima malo število kontaktov zaradi česar se v zrnu pojavijo natezne napetosti v prečni smeri glede na smer obremenjevanje**

**Figure 3.5: a) The Brazilian test; b) Example of a similar grain loading in the sample: the yellow grain is poorly confined, therefore, tensile stresses arise perpendicular to the direction of loading**

Although the Brazilian test only reproduces one loading case that grains within the sample can undergo, it is believed that the crushing can be well described with its application. Vallejo (2009) showed that the majority of grains that crush have a coordination number lower or equal to 3. Every additional contact counteracts the tensile stresses and therefore it causes the reduction of the tensile stresses. But, this does not mean that if the coordination number is greater than 3 the grain cannot crush. If some of the stresses acting upon the grain are big enough to annihilate the confining pressure the grain will still break. Therefore, this needs to be taken into the consideration when determining the breakage criteria.

### 3.4.1.2  Shear failure

Another way of Ž material failure is shear failure. From the nature of this failure it is obvious that it can only take place in grains with a higher coordination number ($C \geq 3$). At least two contacts are needed to immobilize the affected grain and the third to cause the transverse load.
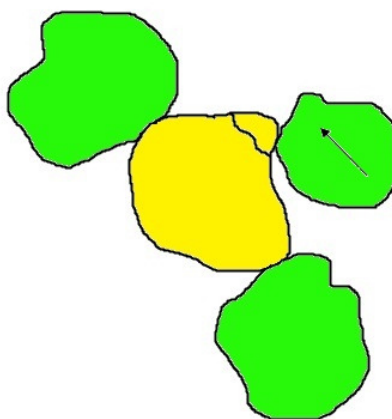
**Slika 3.6: Strižna porušitev zrna**

**Figure 3.6: Shear failure of grain**

While a variety of tests is performed determining tensile strength (Tsoungui, Vallet, Charmet, 1999, Ben-Nun, 2008) no articles on grain shear strength determination have been found. Therefore, the grain shear failure has not been incorporated in the preparation of the computer model. Probably the main reason for the lack of shear strength tests is the difficulty of determining the grain shear strength in laboratory due to the small grain size and broad variety of grain loading modes. Numerical models of a grain are a great tool which enables the investigation of grain shear failure. Because they enable the reproduction of the grain properties, the effect of different parameters can be studied in great detail. Despite the difficulty of measuring the grain shear strength, it is believed that it plays an important role in crushable soil behaviour.

### 3.4.1.3  Abrasion

For this failure mode large relative displacement (slip) of two grains in contact are characteristic. This kind of failure is very hard to measure in laboratory, therefore, the numerical simulation is crucial for modelling this kind of failure. Because the relative displacements will be rather small in the tests performed the influence of this kind of grain *failure* is expected to be rather small. The influence of abrasion would drastically increase in cases such as pile driving (Vallejo, 2007), where the shear displacements would be considerable.

### 3.4.2     Grain size strength dependence (Weibull's Statistics)

Grain strength is one of the properties that depend on the grain structure. A higher amount of imperfections in a material means lower material strength. This is due to the fact that each imperfection causes stress concentrations which lead to the material failure. The amount of defects reduces with decreasing grain size since material naturally fails at the imperfections. Therefore, the amount of flaws within the grain reduces with grain size reduction and consequently the grain strength

increases. The strength continues to increase until the grain reduces to the size where there are no more imperfections within the material. Analogically, the amount of flaws increases with size but stabilizes at certain material specific value, which depends on the size of the imperfections.

There is also strength variation for grains of the same size. Again, this variation depends on the ratio flaw size : grain size. A smaller ratio means a smaller variation in strength for grains of equal size.

McDowell and Bolton (1998) reported that the effect of the flaws on the grain strength can be described well using the Weibull's statistic. McDowell and Bolton stated that for a volume $V$, under applied tensile stress $\sigma$, the survival probability $P_s(V)$ of a block of material is given by:

$$P_s(V) = exp\left[-\frac{V}{V_0}\left(\frac{\sigma}{\sigma_0}\right)^m\right] \tag{3-18}$$

where $\sigma_0$ is the tensile strength that 37 percent of total number of tested blocks survive. $V_0$ is a reference volume of material such that:

$$P_s(V_0) = exp\left[-\left(\frac{\sigma}{\sigma_0}\right)^m\right] \tag{3-19}$$

The exponent $m$ is the Weibull's modulus, and it decreases with increasing variability in tensile strength. For spherical shaped grains the equation (3-19) can be rewritten as:

$$P_s(d) = exp\left[-\left(\frac{d}{d_0}\right)^3 \cdot \left(\frac{\sigma}{\sigma_0}\right)^m\right] \tag{3-20}$$

$d$ – diameter of a grain

The equation above incorporates the two effects of imperfections on grain strength, grain size and the amount of imperfections in a grain. Knowing the characteristic strength $\sigma_0$ for characteristic grain size $d_0$ the strength for a grain of a size $d$ can be expressed as:

$$\sigma = \sigma_0 \cdot \sqrt[m]{\left(\frac{d_0}{d}\right)^3 \cdot \ln\frac{1}{P_s}} \tag{3-21}$$

The graph bellow shows the relation between survival probability and normalized strength for different values of Weibull's modulus. ($m = 1, 5, 10$)
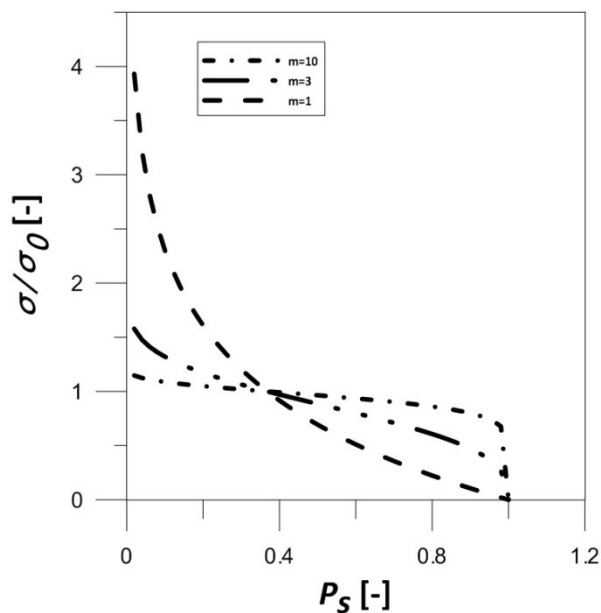
**Slika 3.7: Porazdelitev trdnosti za zrna enake velikosti za različne vrednosti parametra $m$ v skladu z Weibullovo statistiko**

**Figure 3.7: Strength distribution for grains of equal size for different values of $m$ according to Weibull's statistics**

$P_s$ denotes the probability of grain of a diameter $d$ to survive the stress $\sigma$. In other words, it tells us what percentage of grains in a sample will survive such stress. For example, the probability that a grain of a diameter $d_0$ will survive stress $\sigma_0$ is 37 percent, which means that in a sample of 100 grains 37 of them will survive such stress.

### 3.4.3 Crushing modelling

Grain crushing is a comminution of a mother grain into several daughter grains. Due to the fact that there is a great variety of parameters that influence a mode in which grain crushes, the behaviour after grain strength is reached is quite unknown. Therefore, there are several very different approaches trying to best describe this behaviour. Each of them has their advantages and disadvantages. In this chapter two of them are shortly introduced and their advantages and disadvantages are evaluated. The approach believed to best describe the crushing effect is chosen.

#### 3.4.3.1 Replacement method

The particle replacement method is computationally very efficient since each grain is modelled solely by one particle. To incorporate breakage the failure criterion needs to be introduced. When the failure criterion is fulfilled the particle is deleted and smaller particles are generated within the volume that the deleted particle has previously occupied. Since the number of grains can be much greater in this approach, the effect of boundaries on breakage is much smaller.

The negative side of this approach is that the shape of grains is limited to the spherical, therefore, the effect of grain shape on soil behaviour, is neglected. The second disadvantage of this approach is that the number and the distribution of the daughter particles must be predetermined by the user. The problem lies in the influence of different loading cases on grain crushing, which is very limited. In the literature (Vallejo, 2007; Ben-Nun, 2008; Tsoungui, 1999) it was possible to spot that regardless of the grain loading case a single post crushing particle arrangement has been incorporated.



| a) | b) | c) | d) |
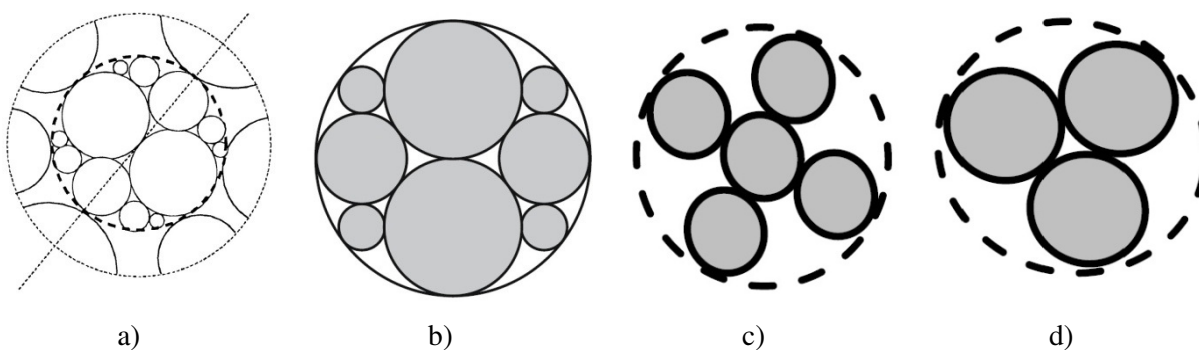
**Slika 3.8: Razporeditev zrn po prekoračitvi trdnostnega kriterija (a – Tsoungui, b – Vallejo, c,d – Ben-Nun)**

**Figure 3.8: Failure modes used by different authors (a – Tsoungui, b – Vallejo, c,d – Ben-Nun)**

**Post crushing particle arrangement**

When each grain is modelled solely by one particle it is necessary to determine the behaviour after the breakage criterion is met. Again, there are several different proposals. Attempts of modelling post crushing behaviour have been made by reducing the particle stiffness and this way reducing the interparticle forces, but the outcome of these attempts was quite poor since great care needs to be taken to avoid energy loss (Brosh, Kalman, Levy, 2011). The most common observed practice in the literature is deleting the mother particle and placing the daughter particles in the same space. Vallejo (2009), Aström and Herman (1998), Tsoungui (1999) have all used this approach but with small distinctions. The main problem with this approach is that you cannot fit all the daughter particles within the volume that mother particle previously occupied. The reason for this is the spherical particle shape, so there are always voids in between the daughter particles. Vallejo, for example, reduced particle size so that they could fit, together with voids, in the volume previously occupied by the mother particle. With this approach the mass conservation requirement is not fulfilled. Aström and Herman tried to fulfil this requirement by seeding the redundant material in the surrounding voids. The problem with this approach is that the computation drastically slows down due to the fact that the void ratio is quite low and. Thus, many random attempts are required to position this material without overlapping other particles. To solve this problem Ben-Nun (2008) and Brosh (2011) have decided to use an approach ž where the radii of daughter particles are reduced so they can all fit in the volume previously occupied by mother particle and then step by step increase their radii so that the mass

conserving criteria would be fulfilled. Due to the higher repulsive forces during the radii increase the affected particles are prevented from breaking.

Although some of the solutions solve the mass conservation problem, the main problem with this approach remains. Only the average stress values within each grain can be evaluated as mentioned in section 3.3.1.5. Several different stress distributions within the grain can result in the same average stress. Therefore, it is not possible to distinguish among them, so a single post crushing particle arrangement can be incorporated in the model. Another question that arises with this approach is: How can the crushing of particles, of which their shapes differ from the spherical shapes, be modelled?

### 3.4.3.2  Particle compound

In this method each grain is composed of several small elementary particles which are then bonded together with bonds in order to compose a grain. The main disadvantage of this approach is the computation time. The time step is determined using the equation:

$$t = \sqrt{\frac{m}{k}} \qquad\qquad (3\text{-}22)$$

mass is calculated with equation:

$$m = \rho \cdot \frac{4 \cdot \pi \cdot r^3}{3} = \frac{\rho \cdot 4 \cdot \pi}{3} \cdot r^3 \qquad\qquad (3\text{-}23)$$

and stiffness is calculated as:

$$k = \frac{E_c \cdot \pi \cdot r^2}{2 \cdot r} = \frac{E_c \cdot \pi}{2} \cdot r \qquad\qquad (3\text{-}24)$$

This means that the calculation step decreases linearly when the size of the smallest particle is decreased. The reduction of a calculation time only plays a role at the beginning of the test. In the particle replacement method the calculation step eventually reduces to the same value. Still, the number of elementary particles is much higher for particle compound method, therefore, it takes longer to solve the force-displacement law equation and dynamic equation.

There are two main advantages of this approach. The computer only calculates the average stress tensor within each elementary particle. Since elementary particles are bonded together, stress distribution is not uniform within each grain. Instead it is determined based on the distribution of forces acting on the grain. This way the natural behaviour of grain crushing is better described since fracture modes actually depend on the stress distribution within the grain.

The second advantage is that by bonding these elementary particles together in a certain manner it is possible to form grains of various shapes. This way you a feature that has a significant effect on soil

behaviour can be modelled. In order to model different shapes, an algorithm is needed that would be able to model grain shape based on a grain photography or X-ray picture.

The precision of the model based on particle compound mainly depends on the number of particles that compose each grain. In Figure 3.11 an example of a particle compound is presented.

Because the author believes that dependence of grain crushing mode should depend on the stress distribution within each grain, and since no proper application could be done with particle replacement method the particle compound method was chosen. Following, the development of a model and algorithms needed to make specific measurements during the test are presented.

## 3.5   Setting the model

In section 3.3 the theoretical background of numeric calculation incorporated in the PFC program is presented. Section 3.4 presents and shortly discusses different ways of crushing modelling. This section is designated to the description of model preparation. First, the servo mechanism used for the test is briefly presented. Next, grain modelling is presented together with description of the effective parameters. Further on, the sample preparation is presented and the steps taken in order to achieve desired stress state and porosity is discussed. At the end of this section, a short section is designated to the measurements that were carried out during the test. Since for some, special algorithms were needed, their logic is schematically described.

### 3.5.1      Servomechanism

To be able to track the stress path correctly, a certain servo mechanism needed to be introduced. In its manual Itasca group (2004) presented an algorithm that sets a defined confining stress to a cylindrically shaped sample. Because the only way to induce the loading with walls is by applying certain displacement, a servo mechanism is needed and it is briefly described here.
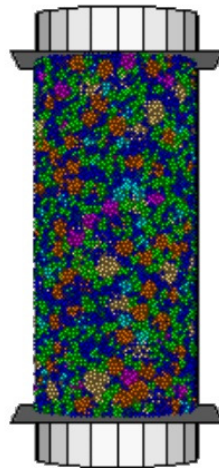
**Slika 3.9: Primer vzorca ($U = 28$) – Različne barve pomenijo različno velika zrna**

**Figure 3.9: Example of a sample ($U = 28$) – Different colours mean different grain sizes**

Every 100 calculation steps the stress conditions of the sample are checked. As mentioned, only displacement can be applied to walls. If a certain force acts on a wall this will not affect its movement, instead, the out of balance force can be tracked. Dividing this force by the sample area, pressure acting on the sample can be evaluated. Based on the difference of the actual wall stresses and the required ones the velocity for the next couple of steps is calculated as:

$$\dot{u}_w = G \cdot \left( \sigma_{meas} - \sigma_{req} \right) = G \cdot \Delta\sigma \qquad (3\text{-}25)$$

Where $G$ represents the gain parameter determined from the approximation of the stiffness of the whole sample, $\sigma_{meas}$ stress acting on a wall, $\sigma_{req}$ required stress acting on a wall. The velocity ($\dot{u}_w$) in the next step needs to be such that the resulting stress will converge towards the required stress state. Imagining the elementary particles as springs linked in series the stiffness of the sample can only be smaller or equal to the sum of stiffness's of all particles touching the wall.

$$\Delta F = K \cdot \Delta U < \Delta\sigma \cdot A \qquad (3\text{-}26)$$

$$\Delta U = \dot{u}_w \cdot \Delta t \qquad (3\text{-}27)$$

$$K = k_n^w \cdot N_c \qquad (3\text{-}28)$$

$A$ – sample area

$k_n^w$ – average normal stiffnesses of all the particles touching the wall

$N_c$ – number of particles touching the wall

For stability, the absolute value of the change in wall stress must be less than the absolute value of the difference between the measured and required stresses (Itasca group, 2004). From the equations (3-26), (3-27), (3-28) the following expression can be derived:

$$\frac{k_n^w \cdot N_c \cdot G \cdot |\Delta\sigma| \cdot \Delta t}{A} < \alpha \cdot |\Delta\sigma| \tag{3-29}$$

Where $\alpha$ is a reduction factor in order to assure the convergence.

$$G = \frac{\alpha \cdot A}{k_n^w \cdot N_c \cdot \Delta t} \tag{3-30}$$

In order to follow the stress path and to be able to track the post peak response the servomechanism has been modified. The displacement of the top and bottom wall has been determined and constant while for the cylindrical wall the servomechanism described above has been used. In order to follow the stress path with constant mean effective stress the required radial stress is determined as:

$$\sigma_{rr\_req} = \frac{3 \cdot p_{const} - \sigma_{zz\_meas}}{2} \tag{3-31}$$

$p_{const}$ – required mean effective stress

$\sigma_{zz\_meas}$ – measured vertical stress in a sample

$\sigma_{rr\_req}$ – required radial stress in a sample

and for isotropic consolidation:

$$\sigma_{rr\_req} = \sigma_{zz\_meas} \tag{3-32}$$

### 3.5.2     Grain modelling

In section 3.4 a theoretical background on different particle breakage models is presented and reasons why a particle compound was chosen are stated. Here, a step-by-step procedure of preparing the grain model is presented. At this stage it is assumed that the stiffness, size and strength properties of elementary particles and bonds, as well as a number of particles in each compound are known.

A)  Material preparation

In the first step of the grain preparation, the highest possible density is tried to be achieved, in order to minimize the effect of imperfections and to maximize the uniformity of the material for a specific size of the elementary particle. For this reason an algorithm prepared by Itasca group was incorporated, designed for true triaxial sample preparation (Itasca group, 2004). The input parameters for this algorithm are presented in the table below:

**Table 3.1: Geometric parameters of the sample (Itasca group, 2004)**

**Preglednica 3.1: Geometrijski parametri vzorca (Itasca group, 2004)**

| parameter | description |
|---|---|
| $h$ | sample height [m] |
| $w$ | sample width [m] |
| $d$ | sample depth [m] |
| $R_{min}$ | minimum ball radius [m] |
| $R_{max}/R_{min}$ | ball size ratio, uniform distribution [ ] |
| $\beta$ | wall normal stiffness multiplier [ ] |
| $\sigma_\circ$ | locked-in isotropic stress [Pa] |
| $N_f$ | min. number of contacts to be a non-floater [ ] |
| $n_f/N$ | remaining floaters ratio [ ] |

**Table 3.2: Material properties for parallel bonded material (Itasca group, 2004)**

**Preglednica 3.2: Materialne lastnosti za zrna pri katerih so uporabljene vzporedne vezi (Itasca group, 2004)**

| parameter | description |
|---|---|
| $\rho$ | ball density [kg/m$^3$] |
| $E_c$ | ball-ball contact modulus [Pa] |
| $k_n/k_s$ | ball stiffness ratio [ ] |
| $\bar{\lambda}$ | parallel-bond radius multiplier [ ] |
| $\bar{E}_c$ | parallel-bond modulus [Pa] |
| $\bar{k}_n/\bar{k}_s$ | parallel-bond stiffness ratio [ ] |
| $\mu$ | ball friction coefficient [ ] |
| $\bar{\sigma}_c$ (mean) | parallel-bond normal strength, mean [Pa] |
| $\bar{\sigma}_c$ (std. dev.) | parallel-bond normal strength, std. dev. [Pa] |
| $\bar{\tau}_c$ (mean) | parallel-bond shear strength, mean [Pa] |
| $\bar{\tau}_c$ (std. dev.) | parallel-bond shear strength, std. dev. [Pa] |

The procedure of the sample preparation used in this algorithm is the following. The maximal porosity is attempted to be achieved for bonded material. For equally sized spheres this is approximately 0.26 (Nimmo, 2004). Due to this, porosity is not among the list of parameters. Following, the number of required particles to achieve such porosity is calculated. The particles are then randomly generated within the geometric boundaries. In order to reduce particle generation steps radii are reduced for a certain factor. Once all the particles are generated, the radii are increased while the particles can move freely. Because of the radii increase there are some locked in stresses within the sample. Therefore, in next step the isotropic stress condition is tried to be achieved, by moving boundary walls. Once the desired isotropic stress is achieved the bonds are assigned to all contacts.

78   Likar, Ž. 2012. Effects of stress path and grain size distribution on mechanical behaviour of crushable granular material

Grad. Th. – University Studies. Ljubljana, UL FGG, Department of Civil Eng.
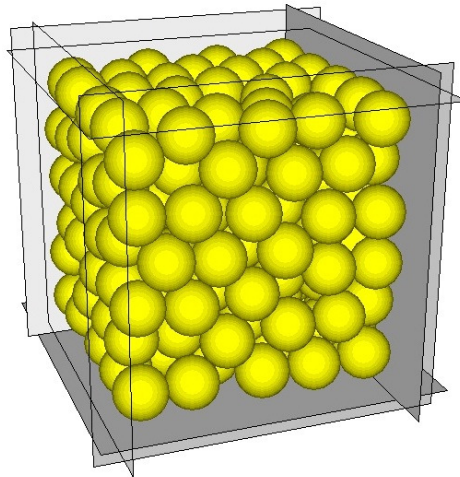


**Slika 3.10: Slika vzorca pred oblikovanjem zrna**

**Figure 3.10: Sample before the grain shaping**

B) Grain shaping

When the stress and density condition is fulfilled the grains need to be formed. Therefore, an algorithm defining particle shape needs to be incorporated. This stage is one of the biggest advantages of this type of grain modelling, since various grain shapes can be achieved. But, due to lack of data and for simplicity of the model in this research only spherical grains have been modelled. Location relative to the grain centre fulfilling the criteria:

$$x^2 + y^2 + z^2 \leq r^2$$

is saved into the computer memory. Later, during the sample preparation this information is called and placed in the sample.
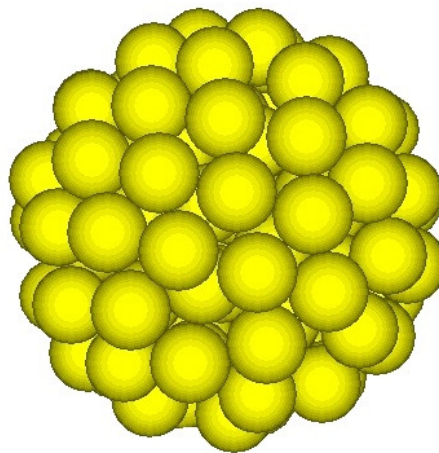


**Slika 3.11: Slika vzorca po oblikovanju zrna**

**Figure 3.11: Sample after the grain shaping**

C)  Micro properties determination:

The most important step in preparing the synthetic material is fitting its properties to the properties measured in the laboratory on a real material. Depending on the type of test that was performed in the laboratory a similar test should be performed in the program. In case of this research no laboratory tests were performed for determining the material properties, so their values were taken from the manufacturer (Leca).

- grain strength for $d = 2$ mm:     1.16 MN/m$^2$

## 3.5.3      Model optimization

The test simulation consumes a lot of computer memory. Parameters such as velocity of loading walls, number of grains in a sample and number of particles in a grain greatly affect the calculation time. In terms of the calculation time, it would be optimal to reduce these three parameters to very low values in order to reduce the calculation time. When reducing the values of these parameters below certain limit the results start to depend on them as well. Therefore, several pre-tests were performed to determine the minimal values of these parameters and to determine how values that are lower than the minimal values affect the results.

### 3.5.3.1  Loading rate

Boundary conditions of a sample are induced by wall movement. While the top and bottom wall are assigned a constant velocity, the velocity of the cylindrical wall is adjusted every 100 steps through the servomechanism as described in section 3.6.1. When the velocities of walls are low, particles have enough time to rearrange. But, when the wall velocity is increased, an increment of wall displacement during each step is too large and, therefore, large repulsive forces are generated affecting the sample behaviour. By varying the velocity of the top and bottom loading wall the maximal velocity, at which particles still have enough time to rearrange, was determined. Below, the behaviour of soil sample during the triaxial shearing at constant mean effective stress $(p')$ for three different velocities is presented. The test was performed on a cylindrical sample with 2000 equally sized particles at constant mean effective stress of 175 kPa.
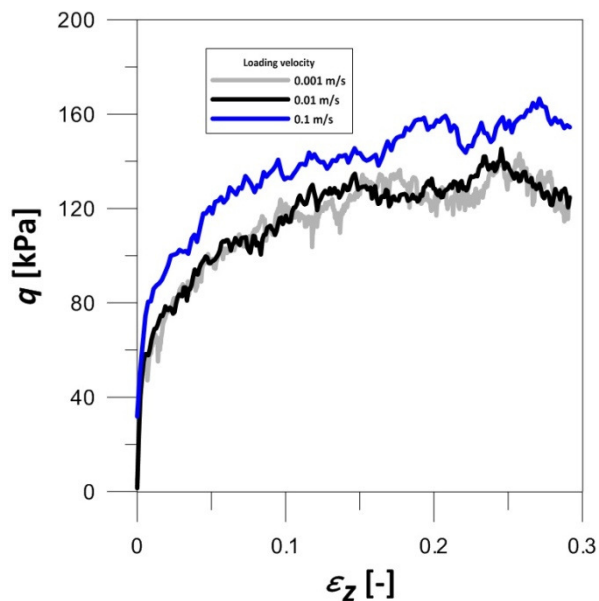
**Slika 3.12: Odziv modela med triosnim strižnim preskusom pri konstanti srednji vrednosti efektivne napetosti ($p'$) za različne hitrosti obremenjevanja**

**Figure 3.12: Response of a model during triaxial shearing at constant mean effective stress ($p'$) for different velocities of loading walls**

Figure 3.12 presents the maximal allowable velocity of loading walls, which is 1 cm/s. For higher velocities the behaviour of a sample is stiffer since the particles cannot rearrange fast enough. In this research the behaviour within each particle is also important. Therefore, the effect of loading velocity on grain stiffness and strength was checked as well. The effect of loading velocity on an artificial increase of grain strength was checked on a grain with 104 particles connected with parallel bonds.
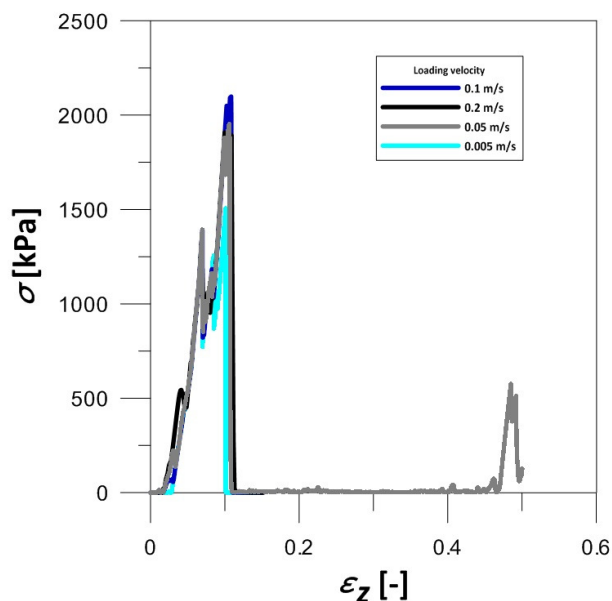


**Slika 3.13: Odziv zrna v odvisnosti od hitrosti obremenitve**

**Figure 3.13: Grain response depending on the loading velocity**

As seen in Figure 3.13 grain strength is even more sensitive to loading velocity. But, it is not expected to experience such loading condition within the sample since particles rearrange and the effect of the artificial increase of grain strength due to the high loading rate is reduced. Figure 3.13 clearly shows that grain strength artificially increases if the loading rate is too fast.

### 3.5.3.2 Elementary particle size

Another parameter that drastically increases the calculation time is the number of particles in a sample. In case of a compound model each grain is composed of several bonded particles. For constant material parameters the grain strength changes as the number of elementary particles that compose each grain varies. But, the material parameters can be adjusted in order to achieve certain macro grain properties. Therefore, the number of particles does not affect the crushing behaviour directly. Nevertheless, more particles that compose each grain the better the crushing behaviour is described. For the simulation the grains were composed of elementary particles with a diameter of 0.4 mm meaning that the maximal grain, with a diameter of 2 mm, is composed of 104 elementary particles.

### 3.5.3.3 Sample size (number of grains in a sample)

The number of grains in a sample has much bigger effect on macro properties than number of particles in a grain. In other words, the ratio between the maximal grain size and the sample diameter has a great influence. Several pre tests were carried out on simple sample that was composed of equally sized grains ($d_{max}$ = 2 mm), where each grain was represented by a single particle. Each consecutive sample was prepared with a smaller dimension until the influence of sample size on the results was observed.
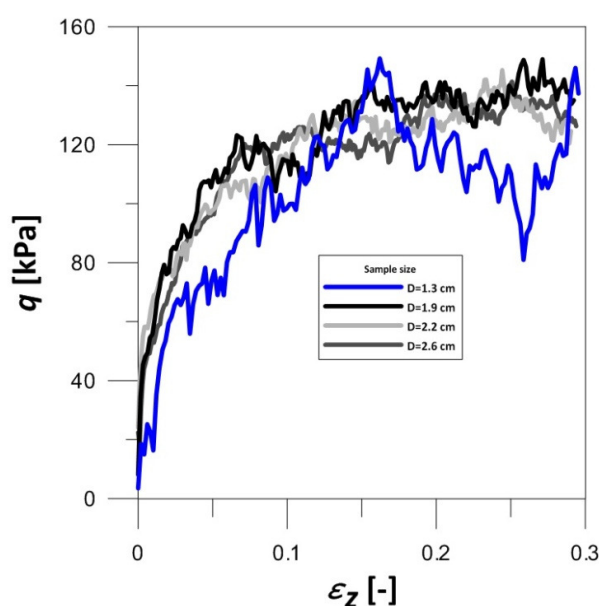


Slika 3.14: Vpliv velikosti vzorca na izmerjene strižno trdnost in togost zemljine

Figure 3.14: The influence of a sample size on sample strength and stiffness

In geotechnic sample testing is widely accepted that the radius of a sample needs to be at least 10 times larger than the maximal grain size. In Figure 3.14 this was confirmed by the tests performed in the PFC3D program. For samples with a diameter larger than $10 \cdot d_{max}$ the shear stiffness and the sample shear strength only slightly varies. Sample with a diameter smaller than $10 \cdot d_{max}$ experiences a decrease in shear stiffness. The noise caused by the particles rearrangement drastically affects the measurements.

### 3.5.3.4 Parameters chosen for test simulation

If all the limitations described in sections 3.5.3.1 – 3.5.3.3 were fulfilled the calculation time would drastically increase. Based on the computer specification presented in Table 3.3 the parameters were chosen so that the duration of each test simulation is limited to 7 days.

- Loading rate:                    1mm/s
- Number of particles in a grain:   104
- Elementary particle diameter:     0.4 mm
- Sample dimensions:                height = 2.6 cm
  
  diameter = 1.3 cm ($6.5 \cdot d_{\max}$)

The loading rate and the number of particles in a grain does not affect the results. Still, the number of grains modelled in a sample indeed influences the results. It is obvious that the values are all far below the limitations that assure exact results. The calculation was still performed in order to test the model and to try to determine if any of the parameters has a smaller effect than determined with a pre-tests so the model could be adjusted.

**Table 3.3: Computer specification/characteristics used for the simulation[2]**

**Preglednica 3.3: Karakteristike računalnikov uporabljenih za izvedbo simulacije[2]**

|                  | Computer 1                                              | Computer 2                                          |
|------------------|---------------------------------------------------------|------------------------------------------------------|
| Processor        | 3 GHz                                                   | 3 GHz                                                |
| RAM              | 4 GB                                                    | 8 GB                                                 |
| Operating system | Windows 7 – 64-bit                                      | Windows 7 – 64-bit                                   |
| PFC3D version    | 3.10 (supports 32-bit calculation and up to 2GB RAM)   | 4.0 (supports 64-bit calculation, unlimited RAM)     |
| DURATION         | 7 days                                                  | 2 days                                               |

[2] Two months before the thesis presentation the computer 1 broke down. So the work was continued on a different computer.

Based on the comparison displayed in Table 3.3 the calculation time drastically decreased on a more powerful computer.

### 3.5.4    Sample preparation

The size of a sample was chosen as H : D = 2.6 cm : 1.3 cm. The total number of equally sized particles in such a sample is approximately 40 000. With an estimation that parallel bonds require the same amount of memory as each particle and knowing that number of parallel bonds is 2.7 times the number of particles, that would mean a total number of basic elements of about 160 000. Such number of basic elements requires a lot of computer memory and, therefore, a long calculation time for the sample preparation. For this reason a shortcut was taken in order to speed up the preparation. Instead of particle compounds, single spheres with elastic properties equal to elastic properties of the compounds were used for first couple of steps. All samples were prepared with an initial porosity of 0.5. Because the isotropic pressure and porosity cannot be adjusted at the same time, samples with different porosities ended up with different isotropic stress. To adjust the mean effective stress walls were moved so that the mean effective stress of 50 kPa is achieved. At this stage compounds were placed in a sample. Because of the slight difference in grain size additional calculation cycles were taken in order to achieve the desired initial isotropic stress state. In case of this research it was 50kPa. During these steps the particles were prevented from breaking apart by setting the strength parameters to a very high value. When the pressure of 50 kPa was reached again, the bond strengths were reduced to the actual value depending on the grain size (Weibull). After this pressure was achieved samples were isotropically compressed to the pressure at which the triaxial shearing was then performed.

### 3.5.5    Measurements

In PFC3D a wide variety of predefined parameters that can be tracked during the test is incorporated, for example: particle displacement and location, particle stress condition, wall displacement, forces acting on a wall, etc.. In most cases these are sufficient, but when an extra parameter is needed it can be pre-programmed into the test procedure. Some trivial parameters that can be incorporated into the test procedure with a single function are deviatoric stresses and shear strains, mean effective stress and volumetric strains, axial and radial strains. The integrated FISH language also allows predefining the function that will track the grain size distribution and the coordination number of grains. These two functions as well as an algorithm evaluating GSD were prepared for the need of this research and it is shortly presented here while the algorithms can be found in the appendices.

### 3.5.5.1 Grain size distribution tracking

The grain size distribution of crushable material changes during the test. To be able to determine how it changes, an algorithm that tracks the GSD needed to be incorporated into the program. In case of the replacement method this can be done by looping through the particles and extracting their radii from the program. With particle compound method this task is a little bit more challenging. An algorithm that was prepared to serve this need is step by step described below.

(i)     Create a matrix with two columns and as many rows as there is a total number of particles in a sample (number of grains times the number of particles in each grain). Create an array with the number of rows that is equal to the maximal number of particles in a grain.

(ii)    Loop through all the particles in the sample. Each particle that was already scanned is flagged. If the particle, currently under investigation is already flagged jump to the next particle in the loop.

(iii)   For each particle: save its pointer into the array, mark it with a flag (for example, change its colour) and loop through all the particles that are parallel bonded with the particle currently under investigation.

(iv)    If the particle is already flagged go to the next particle in bonded contact, otherwise save its pointer to the array. Flag the particle and go to the next particle in contact with the particle currently under investigation.

(v)     Loop until all particles within a grain are scanned.

(vi)    Copy the information from the array to the matrix and assign all the particles, from the last grain, a common compound number.

(vii)   Go to step (ii).

In order to make sure that each grain is scanned and assigned to a compound that it belongs to, two levels of looping are incorporated, one on a sample level and the other one on a grain level.  After all of the particles are assigned to a compound, the size of all the compounds is checked and the colour of the constituent particles is assigned depending on the compound size. By colouring the particles grain size distribution changes can be visualised by plotting a complete sample. In Figure 3.15 the two phases of single grain crushing are showed where the different colours mean different daughter grain sizes.
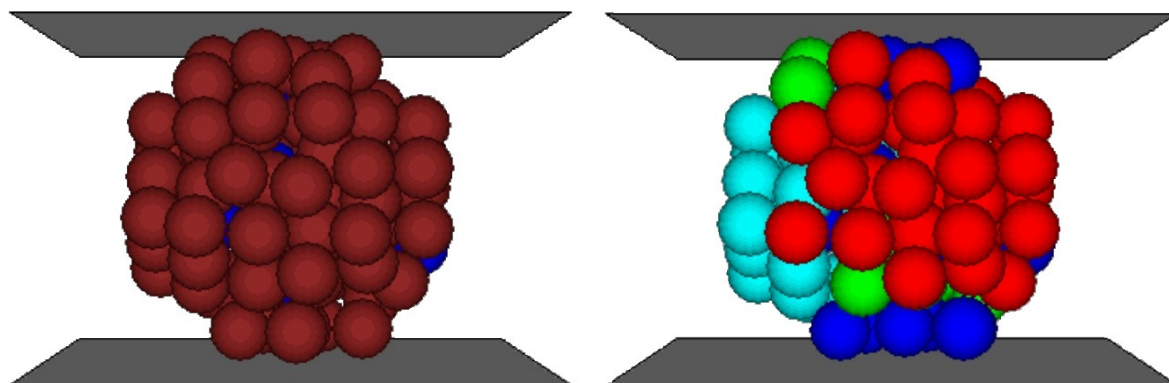
**Slika 3.15: Preverjanje zrnavosti med izvajanjem brazilskega testa**

**Figure 3.15: Grain size distribution tracking during Brazilian test**

### 3.5.5.2  Coordination number

Every time the GSD is evaluated the coordination number of each grain (compound) is also checked.

- (i)     Loop through all the particles in the sample.
- (ii)    The pointers of all the particles that are in contact with the particle currently investigated, but are not connected with a bond, are saved to an array.

After a test simulation is finished a program such as Matlab is used to determine the coordination number of each grain.

- (iii)   A matrix with as many rows as there are grains is made
- (iv)    For every ball from the grain, pointers saved in the array (during step (ii))  are copied to a single row.
- (v)     Each ball pointer is replaced with a compound pointer that it belongs to.
- (vi)    Two grains could have several contacts through several different particles. But it was assumed that each two grains could be in contact only once. Therefore, unique values were extracted from the list produced by step (v).
- (vii)   If the pointer of a grain currently under investigation was among the unique values it was deleted (the grain cannot be in contact with itself).
- (viii)  For each grain, a number of unique values are counted. The result is equal to the coordination number of a grain.

### 3.5.5.3  Grain size distribution

To be able to track the grain size distribution changes during loading, a size of every grain needs to be evaluated. When a test is performed in the laboratory a grain size is determined with a sieving analysis. Although, it is possible to model a sieving analysis in PFC3D its execution would take a very

long time. Plus, it would not be possible to determine the grain size distribution during the test. For this reason a different approach needed to be incorporated. The best way to determine a grain size would be to measure a grain in three perpendicular directions. This could be done with a projection of the grain location on three perpendicular planes. And on these planes determine the maximal and minimal dimensions. With this approach also the angularity of a grain could be determined. While this kind of algorithm should be developed to exactly track the grading changes in this model a simpler algorithm was prepared. It is measuring the average distance of elementary particles composing each compound from its centre of gravity.

For each grain the location of all constituent particles can be tracked. First, the centre of gravity of all the grains was determined with an equation:

$$i_T = \frac{\sum_{j=1}^{n} i_j \cdot m_j}{\sum_{j=1}^{n} m_j} \qquad (3\text{-}33)$$

$i$ – the coordinate $x, y$ or $z$

$i_T$ – the coordinate of a grain centre of gravity

$m_j$ – mass of the elementary particle

n – number of elementary particles in a grain

Because mass is constant for all elementary particles this equation simplifies into:

$$i_T = \frac{\sum_{j=1}^{n} i_j}{n} \qquad (3\text{-}34)$$

Then, the average distance of elementary particles from the centre of gravity was determined:

$$\bar{s} = \frac{\sum_{j=1}^{n} \left[ \sqrt{(x_T - x_j)^2 + (y_T - y_j)^2 + (z_T - z_j)^2} \right]}{n} \qquad (3\text{-}35)$$

and this value was taken as a parameter determining the grain size. This approach is not suitable for grains composed of a single grain since the average distance from the centre of gravity is equal to zero. This means that the increase of fine grains could not be tracked. Therefore, the method has been adapted in a way that if a grain is composed of a single grain its weight for the size was defined as:

$$\bar{s} = \frac{r}{4} \qquad (3\text{-}36)$$

$r$ – radius of an elementary particle

$\bar{s}$ – average distance from the grain centre of gravity



| a) $\bar{s} = \dfrac{r}{4}$ | b) $\bar{s} = \dfrac{r}{2}$ | c) $\bar{s} = r$ | d) $\bar{s} = r \cdot \sqrt{3}$ |
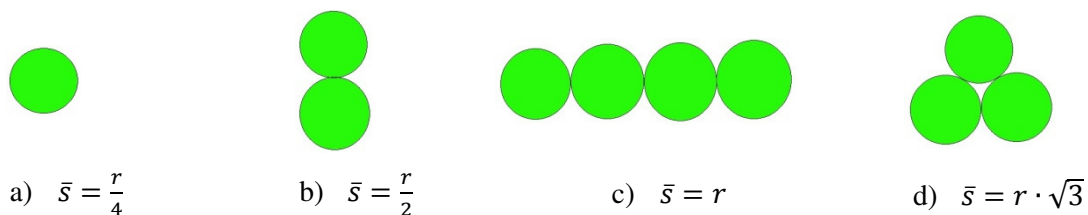
**Slika 3.16: Primeri povprečnih oddaljenosti od težišča zrna za zrna različne oblike**

**Figure 3.16: Examples of average distances from the grain centre of gravity**

## 3.6 Analysis

In this section the model and the results of the numerical simulation are shortly analysed. The input material properties were not acquired from the laboratory tests, instead they were taken from the literature or estimated. For example the grain strength was taken from the brochure on LECA (Leca). In the Table 3.4 parameters of the material that was used for the test simulations are specified.

**Table 3.4: Input parameters for elementary particles and parallel bonds**

**Preglednica 3.4: Vhodni podatki za posamezno zrno**

| Parameter | Value | Units |
|---|---|---|
| Ball normal stiffness | 80 | kN/m |
| Ball shear stiffness | 80 | kN/m |
| Ball density | 2.65 | $10^3$ kg/m$^3$ |
| Ball friction | 0.5 | - |
| Parallel bond normal stiffness | $2.65 \cdot 10^{10}$ | kPa/m |
| Parallel bond shear stiffness | $2.65 \cdot 10^{10}$ | kPa/m |
| Parallel bond normal strength | $3.5 \cdot 10^4$ | kPa |
| Parallel bond shear strength | $3.5 \cdot 10^4$ | kPa |
| Ratio between bond and particle radius | 0.5 | - |

**Table 3.5: Basic sample parameters**

**Preglednica 3.5: Osnovne lastnosti vzorcev**

| Parameter | | Value | Units |
|---|---|---:|---|
| Sample height | | 2.6 | cm |
| Sample diameter | | 1.3 | cm |
| Number of grains | $U = 1$ | 411 | - |
| in a sample | $U = 28$ | 10583 | - |
| Number of particles | $U = 1$ | 42744 | - |
| in a sample | $U = 28$ | 52987 | - |
| Number of parallel bonds | $U = 1$ | 113658 | - |
| in a sample | $U = 28$ | 88776 | - |
| Top and bottom wall velocity | | 0.1 | m/s |
| Maximal number of particles in a grain | | 104 | - |
| $d_{max}$ | | 2 | mm |
| $d_{min}$ | | 0.4 | mm |
| Maximal strain | | 0.3 | - |

For the two main parameters affecting the sample behaviour, sample size and wall velocity, unfavourable values were chosen for the simulations performed. These values were taken in order to reduce the calculation time to 7 days, as showed in Table 3.3. Although it follows from the pre-tests described in sections 3.5.3.1 - 3.5.3.3 that the results are be affected by these parameters, the tests were still performed. The goal of performing these tests was to test the model preparation procedure and the effect of parameters specified in section 3.5.3.4 on crushing. The results from such tests will deviate from the real behaviour of such soil. Still, the crushing mechanism should not be greatly affected by the chosen testing procedure.

### 3.6.1    Results

All samples were prepared with the same initial porosity of 0.5. Section 3.5.4 describes the procedure of sample preparation. During the sample preparation, due to the radii increase of the elementary particles, the sample is isotropically loaded. This means that the sample is at the normal compression line at all times. Because of different GSD the samples were consolidated to different mean effective stresses. Before the spheres were replaced by the compounds the mean effective stress was again adjusted to 50 kPa. After the replacement of spheres with grain compounds, the samples were isotropically compressed to 3 different mean effective stresses: $p' = 87$ kPa, 175 kPa, 350 kPa. Below, the isotropic compression lines for the two different coefficients of uniformity are shown:
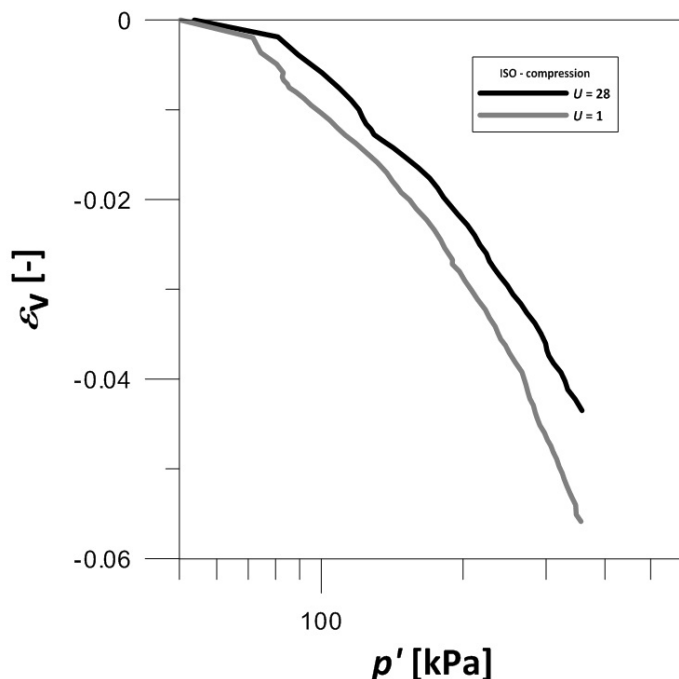
**Slika 3.17: Krivulja izotropne sisljivosti za vzorca U = 1 in U = 28**

**Figure 3.17: Isotropic compression lines for $U = 1$ and $U = 28$**

Figure 3.17 depicts nice behaviour similar to the one observed in the laboratory. During this phase the grain size distribution changed only slightly which is also in agreement with the laboratory results. During the isotropic compression, tests were stopped at three different pressures ( $p' = 87\,\text{kPa},\ 175\,\text{kPa},\ 350\,\text{kPa}$) and saved so later the triaxial shearing could be performed. Below, the diagrams for the three different mean effective stresses and two different coefficients of uniformity are presented.



a)                                              b)
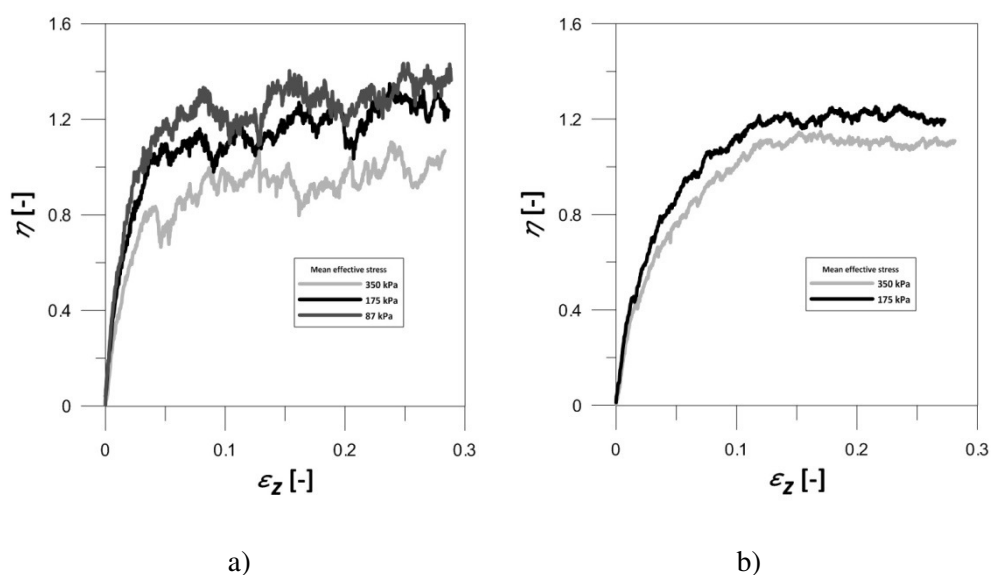
**Slika 3.18: Zmanjševanje parametra $\eta_{max}$ s povečevanjem srednje vrednosti efektivne napetosti za vzorca z začenim koeficientom enakomerosti: a) $U = 1$ in b) $U = 28$**

**Figure 3.18: Reduction of parameter $\eta_{max}$ with increasing mean effective stress: a) $U = 1$ and b) $U = 28$**

Comparing the graphs in Figure 3.18 the different effect of sample size on the distribution with initial uniform grading ($U = 1$) and the uniformly distributed grading ($U = 28$) can be observed. The noise is much bigger in the results of the sample with $U = 1$. Comparing the Figures 3.12 and 3.14 a reason why it can be said that the noise is due to the inappropriate sample size can be seen. While the loading velocity only influences the peak shear strength, the sample size greatly influences the noise of the results. When the sample is too small the stresses are greatly influenced even when only a couple of grains are rearrange. This effect is much smaller in the sample with more uniform distribution since the stress drops are not as significant due to the lower grain interlocking.

Despite this influence the reduction of shear angle was still compared, and it is presented in Figure 3.19. While for the sample with initial uniformity of 28 the noise is small and it is easy to determine the peak shear strength, for the sample with initial uniformity of 1 the peak values were taken to determine the peak shear strength. The peak values were chosen since in Figure 3.14 the peaks seem to almost coincide with the actual peak shear strength.
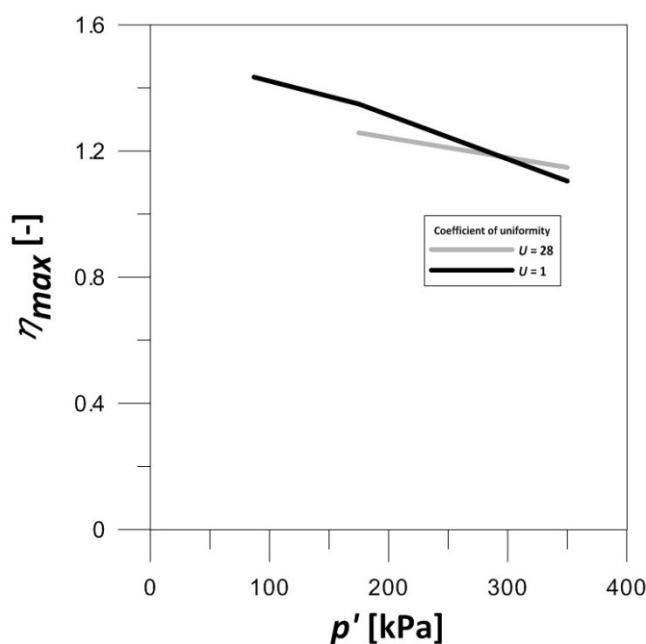


**Slika 3.19: Zmanjševanje vrhunske strižne trdnosti s povečevanjem srednje efektivne napetosti**

**Figure 3.19: The reduction of peak shear strength with the reduction of mean effective stress**

The reduction of peak shear strength is much larger for the sample with uniformity of $U = 1$. The samples were overconsolidated to different confining pressure and, therefore, they experience different amount of dilatancy. It is impossible to say what percent of this reduction is due to the grain crushing and what percentage due to the decrease of overconsolidation ratio defined by:

$$R_0 = \frac{p_y'}{p_0'}$$

(3-37)

$p'_y$ - yield point which lies at the intersection of the swelling line through the point defined with current void ratio and mean effective stress with the normal compression line

$p'_0$ - current mean effective stress



a)   $U = 1$                                                          b)   $U = 28$
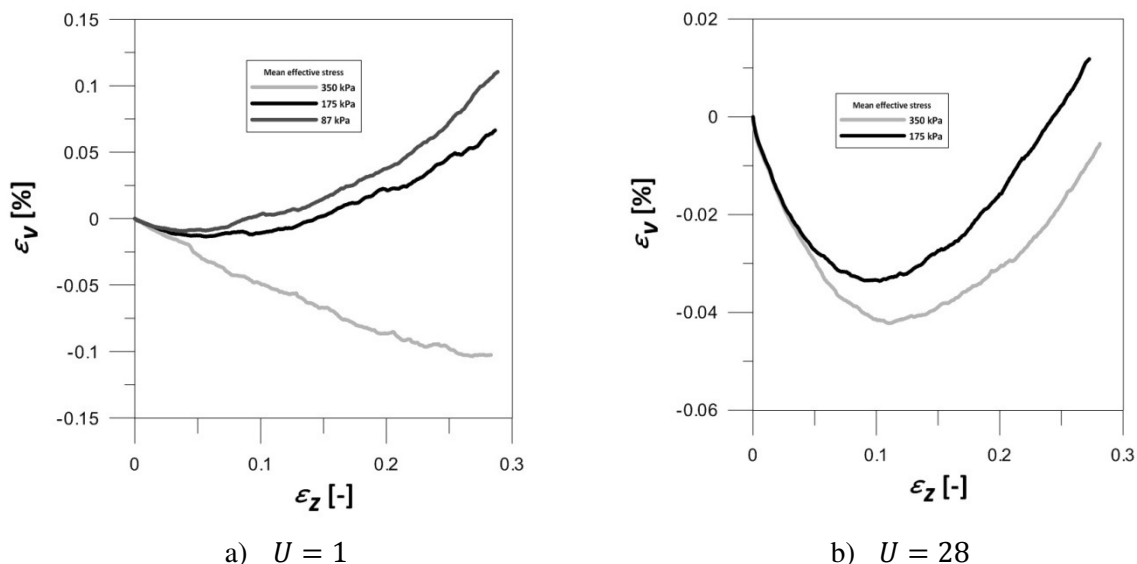
**Slika 3.20: Volumske strižne deformacije med triosnim strižnim preskusom**

**Figure 3.20: Volumetric strains during triaxial shearing test**

When preparing the sample, either void ratio or stress condition can be defined. In case of the tests performed for this research the initial void ratio was defined. Because of different initial grading during the step at which the radii are increased different mean effective stresses arise within the sample. This means that samples are initially overconsolidated to different mean effective stresses. Comparing the graphs a) and b) in Figure 3.20 it is possible to infer that the overconsolidation pressure for sample with initial uniformity $U = 1$ was somewhere between 175 kPa and 350 kPa while for sample with initial uniformity $U = 28$ it was slightly higher than 350 kPa. The difference in the overconsolidation pressures is a result of different initial grain size distributions and the sample preparation procedure.

a)  $U = 1$                                            b)  $U = 28$
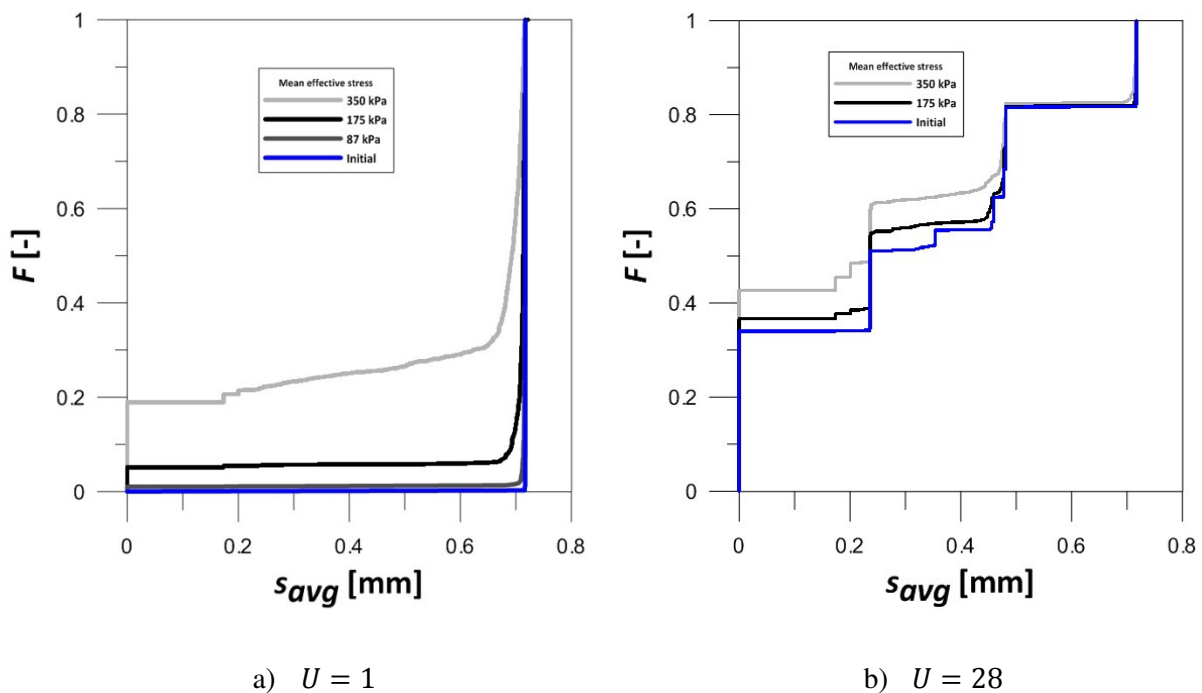
**Slika 3.21: Zrnavostna sestava po opravljenih testih**

**Figure 3.21: Grain size distributions after tests**

Figure 3.21 shows that samples experienced a great increase of the amount of fine material while the gradings only slightly changed for bigger grain sizes. This suggests the crushing takes place only at contacts where the edges chip away. This way the amount of smaller grains increases while the size of bigger grains only slightly reduces. Figure 3.22 displays the coordination numbers for all the grains in the sample at the end of the test. This explains why only an increase of fine material can be observed. Even in a sample with very uniform grain size distribution ($U = 1$) grains have high coordination numbers. Because every additional contact reduces the tensile stresses within the grain it is not to be expected that grains would crush due to the tensile stresses as in Brazilian test.
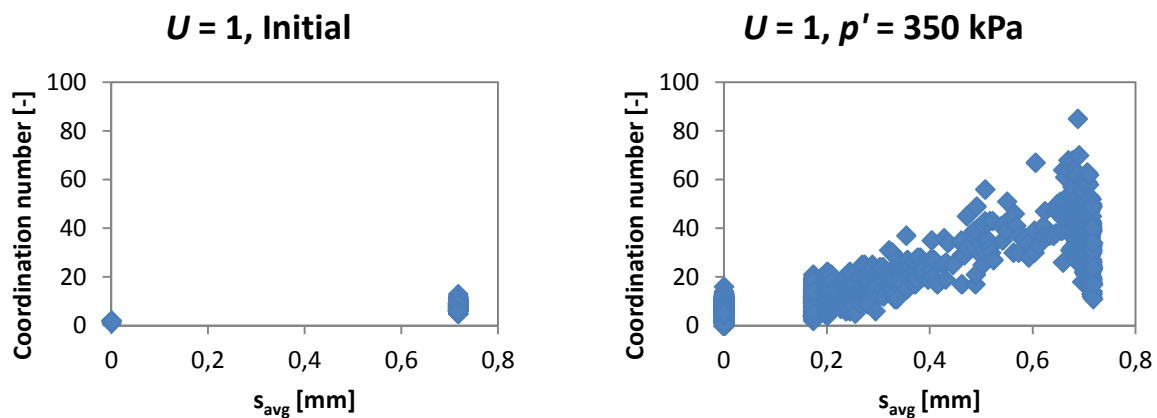


**Slika 3.22: Število medzrnskih kontaktov v odvisnosti od velikosti zrna ($U = 1$)**

**Figure 3.22: Coordination number for different grain sizes ($U = 1$)**
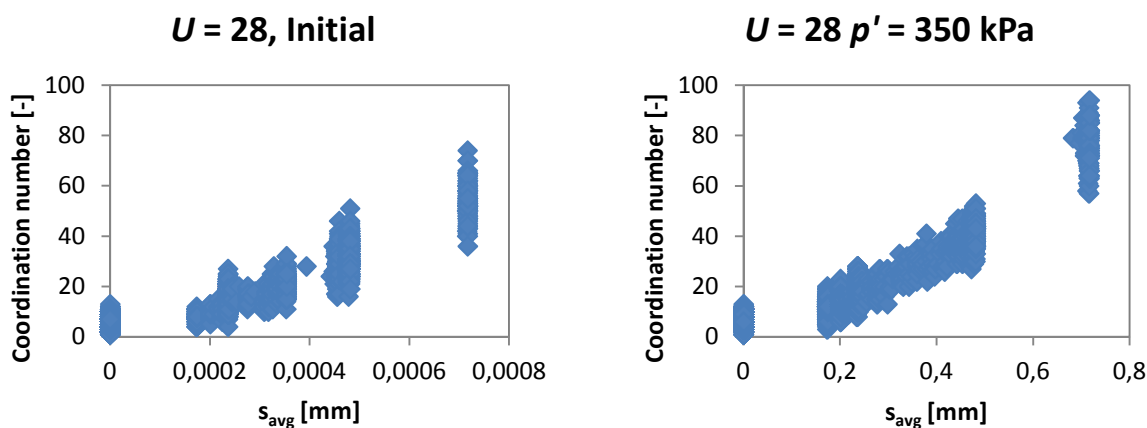
**Slika 3.23: Število medzrnskih kontaktov v odvisnosti od velikosti zrna ($U = 28$)**

**Figure 3.23: Coordination number for different grain sizes ($U = 28$)**

When a contact force is low and a relative shear displacement of the two grains in contact is enforced, they only slip at a contact. But, when the contact normal force increases the contact shear strength increases as well. At some point the contact shear strength is higher than the grain shear strength. At this point instead of a slip at a contact a tip of a grain chips away. With an increase in the coefficient of uniformity the load acting on a grain is distributed among higher amount of grains. Because the reduction of normal contact force means the reduction of contact shear strength, the grain shear strength overrules and the grains slip rather than break at the contact. The same happens at lower mean effective stresses where despite the low coordination number the normal contact forces are too low that the contact shear strength would overrule the grain shear strength.

This points out another parameter that for a specific soil influences the reduction of internal friction angle, and that is angularity. It is known that the friction angle increases with increased angularity. During the loading the grains crush at contacts and, therefore, the angularity of the grains reduces. Consequently, the internal friction angle reduces as well.

In Figure 3.24 the number of bond breaks as a function of shear strains is presented. For samples with an initial coefficient of uniformity equal to 1, the rate of bond breaking is increasing with increasing shear strains while for sample with an initial coefficient of uniformity equal to 28 is reducing. This result is in favour of the theory of ultimate fractal grading. While the sample with $U = 1$ is far from the ultimate grading and it needs to experience considerable crushing, the sample with $U = 28$ is very close to the ultimate grading and, therefore, the crushing rate diminishes with increasing shear strains.
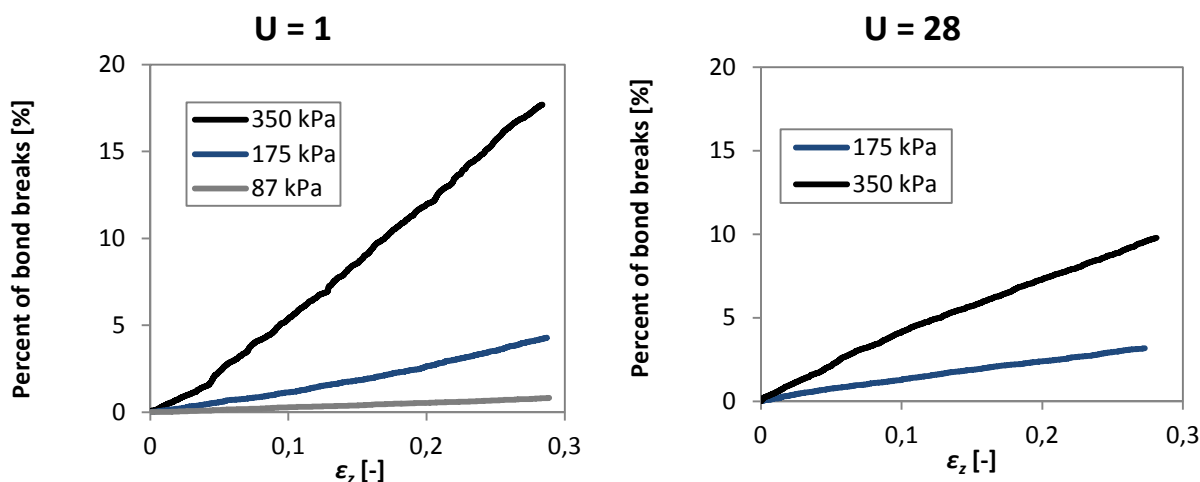
**Slika 3.24: Število prekinjenih vezi v odvisnosti od strižnih deformacij**

**Figure 3.24: Bond breakage as a function of shear strains**

## 3.7   Model improvements

Based on the test results several improvements of a model and of sample preparation procedure can be proposed. The first one is the grain modelling. Parallel bond require far more computer memory than contact bonds. From the single grain crushing test it was clear that the grain crushing behaviour can be better described with parallel bonds. Therefore, it was decided to incorporate them in the model. From the results of the simulation it is evident that the coordination number of grains is too high that the grains would crush due to the tensile stresses. Instead, grains only crush at contacts and this can be considered as a shear failure, as displayed in Figure 3.6. This kind of failure can be also well described with grains composed of contact bonded material. Contact bonds, unlike parallel bonds, do not require any additional computer memory compared to the grain stiffness model. The only difference is that it can, besides the compression, also resist the tension. Therefore, using this kind of bond the number of elementary particles can be increased approximately four times. The calculation time would only slightly increase due to the increase of the sample height.  By increasing the number of grains four times, the critical value of a sample size would be satisfied and the influence of the sample size on test results would be eliminated. Figure 3.18 presents the different effect of sample size on samples with different initial GSD. By eliminating the sample size effect on the test results the only negative effect that remains is the influence of high loading rate. While the sample size effect is reduced by increasing the value of coefficient of uniformity, the effect of the loading rate is much more consistent regardless of the $U$ −value.

The second correction that would need to be carried out is the sample preparation procedure. In case of the simulations that were carried out the number of grains in a sample was determined based on the porosity that was predefined. The grains were generated within the sample with reduced radii and then their radii were increased to the specified size. This way the sample was uniformly compacted and the

preparation time was reduced. With this approach the overconsolidation pressure could not be controlled. Porosity is a GSD and mean effective stress dependent parameter which means that the pressure at which the specified porosity is achieved for a specific GSD varies. When comparing the effect of crushing, at the same mean effective stress the effect of overconsolidation should be eliminated. In such a case the sample should be prepared by generating and compressing particles in layers. This way the overconsolidation of a sample is eliminated. The preparation of a sample layer by layer is important in order to achieve a homogenous sample. Compressing large samples all at once would result in highly compacted regions while other regions would remain in loose condition.

# 4    CONCLUSION

In this thesis the effect of stress path and grain size distribution on grain crushing and on internal shear angle is studied. On artificial material known as LECA a series of laboratory tests were performed. Because of low grain strength, tests could be performed in standard oedometer and trixial apparatus. The amount of grading changes that the material undergoes was showed to greatly depend on the initial grain size distribution and is increasing with increasing coefficient of uniformity. During the isotropic compression the changes of the grain size distribution are negligible, while during oedometer test, triaxial shearing test at constant cell pressure and triaxial shearing test at constant mean effective stress the material experienced grading changes. Still, the effect of mean effective stress is important since it increases the particle interlocking forces which are important when shear strains are induced to the sample. The reduction of the internal shear angle depends on the grain size distribution changes while the influence of the grain ovalization could not be tracked during the laboratory tests. Based on results, a simple model describing the grading changes and reduction of internal shear angle was prepared. The model is based on the stress path that is induced to the sample and is defined with mean effective stress at the end of the test and the inclination of the stress path.

Grain crushing is a micro scale phenomenon affecting the macro scale behaviour of crushable material. During the laboratory tests it is not possible to track the behaviour of the sample on the grain scale. Therefore, a numerical model describing the grain crushing was prepared in program Particle Flow Code 3D. To achieve reasonable calculation times, model needed to be simplified to such extent that the results were affected by the loading velocity and the sample size. The simulations were still performed to observe the crushing mechanism, which is not expected to be influenced by the two parameters, and to evaluate the model itself.  It was observed that due to the high number of contacts, grains are unlikely to experience tensile failure. The most common type of grain failure was due to the exceeded grain shear strength close to contacts. For this reason the application of parallel bonds, which are able to resist the normal and shear forces as well as the moment, in grain modeling is unnecessary. Instead, contact bonds, which are computationally more efficient, should  be used. This would enable to increase the sample size and to eliminate its effect on the results. To reduce the calculation time and to increase the sample homogenity the radius expansion procedure was incorporated in sample preparation. This way sample stress condition was hard to control, therefore, this approach was evaluated as inappropriate for such application. Instead, by compacting a sample layer by layer the desired stress condition should be achieved.

Grain crushing is a complex phenomenon influenced by a range of parameters. Of which, not all can be tracked during laboratory testing. The application of numerical simulation can be a helpfull tool in such cases. Programs like PFC3D are very computationally intensive, therefore, models need to be simplified to certain extent. Still, on these models many things can be observed, but one should be

aware of the influence of the model simplification. If a precise simulation, because of the comparison with the laboratory results, is needed, a more powerfull computer should be used for the calculation. In order to assure the reliability of the results the grain material modelled in the program needs to be related to the laboratory tests.

## 5    RAZŠIRJEN POVZETEK V SLOVENŠČINI

### 5.1 Uvod

### 5.1.1 Motivacija

Uporaba grobo zrnatega materiala je v geotehniki zelo razširjena zaradi njegove velike prepustnosti in visokih vrednosti tako trdnostnih kot tudi togostnih karakteristik. Trdnost grobo zrnatega agregata je normalno dovolj velika, tako da pri povečanih obremenitvah ni pričakovati večjih sprememb pri sami zrnavostni sestavi kot tudi pri mehanskih lastnostih materiala. Vendar pa se v geotehniki srečamo tudi s primeri, ko so napetosti znotraj samega materiala zelo visoke, na primer pri gradnji visokih zemeljskih pregrad (Marsal, 1967) in v primerih globokega temeljenja, kjer se uporablja metoda vtiskanja pilotov (Lobo-Guerrero, Vallejo, 2007). V takih primerih se lahko zgodi, da bo presežena trdnost uporabljenega materiala in se bo njegova sestava pričela spreminjati in z njo tudi njegove mehanske lastnosti. Zaradi teh sprememb prihaja do zmanjšanja prepustnosti materiala, do dodatnih posedkov in ne nazadnje do zmanjšanja strižnega kota samega materiala. Seveda pa do takih situacij ne prihaja zgolj pri geotehničnih objektih, temveč lahko do pojava drobljenja materiala prihaja tudi pri naravnih pojavih, kot so zemeljski plazovi (Gerolymos, Gazetas, 2007).

V naravi se večinoma srečujemo z grobozrnatim materialom z visoko trdnostjo agregata, pri katerem do sprememb v zrnavostni sestavi prihaja šele pri visokih napetostih. Vendar pa nemalokrat pridemo v stik tudi s peski, pri katerih je trdnost samega agregata razmeroma nizka in lahko spremembe mehanskih karakteristik materiala povzročajo že razmeroma nizke napetosti. Primeri takih materialov so peski iz npr. piroklastičnega materiala, preperelega granita.

Zaradi spremenljivih lastnosti takega materiala in predvsem njegovega na prvi pogled nepredvidljivega obnašanja, marsikdo podvomi v ustreznost njegove uporabe.  Vendar v večini primerov take materiale odlikuje nizka specifična teža v povezavi z visokimi vrednostmi trdnostnih karakteristik. To pa sta verjetno tudi glavna razloga, da nemalo raziskovalcev nameni svojo pozornost raziskovanju obnašanja takega materiala. Cilj projektiranja je v naprej predvideti obnašanje konstrukcij. Da bi to lahko naredili, je potrebno razumevanje fizikalnih procesov, do katerih prihaja pri povišanih napetostih v grobo zrnatih materialih.

### 5.1.2 Struktura raziskave

Drobljenje agregata je pojav pri katerem lastnosti na nivoju zrna vplivajo na obnašanje celotnega materiala, zaradi česar je raziskava sestavljena iz dveh delov. Prvi del predstavlja analiza serije preskusov opravljenih v laboratoriju, pri katerih so bili vzorci izpostavljeni različnim napetostnim potem, in sicer:

- izotropna obremenitev vzorca,

- vertikalna obremenitev vzorca s preprečenimi vodoravnimi pomiki (Edometerski preskus),
- vertikalna obremenitev vzorca pri konstantnem celičnem tlaku,
- vertikalna obremenitev vzorca pri konstantni srednji vrednosti efektivne napetosti.

Vsi omenjeni testi so bili opravljeni na vzorcih z različnimi začetnimi zrnavostnimi sestavami. Z namenom enostavnejše primerjave je bila vsem vzorcem v posamezni seriji (skupno 3 serije) skupna končna vrednost srednje efektivne napetosti.

Ker je za razumevanje pojava drobljenja pomembno tudi razumevanje obnašanja materiala na nivoju posameznega zrna, je drugi del raziskave potekal z uporabo računalniškega programa PFC3D, ki deluje na osnovi metode ločenih končnih elementov. V tem delu raziskave so bili raziskani načini modeliranja drobljenja agregata v numerični simulaciji in opravljena analiza primernosti posameznega načina. Za način, ki je bil izbran za najbolj primernega, se je nato pripravil model skupaj s potrebnimi spremljajočimi meritvami. Na koncu se je pripravljen model preskusil, na podlagi dobljenih rezultatov pa so bile predlagane potrebne spremembe in izboljšave modela.

## 5.2 Laboratorij

### 5.2.1 Material

Peski, katerih agregat predstavlja material naravnega izvora, imajo v večini primerov razmeroma visoko trdnost agregata. Za raziskovanje vpliva drobljenja pri takih materialih bi bilo potrebno preskuse opraviti pri izredno visokih napetostih, za kar bi bila potrebna uporaba visokotlačnih preskusnih naprav. Alternativna možnost uporabi peskov z visoko trdnostjo agregata in visoko tlačnih preskusnih naprav je uporaba agregata z nizko trdnostjo. Pri takem agregatu se drobljenje pojavi že pri napetostih, ki so jih sposobne zagotoviti standardne preskusne naprave. V ta namen se je za potrebe laboratorijskih testov uporabil umeten material znan pod komercialnim imenom LECA (Light Expanded Clay Agreggate). Glavni značilnosti uporabljenega materiala sta visoka vrednost strižnega kota in nizka navidezna specifična teža. Slednja je posledica izgorevanja organskega materiala med procesom segrevanja materiala. Značilna oblika LECA-e je posledica posebnega proizvodnega cikla, pri katerem se razpadel glinen material med segrevanjem v rotacijski peči oblikuje v okrogla zrna. Zaradi omejenosti z velikostjo preskušanca je bil za namene te raziskave uporabljen agregat velikosti 0-2 mm, ki pa je za razliko od običajnega LECA agregata drobljen in zaradi tega mnogo bolj ostrorob. Ostrorobost je lepo vidna na sliki 5.1.

Razlog za uporabo izraza »navidezna specifična teža« omenjenega v prejšnjem odstavku, je, da se delež por spreminja v odvisnosti od velikosti zrna. Na sliki 5.1 je prikazanih nekaj posnetkov zrn različnih velikosti, na katerih se lepo vidi, kako se delež por spreminja z velikostjo zrna.
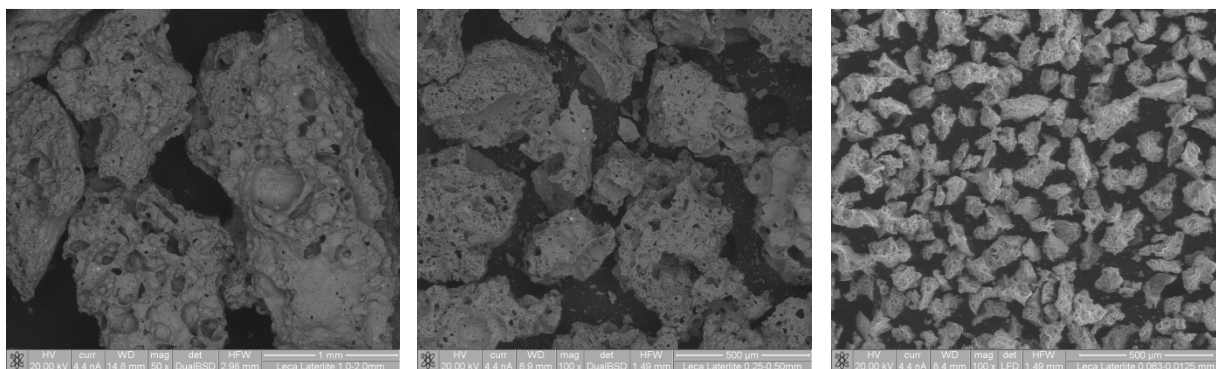
| 1 – 2 mm (mag.: 50 x) | 0.25 – 0.5 mm (mag.: 100 x) | 0.063 – 0.125 mm (mag.: 100 x) |

**Slika 5.1: Slike zrn različnih velikosti, na katerih sta lepo vidni poroznost značilna za LECA-o in ostrorobost agregata, ki je razlog za visok strižni kot materiala**

Zaradi spreminjanja deleža por se spreminja tudi navidezna specifična teža materiala, kar se lahko opiše z eksponentno funkcijo (Casini & Viggiani, 2011):

$$\gamma_s = a \cdot d^{-b} = 12.64 \cdot d^{-0.268} \text{ za } d \geq 0.063 \text{ mm} \tag{5-1}$$

$\gamma_s$ – navidezna specifična teža [kN/m$^3$]

$a, b$ – parametra za prilagajanje funkcije

$d$ – premer zrna [mm]

### 5.2.2 Mejna zrnavostna sestava

Pri obravnavanju drobljenja agregata se pojavlja vprašanje, ali obstaja neka mejna zrnavostna sestava, kateri se približujejo zrnavostne sestave obremenjenega materiala. V preteklosti je bilo predlaganih več različnih primerov mejnih zrnavostnih sestav. Primer ene od njih je glinen material, ki je, kot je predvideval Hardin (1985), posledica povečevanja števila kontaktov s sosednjimi zrni ter povečevanja števila nepravilnosti z velikostjo zrna. Hardin je predvideval, da se s povečevanjem rezultante kontaktnih sil, ki delujejo na zrno, povečuje tudi verjetnost drobljenja agregata. V zadnjem času pa ima vse več zagovornikov teorija, ki trdi, da se s povečevanjem števila kontaktov povečuje enakomernost porazdelitve napetosti znotraj zrna.

Posledica te teorije je, da se z drobljenjem velikost večjih zrn le malenkostno zmanjšuje, medtem ko se zrnavostna sestava na območju manjših zrn močno spreminja. Ker vsaka pora (nepravilnost) pomeni oslabitev materiala, material med drobljenjem strmi k čim boljši zapolnitvi prostora. Fuller in Thompson (1907) sta pokazala, da je zrnavostna sestava, ki najbolje zapolni prostor, fraktalna. Še več pokazala sta, da ima taka zrnavostna sestava fraktalno dimenzijo 2,5. To specifično zrnavost lahko zapišemo z naslednjo enačbo (Casini in Viggiani, 2011):

$$N(d > \Delta) = C \cdot \Delta^{-\alpha} \tag{5-2}$$

Kljub temu, da je teorija o mejni fraktalni distribuciji splošno sprejeta, pa njena fraktalna dimenzija še ni povsem določena. Zaradi tega je bilo za namen raziskave predpostavljeno, da je mejna zrnavostna sestava tista končna zrnavostna sestava, ki bo imela največji koeficient enakomernosti. Taka končna zrnavostna sestava ima fraktalno dimenzijo 2,39. Na tem mestu pa je potrebno poudariti, da je, pri materialu kot je LECA, potrebno razlikovati med zrnavostno sestavo vrednoteno po prostornini in zrnavostno sestavo vrednoteno po teži. Primerjava obeh načinov vrednotenj je predstavljena v naslednji točki.

### 5.2.3 Spremljanje spreminjanja zrnavostne sestave

Za potrebe vrednotenja količine drobljenja je potreben parameter, ki bo predstavljal razliko med začetno in končno zrnavostno sestavo. Kadar govorimo o zrnavostni sestavi običajnih peskov, ne razlikujemo med zrnavostno sestavo vrednoteno po prostornini in zrnavostno sestavo vrednoteno po teži. Razlog za to je konstantna specifična teža. Pri LECA-i pa se navidezna specifična teža spreminja z velikostjo zrna, zato je potrebno zrnavostno sestavo vrednoteno po teži glede na zrnavostno sestavo vrednoteno po prostornini utežiti s funkcijo, ki opisuje spreminjanje navidezne specifične teže (5-1). Za fraktalno zrnavostno sestavo velja, da jo lahko opišemo z naslednjima funkcijama:

$$F_V(d) = \left(\frac{d}{d_{max}}\right)^{\beta_V} \quad \text{in} \quad F_W(d) = \left(\frac{d}{d_{max}}\right)^{\beta_W} \tag{5-3}$$

$F_V$ – kumulativna funkcija zrnavostne sestave vrednotene po prostornini

$F_W$ - kumulativna funkcija zrnavostne sestave vrednotene po teži

Pri čemer je $\beta_V$ funkcija fraktalne dimenzije, $\beta_W$ pa funkcija tako fraktalne dimenzije in parametra $b$, ki določa hitrost spreminjanja navidezne specifične teže:

$$\beta_V = 3 - \alpha \tag{5-4}$$

$$\beta_W = \beta_V - b \tag{5-5}$$

Potencial drobljenja, ki ga ima zrnavostna sestava, je definiran kot površina med krivuljo začetne zrnavostne sestave po prostornini in krivuljo mejne zrnavostne sestave po prostornini, in je poenostavljeno izražen kot:

$$B_p = 0.434 \cdot \left(\frac{1}{\beta_u} - \frac{1}{\beta_0}\right) \tag{5-6}$$

Celotno drobljenje, ki se izvrši v posameznem vzorcu, je definirano kot površina med krivuljo začetne zrnavostne sestave po prostornini in krivuljo končne zrnavostne sestave po prostornini, in je poenostavljeno izraženo kot:

$$B_t = 0.434 \cdot \left( \frac{1}{\beta} - \frac{1}{\beta_0} \right) \qquad (5\text{-}7)$$

Koliko drobljenja relativno glede na potencial se je izvršilo pa lahko zapišemo z:

$$B_r = \frac{B_t}{B_p} \qquad (5\text{-}8)$$

### 5.2.4 Program testov

Analiza, predstavljena v tem diplomskem delu, je del razširjene raziskave, ki poteka na inštitutu ETH IGT. Cilj analize je izboljšanje razumevanja vpliva različnih napetostnih poti in začetnih zrnavostnih sestav na drobljenje agregata. S tem namenom so bili poleg triosnih preskusov pri konstantni srednji vrednosti efektivne napetosti (TXP) v analizo vključeni tudi rezultati drugih študentov. Wanninger in Pascal sta opravila preskuse v oedometru (OED), medtem ko so Leu, Low in Zimmermann vzorce izpostavili izotropni obremenitvi ter opravili triosne preskuse pri stalnem celičnem tlaku.

Podatki o vzorcih, ki so bili pripravljeni z različnimi začetnimi zrnavostnimi sestavami, so zbrani v spodnji preglednici.

**Preglednica 5.1: Parametri za določitev izhodiščnih zrnavostnih krivulj**

| $U_W$ | $d_{50,W}$ [mm] | $\beta_W$ | $d_{max,W}$ [mm] | $\beta_V$ | $d_{max,V}$ [mm] | $U_V$ | $d_{50,V}$ [mm] | $B_{p,V}$ |
|---|---|---|---|---|---|---|---|---|
| 3.5 | 0,5 | 1,43 | 0,81 | 1,69 | 081 | 2,89 | 0,54 | 0,45 |
| 7 | 0,5 | 0,92 | 1,06 | 1,16 | 1,06 | 4,7 | 0,58 | 0,34 |
| 14 | 0,5 | 0,68 | 1,39 | 0,89 | 1,39 | 7,48 | 0,64 | 0,22 |
| 28 | 0,5 | 0,54 | 1,81 | 0,75 | 1,81 | 10,9 | 0,72 | 0,13 |

Kot je razvidno, so bili vzorci pripravljeni s konstantno velikostjo zrna $d_{50}$ glede na masno zrnavostno sestavo in z različnimi začetnimi vrednostmi koeficienta enakomernosti.

Vzorci z začetnimi koeficienti enakomernosti ($U_W$) 3,5, 14 in 28 so bili izpostavljeni vsem štirim napetostnim potem, medtem ko so bili na vzorcih z $U_W = 7$ opravljeni le edometerski preiskusi in triosna obremenitev vzorca pri konstanti srednji vrednosti efektivne napetosti. Na sliki 5.2 je prikazan program napetostnih poti:
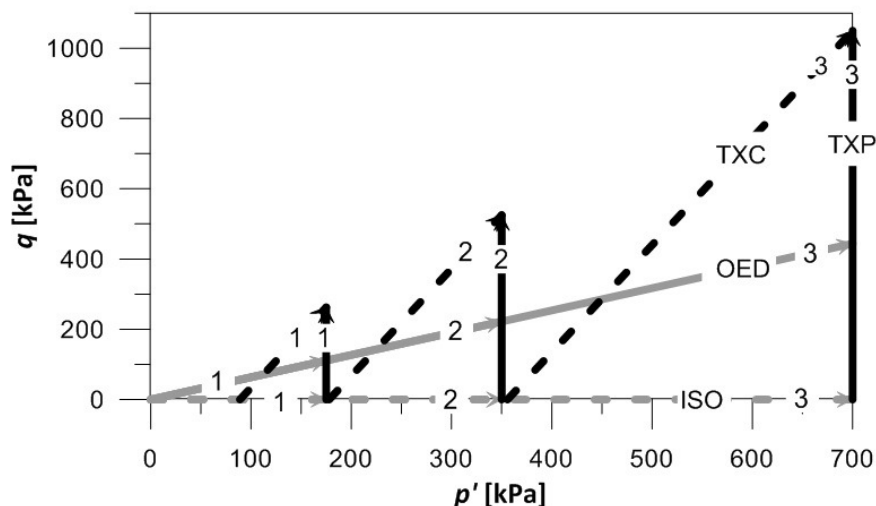
**Slika 5.2: Program napetostnih poti**

## 5.2.5 Analiza rezultatov

### 5.2.5.1 Vpliv napetostne poti

Rezultati izotropne obremenitve vzorcev kažejo, da srednja vrednost efektivne napetosti nima direktnega vpliva na spreminjanje zrnavostne strukture ne glede na začetno vrednost koeficienta enakomernosti. V vzorcu, ki je obremenjen enakomerno v vseh smereh, je enakomerno obremenjen tudi agregat, zaradi česar ne prihaja do povečanih nateznih napetosti v prečni smeri. Hkrati pa vzorec zaradi značilnosti napetostne poti ni izpostavljen strižnim deformacijam, ki bi povzročile krušenje robov. Na spodnji sliki so prikazane krivulje zrnavostne sestave pred in po opravljenih preizkusih:
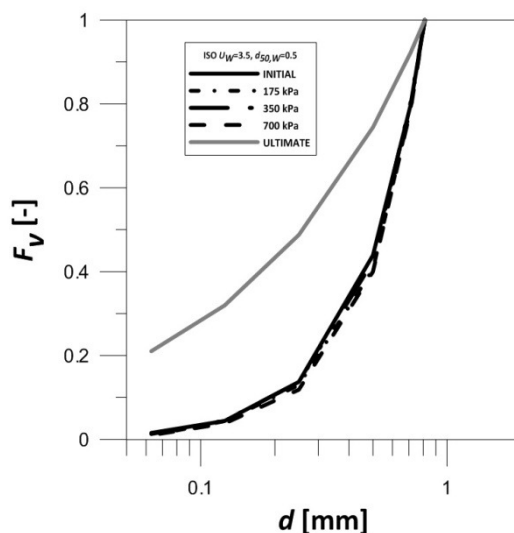


**Slika 5.3: Volumska zrnavostna sestava po izotropni tlačni obremenitvi za vzorec z $d_{50,W} = 0,5$ mm $U_W = 3,5$ (Leu, 2011)**

Nekatere izmed končnih krivulj na zgornjem grafu so pod krivuljo začetne zrnavostne sestave, kar pa je fizikalno nemogoče. Pojav je posledica napak, do katerih prihaja pri odvzemu vzorca preizkuševalne naprave in pri sejalni analizi.

Za razliko od izotropne obremenitve vzorca pri OED, TXC in TXP preizkusih prihaja do opazne razlike med začetno in končno zrnavostno sestavo. Ti rezultati kažejo na vpliv deviatoričnih napetosti in strižnih deformacij na pojav drobljenja.



a) OED, $U_W = 3,5$          b) TXC, $U_W = 3,5$          c) TXP, $U_W = 3,5$
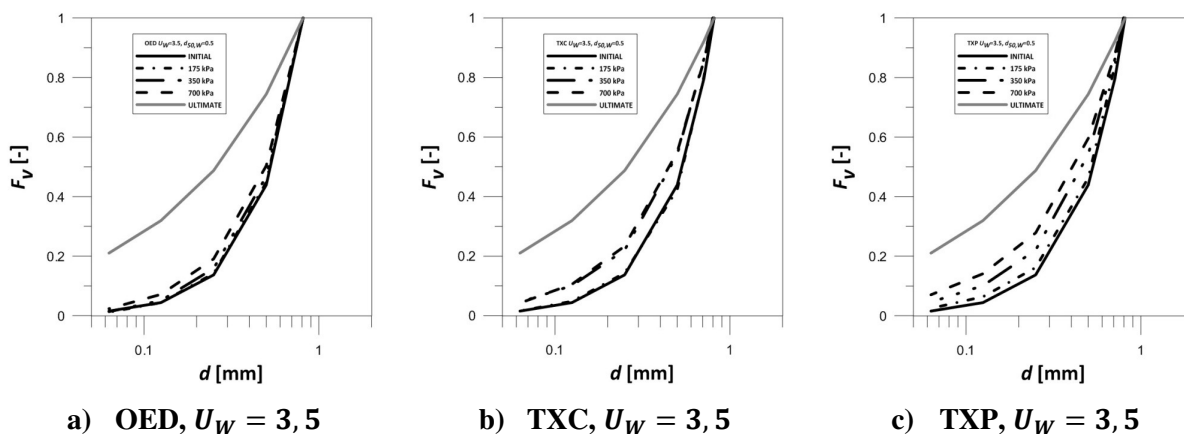
**Slika 5.4: Primerjava količine drobljenja za različne napetostne poti**

Na sliki 5.4 je razvidno, kako različne napetostne poti vplivajo na količino drobljenja, ki se izvrši v posameznem vzorcu. Poleg tega je lepo vidno tudi, kako se velikost maksimalnega zrna, kljub opazni količini drobljenja, skoraj ne spreminja. Ta rezultat potrjuje teorijo, ki govori o zmanjšanem drobljenju pri večjih zrnih zaradi povečanega števila kontaktov s sosednjimi zrni. Povečano število kontaktov preprečuje pojav nateznih napetosti v zrnu, hkrati pa zaradi povečane kontaktne površine zmanjšuje tudi kontaktne normalnih napetosti. Zaradi zmanjšanja slednjih se zmanjša tudi kontaktna strižna trdnost. Dokler je vrednost kontaktne strižne trdnosti nižja od strižne trdnosti agregata, ne prihaja do krušenja robov, temveč se zrna zgolj prerazporejajo.

Parametri, ki vplivajo na količino drobljenja, so torej:

- deviatorične napetosti – povečujejo neenakomernost obremenitve zrna,
- srednja efektivna napetost – povečuje kontaktne napetosti,
- strižne deformacije – povzročajo relativne premike zrn,
- število medzrnskih kontaktov – zmanjšujejo natezne napetosti znotraj zrna in povečuje razporejanje obremenitve na nivoju zrna.

Na sliki 5.5 so prikazane vrednosti maksimalnega zrna pred in po opravljenih TXP preskusih. Lepo je vidno, kako se velikost maksimalnega zrna zmanjšuje s povečevanjem vrednosti koeficienta enakomernosti ($U$) ter srednje vrednosti efektivne napetosti. To namiguje na obstoj dveh stopenj drobljenja. Med prvo stopnjo, ki traja vse dokler zrnavostna krivulja ne doseže mejne, je velikost

maksimalnega zrna konstantna. Ko je mejna krivulja dosežena, so vsa zrna enakomerno obremenjena. Ker pa za večja zrna velja, da imajo več nepopolnosti, se med drugo stopnjo pričnejo drobiti tudi večja zrna.
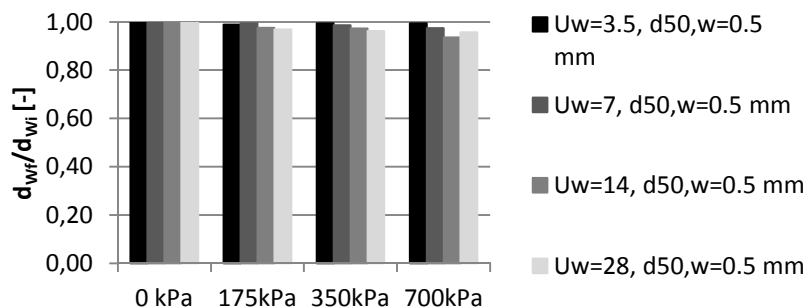


**Slika 5.5: Zmanjševanje velikosti maksimalnega zrna s povečevanjem srednje efektivne napetosti**

### 5.2.5.2 Vpliv začetne zrnavostne sestave

Ena od glavnih lastnosti, ki vplivajo na količino drobljenja, je zrnavostna sestava. Kot je omenjeno že v poglavju 5.2.5.1, je drobljenje v veliki meri odvisno od števila medzrnskih kontaktov. To število je v direktni povezavi z zrnavostno sestavo. Večji kot je koeficient enakomernosti materiala, večje je število kontaktov, s tem pa se zmanjšuje potencial za drobljenje. Eden izmed načinov opisa potenciala drobljenja je površina med krivuljo začetne zrnavostne sestave in krivuljo mejne zrnavostne sestave.



a)                                                                  b)
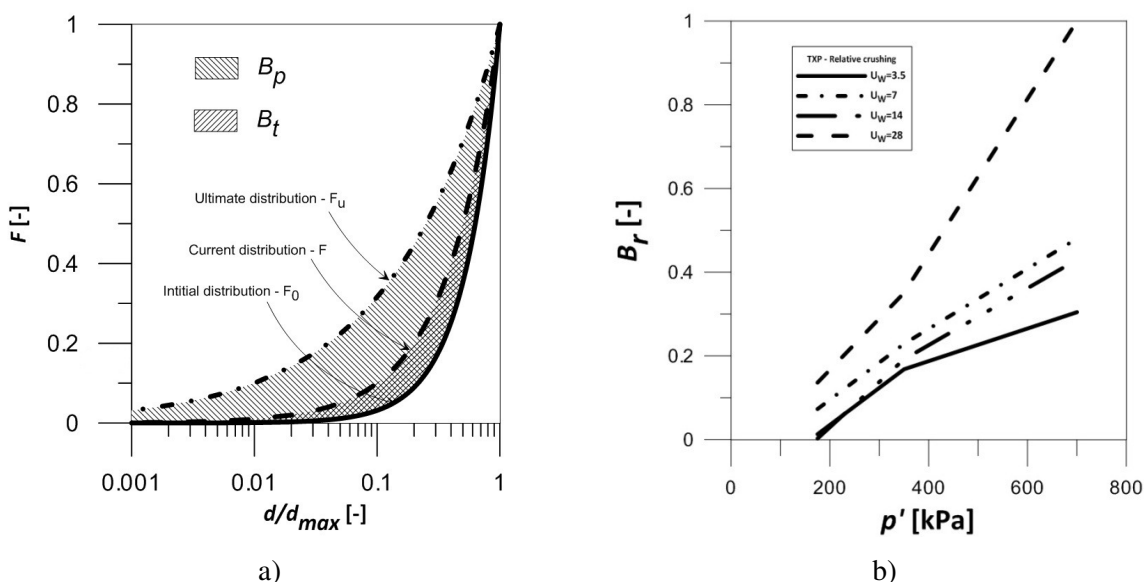
**Slika 5.6: a) Definicija potenciala drobljenja ($B_p$) in celotnega drobljenja ($B_t$), b) Relativno drobljenje ($B_p$) za primer TXP preskusa**

Slika 5.6 b) prikazuje kako je relativno drobljenje, ki je definirano kot:

$$B_r = \frac{B_t}{B_p} \tag{5-9}$$

odvisno od potenciala drobljenja. Na sliki sta vidni tudi dve anomaliji:

- preskus na vzorcu $U_W = 3,5$ pri $p' = 700$ kPa ni dosegel strižne trdnosti, saj je preskusna naprava dosegla maksimalen možen pomik,

- vzorci z $U_W = 28$ so dosegali velike vrednosti drobljenja (tako relativnega kot tudi celotnega), za kar ni bilo najdene ustrezne razlage.

### 5.2.5.3 Prostorninske spremembe

Za teorijo kritičnega stanja je značilno, da se ob dosegu kritične napetosti prostorninske spremembe prenehajo spreminjati. Samo iz diagrama $q : \varepsilon_s$ ni mogoče povedati, ali je bilo ob porušitvi doseženo kritično stanje. Za preskuse opravljene na materialu, ki med obremenjevanjem doživi spremembo zrnavostne sestave, se je izkazalo, da se ob dosegu strižne trdnosti prostorninske spremembe še niso umirile. Gradient spreminjanja prostornine ob koncu preskusa je odvisen od koeficienta enakomernosti začetne zrnavosti ter končno srednjo efektivno napetostjo. Z zmanjševanjem vrednosti $U$ in povečevanjem $p'$ se gradient ob dosegu strižne trdnosti povečuje, kar kaže na povečano količino drobljenja, ki se je izvršila v vzorcu. Kritični količnik por, ki je odvisen od zrnavostne sestave, se namreč z drobljenjem zmanjšuje, zato so potrebne večje prostorninske spremembe.

### 5.2.5.4 Redukcija strižnega kota

Za strižni kot je značilno, da je odvisen od zrnavostne sestave materiala in njegove ostrorobosti, medtem ko se s povečevanjem srednje efektivne napetosti ne spreminja. Ker se pri materialu z nizko trdnostjo agregata zrnavostna sestava in ostrorobost spreminjata, je pričakovati, da se bo temu primerno spreminjal tudi strižni kot. S povečevanjem srednje efektivne napetosti in posledično povečevanjem količine drobljenja se strižni kot zmanjšuje. S tem, ko se zrna znotraj vzorca drobijo, se povečuje koeficient enakomernosti, zato je zanimivo, da vzorci z večjim začetnim koeficientom enakomernosti dosegajo višje vrednosti strižnega kota. Kot je razvidno iz preglednice 5.1 imajo vzorci z različnimi koeficienti enakomernosti različne vrednosti $d_{max}$. Na sliki 5.8 pa je prikazano, kako se strižni kot s povečevanjem velikosti zrna povečuje. Zaradi tega je mogožno sklepati, da je povečan strižni kot pri vzorcih z višjimi vrednosti koeficienta enakomernosti posledica povečevanja velikosti maksimalnega zrna.
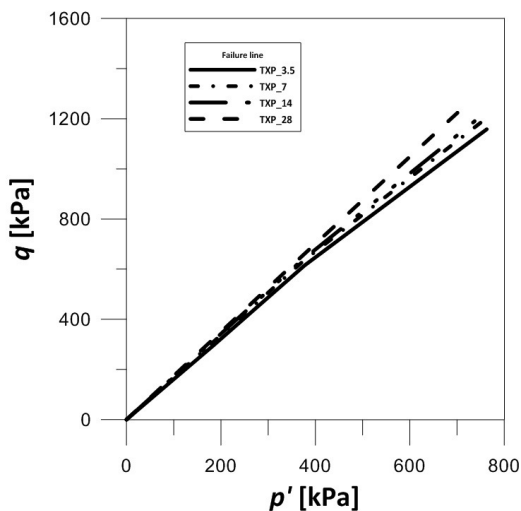
**Slika 5.7: Porušne linije za različne začetne zrnavosti**
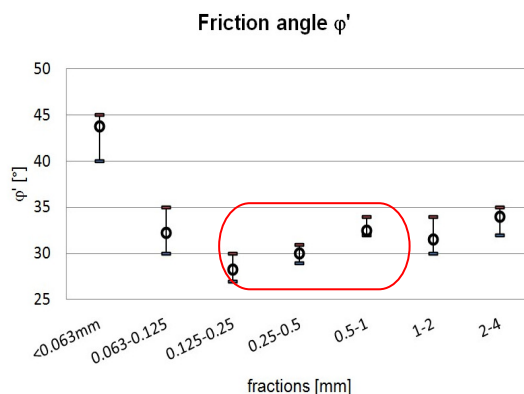


**Slika 5.8: Odvisnost strižnega kota od velikosti zrna**

## 5.2.6 Model

### 5.2.6.1 Drobljenje

Na podlagi rezultatov je bil pripravljen enostaven model, ki opisuje obnašanje drobljivega materiala. Pri formulaciji modela, se je poskušalo upoštevati, da bi čim bolje opisoval tudi samo fizikalno dogajanje med drobljenjem.

Za relativno drobljenje se je izkazalo, da je razmeroma neodvisno od začetne zrnavosti, da pa njegova vrednost v večji meri odvisna od napetostne poti, kateri je vzorec izpostavljen. Zaradi tega se je za posamezno napetostno pot določilo funkcijo, ki opisuje odvisnost relativnega drobljenja od končne vrednosti srednje efektivne napetosti. Omenjena funkcija je bila dobljena kot povprečje funkcij, ki opisujejo naraščanje drobljenja za posamezno začetno zrnavostno strukturo. Omenjene funkcije so prikazane na sliki 5.11
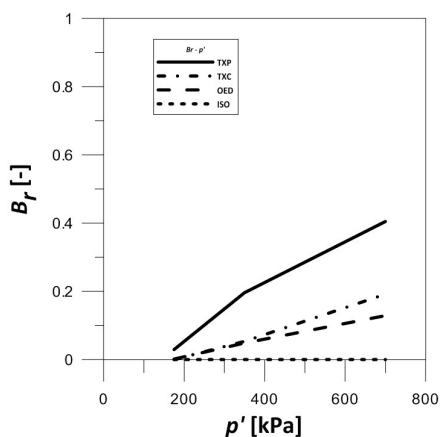


**Slika 5.9: Primerjava relativnega drobljenja kot funkcija napetostne poti in končne srednje efektivne napetosti**
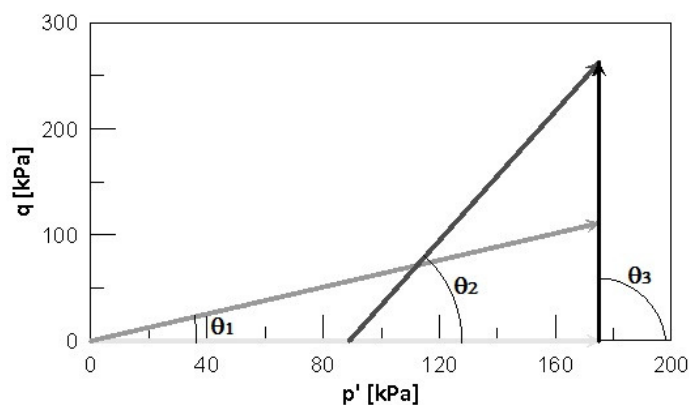


**Slika 5.10: Definicija naklona napetostne poti $\theta$**

Iz analize, ki je predstavljena v točki 5.2.6, je razvidno, da je količina drobljenja odvisna predvsem od napetostne poti in potenciala drobljenja začetne zrnavostne sestave. Zaradi tega se funkcija, ki opisuje drobljenje vzorca, lahko zapiše na naslednji način:

$$B_r = k(\theta) \cdot \ln[f(p')] + n(p'_{br\_start}) \qquad\qquad (5\text{-}10)$$

$\theta$ – naklon napetostne poti, kot je prikazano v sliki 5.11

$p'$ – končna vrednost srednje efektivne napetosti pri posamezni napetostni poti

$p'_{br\_start}$ – končna vrednost srednje efektivne napetosti pri posamezn napetostni poti pri kateri se zrna pričnejo drobiti

Vpliv napetostne poti je v enačbi zajet v parametrih $\theta, p'$ in $p'_{br\_start}$, medtem ko je vpliv potenciala drobljenja zajet z dejstvom, da enačba (5-10) določa vrednosti relativnega drobljenja.

### 5.2.6.2 Strižni kot

Kot je bilo že omenjeno, za strižni kot velja, da je odvisen od zrnavostne sestave ter ostrorobosti agregata. Vpliva omenjenih parametrov na strižni kot se lahko seštevata ali pa se med seboj izničita. Pripravljen model je razmeroma enostaven, zato je predpostavljeno, da je ostrorobost konstantna ne glede na velikost zrna, in je torej strižni kot odvisen zgolj od zrnavostne sestave materiala. Za tak primer velja, da je strižni kot direktna funkcija relativnega drobljenja in se lahko zapiše na naslednji način:

- $M' = M'_{ini} \quad for \quad p' < p'_{br\_start}$
- $M'(p', \theta) = M'_{ini} + \left(M'_{fin} - M'_{ini}\right) \cdot Br(p', \theta)$
  $\rightarrow for \quad p'_{br\_start} \le p' \le p'_{br\_stop}$     (5-11)
- $M' = M'_{fin} \quad for \quad p'_{br\_stop} < p'$

$M'(p', \theta)$ – razmerje $q/p'$ ob porušitvi za $p'_{br\_start} < p' < p'_{br\_stop}$

$M'_{ini}$ – razmerje $q/p'$ ob porušitvi za $p' < p'_{br\_start}$

$M'_{fin}$ – razmerje $q/p'$ ob porušitvi za $p' > p'_{br\_stop}$

Porušna ovojnica, ki je določena s funkcijo (5-11), predstavlja strižno trdnost zemljine. Vendar pa ne opisuje kritičnega stanja, saj je gradient prostorninskih sprememb različen od nič, kar pomeni da se bo zrnavostna sestava in s tem strižni kot, s povečevanjem strižnih deformacij še naprej spreminjala.

### 5.2.6.2 Primerjava modela z rezultati

Na spodnji sliki je prikazana primerjava vrednosti relativnega drobljenja, dobljenih z laboratorijskimi testi, z vrednostmi izračunanih z modelom. Razen v primeru TXC je doseženo razmeroma dobro ujemanje. Kot je prav tako razvidno, so bile za parameter $p'_{br\_start}$ uporabljene različne vrednosti. Glede na to, da je količina drobljenja, pri določeni končni vrednosti srednje efektivne napetosti, odvisna od napetostne poti, enako velja tudi za najnižjo vrednost srednje efektivne napetosti, ki povzroča drobljenje.
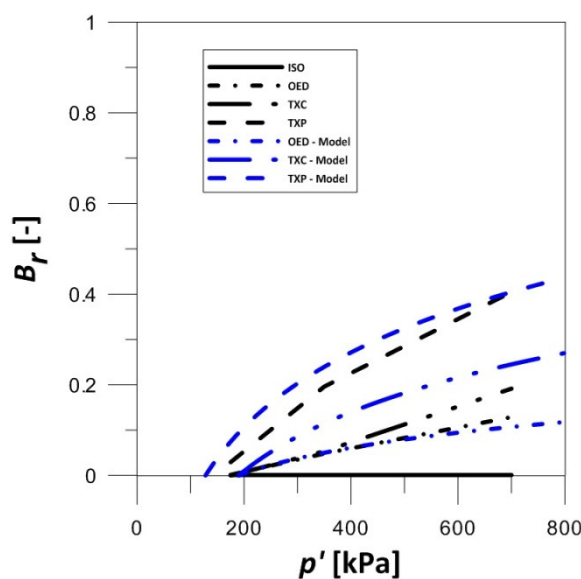


**Slika 5.11: Primerjava računskega modela z rezultati laboratorijskih testov**

### 5.2 Računalniški model

Pri razlaganju naravnih pojavov, kot je drobljenje, kjer spreminjanje lastnosti na nivoju zrna vplivajo na obnašanje celotnega vzorca, je zelo primeren pripomoček računalniško modeliranje samega pojava. Pri računalniškem modelu je namreč mogoče spremljati obnašanje vsakega posameznega zrna, ne da bi pri tem vplivali na obnašanje samega vzorca. Seveda se je pri tem potrebno zavedati, da imaš opravka z računalniškim modelom, ki le v večji ali manjši meri opisuje dejansko obnašanje modeliranega materiala. Z željo, da bi se poglobilo razumevanje pojava drobljenja, se je v računalniškem programu PFC3D, ki deluje na principu ločenih elementov, pripravil model drobljenja agregata.

Najprej so se za potrebe numerične simulacije raziskale različne možnosti modeliranja drobljenja v programu. Izmed vseh možnosti zasledenih v literaturi sta se preizkusili dve izmed njih, nato pa se je za primernejšo pripravil celoten model s spremljajočimi meritvami. Model je na kratko predstavljen tudi v tem povzetku, teoretično ozadje programa in opis ostalih načinov pa je natančneje opisano v angleškem delu diplome.

### 5.2.1 Obremenjevanje vzorca

Za potrebe obremenjevanja vzorca se je pripravil mehanizem, ki na posamezni površini vzorca vsiljuje predvideno napetost oz. pomik. Osnovo je predstavljal mehanizem, pripravljen s stani podjetja Itasca group (2004), ki na mejni ploskvi zagotovi zahtevano napetost. Za potrebe simulacije se je predvidela uporaba deformacijsko vodenega preskusa. Cilindrični vzorec se je na zgornji in spodnji ploskvi obremenjeval s stalno hitrostjo, medtem ko se je vektor hitrosti cilindrične mejne ploskve prilagodil vsakih nekaj korakov.

### 5.2.2 Modeliranje zrna

Najbolj primeren način modeliranja drobljenja za potrebe raziskave je bil s pomočjo gruč. Gruča je zrno, ki je sestavljeno iz več osnovnih sferičnih elementov, ki so med seboj povezani z vezmi. Na ta način je mogoče modelirati zrna različnih oblik. Najprej so se v škatlo kubične oblike, katere dimenzije so bile večje od predvidene velikosti zrna, zgenerirali osnovni elementi ter se povezali z vzporednimi vezmi (obstaja tudi možnost kontaktnih vezi). Nato pa so se zrna, ki so bila izven volumna, ki je določal obliko zrna, izbrisala. Zaradi enostavnosti modela so se modelirala zgolj zrna sferične oblike.

Lastnosti tako pripravljenih zrn so se preverile z brazilskim testom, ki se tudi v laboratoriju ponavadi uporablja za določitev trdnostnih in togostnih karakteristik zrna. Lokacija posameznih osnovnih elementov in vezi glede na težišče zrna se je shranila v pomnilnik računalnika ter se kasneje med pripravo vzorca ponovno priklicala.

### 5.2.3 Priprava vzorca

Izvajanje simulacij zahteva veliko računalniškega pomnilnika, kar hkrati pomeni tudi dolge računske čase. Zato je potrebno, če se le da, pripravo modela kot tudi sam model poenostaviti. Med samo pripravo vzorca se je tako namesto vsake izmed gruč v prvih fazah uporabil po en osnovni element, katerega velikost je bila enaka velikosti gruče. S tem se, na primer za eno zrnat material, število osnovnih delcev iz 40 000 zmanjšalo na zgolj 400.

V vzorec sferične oblike so se najprej zgenerirali (naključno izbrana lokacija) osnovni elementi, tako da se med seboj niso prekrivali. Zaradi zmanjšanja števila poskusov se je začetni radij osnovnih elementov reduciral z določenim faktorjem, ko pa so bila vsa zrna zgenerirana se je njihov radij povečal, pri čemer so se lahko delci prosto prerazporedili. Število delcev modeliranih v vzorec se je izračunalo na podlagi zahtevane poroznosti. Po uravnoteženju vzorca se je vključil mehanizem za določitev napetostnega stanja v vzorcu, ki je bilo v začetku določeno kot 50 kPa. Po dosegu izbrane

napetosti so se osnovni elementi izbrisali, na njihova mesta pa so se vstavile gruče, katerih relativna lokacija je bila shranjena v pomnilniku računalnika. Zaradi malenkostne razlike v velikosti gruč in predhodnje uporabljenih osnovnih elementov se je pred pričetkom preskusa opravilo še nekaj računskih korakov, tako da se je ponovno vzpostavilo izotropno napetostno stanje pri 50 kPa. Med tem časom je bila trdnost delcev močno povečana, tako da se zrna niso mogla drobiti oz. krušiti. Po ponovnem uravnoteženju vzorca se je trdnost gruč zmanjšala na predvideno vrednost. V naravi se trdnost z zmanjševanjem zrn povečuje, saj se s tem zmanjšuje delež napak v materialu. Hkrati pa tudi trdnost dveh enako velikih zrn ni enaka, temveč se spreminja v odvisnosti od količine napak v materialu. Da bi se material čim bolj natančno opisal, se je variiranje trdnosti modeliralo s pomočjo Weibullove verjetnostne funkcije:

$$\sigma = \sigma_0 \cdot \sqrt[m]{\left(\frac{d_0}{d}\right)^3 \cdot \ln\frac{1}{P_s}} \qquad\qquad (5\text{-}12)$$

kjer je $\sigma$ trdnost izbranega zrna velikosti $d$ in se izračuna na podlagi trnosti nominalnega zrna ($\sigma_0$) velikosti $d_0$, pri čemer $P_s$ pomeni verjetnost, da bo zrno velikosti $d$ preneslo napetost velikosti $\sigma$.

Tako pripravljen vzorec se je nato postopoma obremenil do želene srednje efektivne napetosti, pri kateri se je izvedel strižni preskus.

### 5.2.3 Optimizacija modela

Kot je bilo že omenjeno, se s številom osnovnih elementov in modeliranih vezi močno povečuje tudi računski čas. Zaradi tega je bilo potrebno poiskati minimalno število gruč, minimalno število osnovnih elementov, ki sestavljajo gručo, in maksimalno hitrost, ki še ne vplivajo na rezultate simulacije. Izkazalo se je, da bi bil z uporabo teh kritičnih vrednosti računski čas še vedno prevelik, zato se je nadalje analiziral še vpliv izbranih vrednosti omenjenih parametrov na nevarni strani kritičnih vrednosti na rezultate simulacije. V nadaljevanju so prikazani diagrami vplivov posameznih parametrov na rezultate simulacije:
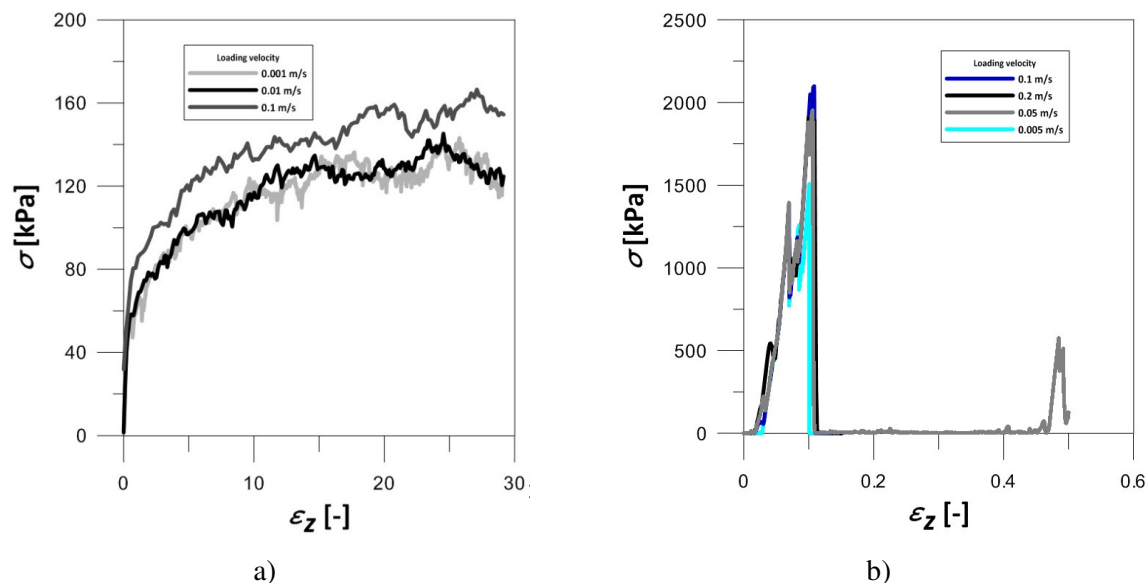
**Slika 5.12: Vpliv hitrosti obremenjevanja na obnašanje a) celotnega vzorca, b) gruče**
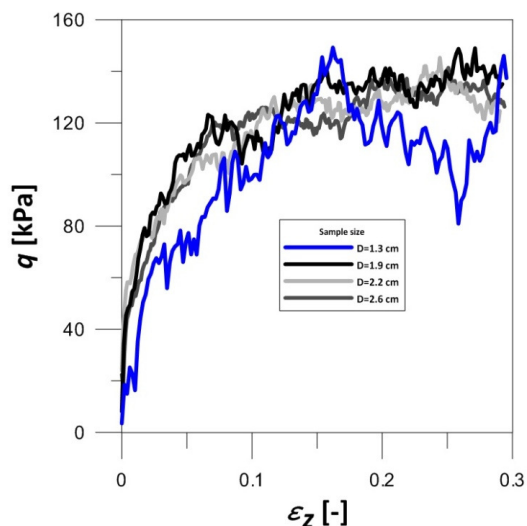


**Slika 5.13: Vpliv velikosti vzorca na rezultate simulacije**

Vse zgoraj prikazane simulacije so se izvajale na poenostavljenih modelih, kjer se je namesto gruče modeliral osnovni element. Seveda pa to ne velja za vpliv hitrosti obremenjevanja na obnašanje posamezne gruče. Za izvedbo simulacije so se izbrali parametri, tako da je celoten račun trajal 7 dni:

- hitrost obremenjevanja:             1 mm/s
- število osnovnih elementov v gruči:     104
- premer osnovnega elementa:          0,4 mm
- velikost zrna:                     višina = 2,6 cm

                                         premer = 1,3 cm $(6,5 \cdot d_{\max})$

Čeprav je računski čas še vedno razmeroma dolg, pa je model vseeno poenostavljen že do te mere, da zgoraj navedeni parametri vplivajo na rezultate. Z namenom izpopolnitve modela so se simulacije

vseeno izvršile, poleg tega pa na sam mehanizem drobljenja te poenostavitve niso imele večjega vpliva.

### 5.2.4 Meritve

Program PFC3D ima vgrajeno široko knjižnico parametrov, ki se jih lahko spremlja med izvajanjem simulacije. Za primere, kadar je potrebno meriti količino, ki ni vključena v knjižnico, pa ima program vgrajen programski jezik FISH, s katerim se spekter možnih meritev še precej razširi. Za potrebe simulacije drobljenja so se v sklopu priprave modela pripravili tudi algoritmi, ki med izvajanjem simulacije razločijo med posameznimi zrni ter merijo zrnavost in koordinacijsko število (število medzrnskih kontaktov za posamezno zrno).

Program obravnava osnovne elemente ločene, zato ne podaja direktne informacije o velikosti gruč. Ker se zrnavost med simulacijo spreminja, je bilo potrebno pripraviti algoritem, ki bi spremljal to spreminjanje. Skupaj z merjenjem same velikosti zrn se je pripravil tudi algoritem, ki v odvisnosti od velikosti zrna pripadajoče osnovne elemente tudi obarva, kar omogoča tudi nazorno vizualizacijo drobljenja.

Ker ima velik vpliv na drobljenje tudi koordinacijsko število, se je med samo simulacijo zbiralo podatke o kontaktih posameznih osnovnih elementov z ostalimi osnovnimi elementi, ki niso pripadali isti gruči. Nato pa se je v programu Matlab ob predpostavki, da imata dve gruči (zrni) med seboj lahko samo en kontakt, izvrednotilo koordinacijsko število posameznega zrna. To bi bilo mogoče opraviti tudi v samem programu PFC3D, vendar bi to drastično vplivalo na računski čas.

Ena od stvari, ki se v laboratoriju zdi samoumevna in enostavna, medtem ko pri izvajanju simulacije temu ni tako, je določanje zrnavostne sestave. Določanje velikosti in oblike zrn zahteva namreč precej zahtevne algoritme. Zato se je za potrebe pričujočega modela uporabila nekoliko poenostavljena metoda določanja velikosti zrn, in sicer se je določala povprečna oddaljenost osnovnih elementov od težišča gruče, ki ji pripadajo.

### 5.2.5. Analiza modela

Kljub temu da je model preveč poenostavljen in bodo parametri kot sta hitrost obremenjevanja in velikost vzorca vplivali na rezultate, se je simulacija vseeno izvedla. Po koncu pa so se rezultati analizirali in podale možne izboljšave. V programu se je izvedla simulacija triosnih strižnih preskusov pri konstanti vrednosti srednje efektivne napetosti ($p'$) in sicer pri treh različnih vrednostih $p'$ (87 kPa, 175 kPa in 350 kPa) ter pri dveh vrednostih koeficientov enakomernosti ($U = 1$ in $U = 28$).

Kot se je izkazalo, so koordinacijska števila posameznih zrn razmeroma velika, tako da ne prihaja do drobljenja zrn zaradi nateznih napetosti. V največji meri do drobljenja prihaja na kontaktih, kjer zaradi

visoke kontaktne strižne trdnosti prihaja do strižne porušitve v zrnih. Zaradi tega je pri eno zrnatem materialu možno opaziti velik porast drobnih zrn (en oz. dva povezana osnovna elementa).  Iz tega sledi, da je uporaba vzporednih vezi, ki so sposobne prenašati tudi momente, nepotrebna. Glavni razlog uporabe vzporednih vezi je bil namreč, da z njihovo uporabo lahko nazorno opišeš drobljenje celotnega zrna (kot v brazilskem testu). Vendar pa je posledica njihove uporabe mnogo večja uporaba računalniškega pomnilnika, približno 4-krat več. Z uporabo kontaktnih vezi bi verjetno drobljenje opisali povsem enakovredno.

Drug popravek pa se tiče same priprave modela. Kot je omenjeno v točki 5.2.3, se je vzorec pripravil s povečevanjem osnovnih elementov, ki so začasno nadomestili gruče. Pri tem se je vnaprej določil količnik por. Razlog za uporabo načina povečevanja osnovnih elementov je bil, da se na ta način doseže veliko bolj enakomerno pripravljen vzorec kot pri izotropnem obremenjevanju do določene napetosti. Iz značilnosti deviške krivulje pa je razvidno, da je za različne zrnavosti pri enakem količniku por pričakovati različne srednje vrednosti efektivne napetosti. V naslednjem koraku se je vzorec razbremenil do vrednosti srednje efektivne napetosti 50 kPa, zaradi česar so bili vzorci različno prekonsolidirani. Pri različno prekonsolidiranih vzorcih pa je primerjava drobljenja otežena, če ne celo onemogočena, saj je vpliv prekonsolidacije na drobljenje težko ločiti od preostalih vplivov. Zato se zdi bolj primeren način priprave vzorcev s pripravo po plasteh, ki bi se sproti utrdile do želene napetosti, na ta način bi se dosegel homogen vzorec in se hkrati izločil vpliv prekonsolidacije.

### 5.2.6. Zaključki

Uporaba računalniških simulacij je zelo uporabno orodje, ki omogoča dostop do marsikaterih stvari, ki pri laboratorijskem delu ostajajo raziskovalcem skrita. V sklopu študije se je pripravil model, ki solidno opisuje pojav drobljenja. Vendar pa zaupanj v rezultate zmanjšuje dejstvo, da je bil model poenostavljen do te mere, da način izvajanja testov vpliva na same rezultate. Delno se natančnost samega modela lahko popravi z uporabo kontaktnih vezi namesto vzporednih vezi za formiranje gruč, za dodatno izboljšanje natančnosti simulacije pa bi bila potrebna uporaba zmogljivejšega (super) računalnika. Podatek, ki nakazuje na to, je primerjava računskih časov simulacije, ki je bila opravljena na dveh različno zmogljivih računalnikih. Medtem ko je na 32 bitnem operacijskem sistemu in z 2 GB bralno-pisalnega pomnilnika potreben čas za izračun simulacije 7 dni, se je na 64 bitnem operacijskem sitemu z 8 GB bralno-pisalnega pomnilnika  čas skrajšal na vsega 2 dni.

Glede na dobljene rezultate je pod vprašaj postavljena uporaba ostalih načinov modeliranja drobljenja. Kot je prikazano prihaja namreč v večji meri do strižnih porušitev na kontaktih, česar pa z modeli kot je metoda z zamenjavo zrn (natančneje je opisana v angleškem delu diplomskega dela), ni mogoče modelirati, vsaj ne brez uporabe metode končnih elementov.

**REFERENCES**

Arenson, L. U. 2002. Unstable alpine permafrost: a potentially important natural hazard – variations of geotechnical behaviour with time and temperature. Zurich, Swiss Federal Institute of Technology Zurich (published by the author L. U. Arenson).

Astrom, J.A., Herrmann, H.J. 1988. Fragmentation of grains in a two-dimensional packing. Eur. Phys. J. B 5: 551-554.

Atkinson, J. 1993. An Introduction to the Mechanics of Soils and Foundations. Maidenhead, McGraw-Hill: 321 p.

Ben-Nun, O. Einav, I. 2008. A Refined DEM Study of Grain Size Reduction in Uniaxial Compression. V: The 12th International Conference of IACMAG, Goa, India, 1-6 October , 2008. New York, Curran Associates: p. 702-708.

Brosh, T., Kalman, H., Levy, A. 2011. Fragments spawning and interaction models for DEM breakage simulation. Granular Matter 13: 765–776.
doi: 10.1007/s10035-011-0286-z

Casini, F., Viggiani, G.M.B. 2011. Experimental investigation of the evolution of grading of an artificial material with crushable grains under different loading conditions. V: International Symposium on Deformation Characteristics of Geomaterials, Seoul, Korea, September 1-3, 2011. IOS Press (sep. pag.)

CEN ISO/TS 17892-4:2004. Geotechnical investigation and testing - Laboratory testing of soil - Part 4: Determination of particle size distribution.

Colliat-Dangus, J.L., Desrues, J., Foray, P. 1988. Triaxial testing of granular material under elevated cell pressure. ASTM:  290-310.

Cui, L., O'Sullivan, C., O'Neill, S. 2007. An analysis of the triaxial apparatus using a mixed boundary three-dimensional discrete element model. Geotechnique 57, 10: 831–844.
doi: 10.1680/geot.2007.57.10.831

Einav, I. 2007. Soil mechanics: breaking ground. Philosophical Transactions of the Royal Society A 365: 2985–3002.
doi:10.1098/rsta.2007.0009

Fuller, W.B., Thompson, S.E. 1907. The laws of proportioning concrete. ASCE Transactions 59: 67–143.

Geotech. Lightweight aggregate soil mechanics – properties and application. 2012.
http://geotech.maxit-cms.com/media/68/Soil%2520Mech2.pdf (Obtained January 2012).

Gerolymos, N., Gazetas, G. 2007. A model for grain-crushing-induced landslides - Application to Nikawa, Kobe 1995. Soil Dynamics and Earthquake Engineering 27: 803–817.
doi: 10.1016/j.soildyn.2007.01.003

Hardin, B.O. 1985. Crushing of soil particles. Journal of Geotechnical Engineering 111, 10: 1177-1192.

Itasca group. 2004. Manual: Particle Flow Code in 3 Dimensions. Minneapolis, Itasca group.

Leca. Lightweight, Insulating Building Materials. 2012.

http://www.gpnm.org/e/uploads/131-b810984952.pdf (Obtained March 2012).

Lee, K. L., Farhoomand, I. 1967. Compressibility and crushing of granular soil. Canadian Geotechnical Journal 4, 1: 68-86.

Leslie, D.D. 1975. Shear Strength of Rockfill. Physical Properties Engineering Study No. 526, South Pacific Division, Corps of Engineers Laboratory: 124 p.

Leu, J. 2011. Effects of grain size distribution and confining stress on mechanical behaviour of an artificial crushable material: application to retaining wall. Project Thesis, Zurich, Swiss Federal Institute of Technology Zurich (published by the author J. Leu).

Lobo-Guerrero, S., Vallejo L. E. 2007. Influence of pile shape and pile interaction on the crushable behavior of granular materials around driven piles: DEM analyses. Granular Matter   9: 241–250.
doi: 10.1007/s10035-007-0037-3

Marketos, G., Bolton, M.D. 2010. Flat boundaries and their effect on sand testing. International Journal for Numerical and Analytical Methods in Geomechanics 34: 821–837.
doi: 10.1002/nag.835

Marsal, R.J. 1965. Discussion of shear strength. V: Proceedings of the 6th International Conference on Soil Mechanics and Foundation Engineering, Montreal, September  8-15, 1965. Toronto, Ontario, Canada, University of Toronto Press: p. 310-316.

McDowell, G. R., Bolton, M. D. 1998. On the micromechanics of crushable aggregates. Geotechnique 48, 5: 667-679.

Nazari, A., Riahi, S. 2011. Effects of CuO nanoparticles on compressive strength of self-compacting concrete. Sadhana 36, 3: 371–391.

Schoutens, J.E. 1979. Empirical analysis of nuclear and high-explosive cratering and ejecta. Nuclear Geoplosics Sourcebook 55, 4: 237-256.
doi: 10.1007/3-540-45256-7_14

Towhata, I. 2008. Geotechnical Earthquake Engineering. Berlin, Springer Series in Geomechanics and Geoengineering: 394-395.

Tsoungui , O., Vallet, D.,Charmet, J.C. 1999. Numerical model of crushing of grains inside two-dimensional granular materials. Powder Technology 105: 190–198.

Vallejo L. E., Lobo-Guerrero, S. 2009. Fractal Fragmentation of Granular Materials under Compression. V: Nakagawa, M. (ed.), Luding S. (ed.). Proceedings of the 6 International Conference on Micromechanics of Granular Media, Golden, Colorado, July 13-17, 2009.  Melville, New York, American Institute of Physics: 847-850.
doi: 10.1063/1.3180061

Wanninger, F. 2010. Effects of grain crushing on compressibility of an artificial material. Project Thesis. Zurich, Swiss Federal Institute of Technology Zurich (published by the author F. Wanninger).

Wikipedia. Appollonian gasket. 2012.
http://en.wikipedia.org/wiki/Apollonian_gasket (Obtained June 2012).

Wood, D.M., Maeda, K. 2008. Changing grading of soil: effect on critical states. Acta Geotechnica 3:3–14.

**APPENDIX**

**APPENDIX A: Laboratory test results**

**APPENDIX B: Algorithms for PFC3D**

## APPENDIX A: Laboratory test results

**(i)    ISO**

- $v - p'$
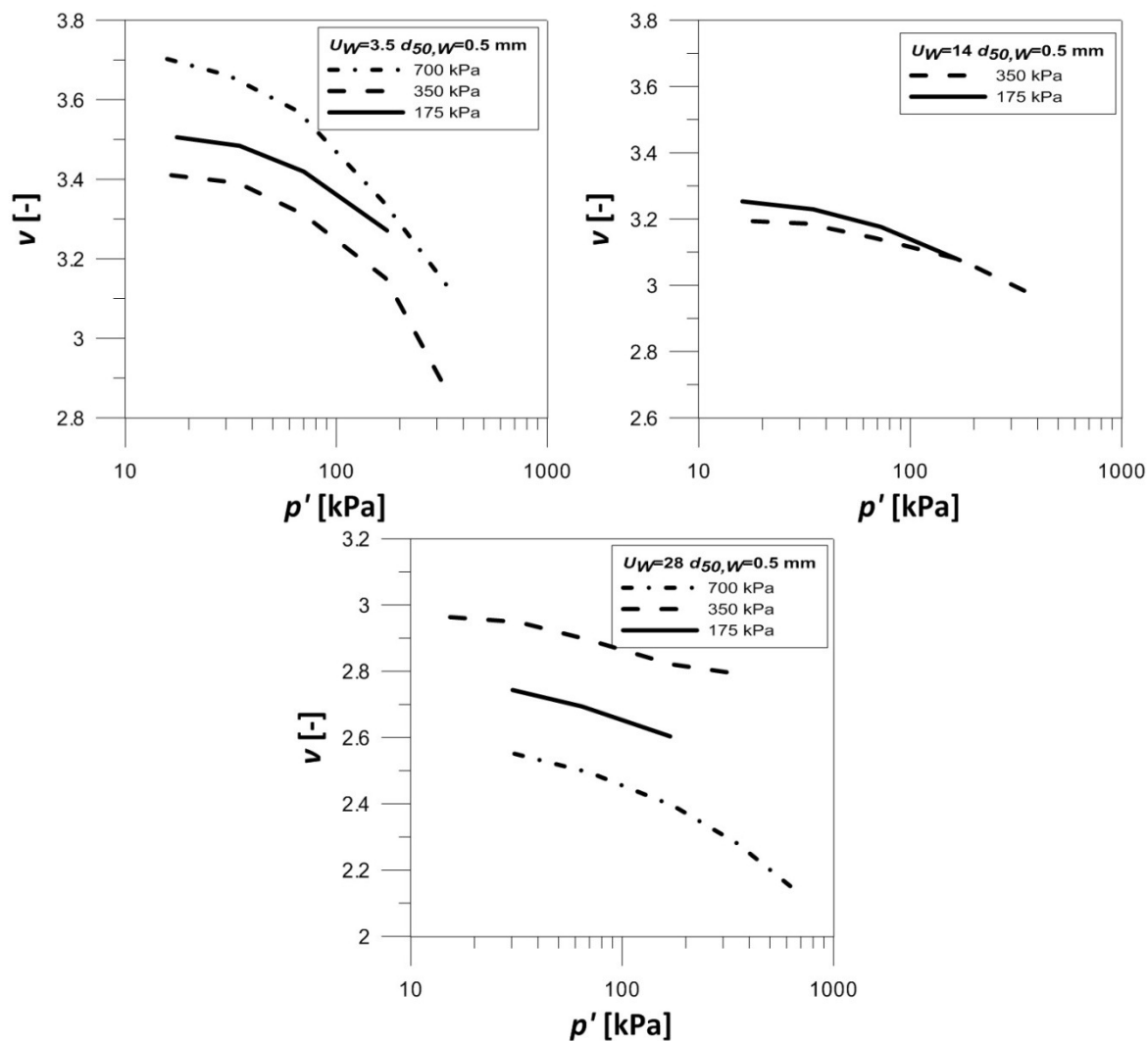


**Slika A.1 : Linije izotropne kompresije**

**Figure A.1 : Isotropic compression lines**

- **GSD**
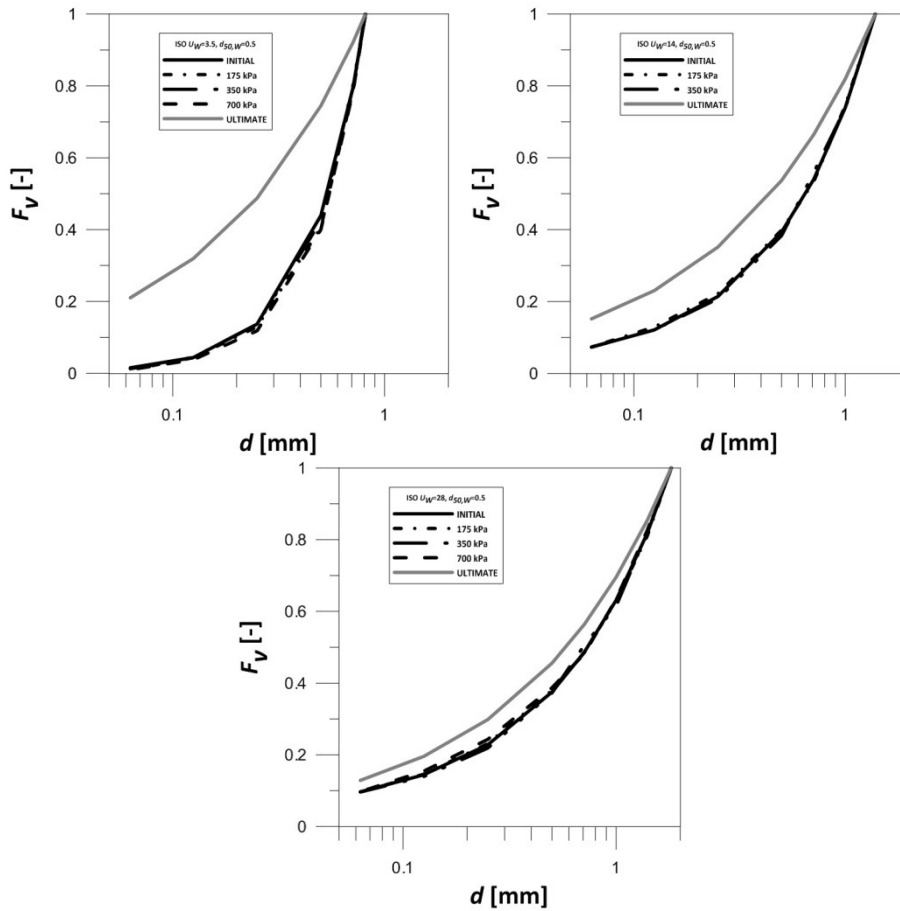


**Slika A.2 : Zrnavostne krivulje po opravljenih ISO testih**

**Figure A.2 : Grain size distribution curves after the ISO tests**

- **Total and relative crushing**
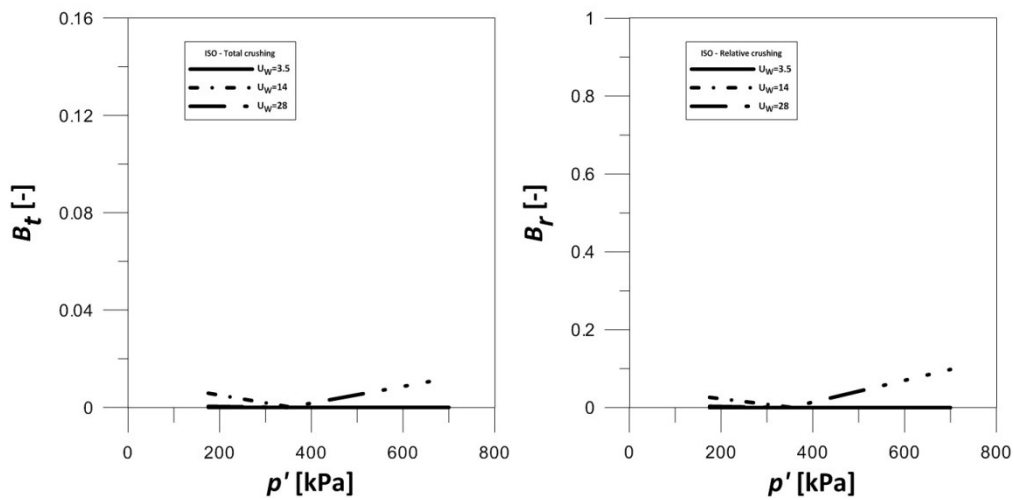


**Slika A.3 : Celotno in relativno drobljenje po opravljenih ISO testih**

**Figure A.3 : Total and relative grain crushing after the ISO tests**

**(ii)    OED**

- **Stress-strain curve**
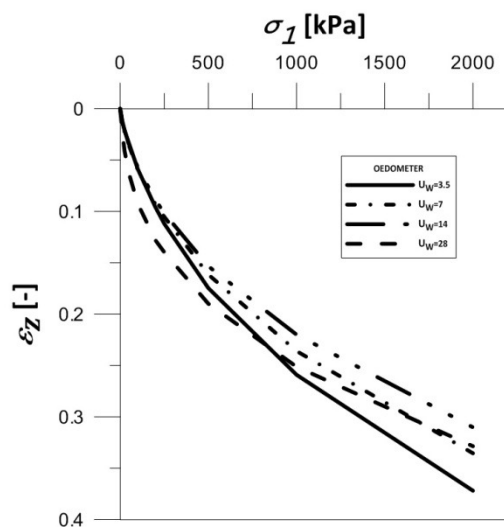


**Slika A.4: Diagram napetosti in deformacij med oedometerskimi testi**

**Figure A.4: Stress-strain curve during the OED tests**

- **Total and relative crushing**
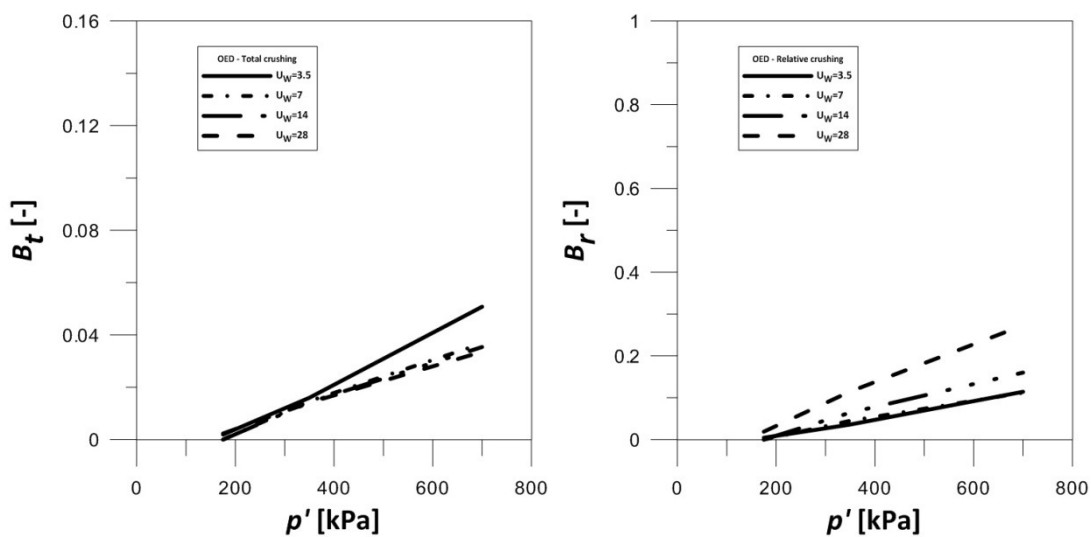


**Slika A.5: Celotno in relativno drobljenje po opravljenih oedometerskih testih**

**Figure A.5: Total and relative crushing after OED test**

- **GSD**
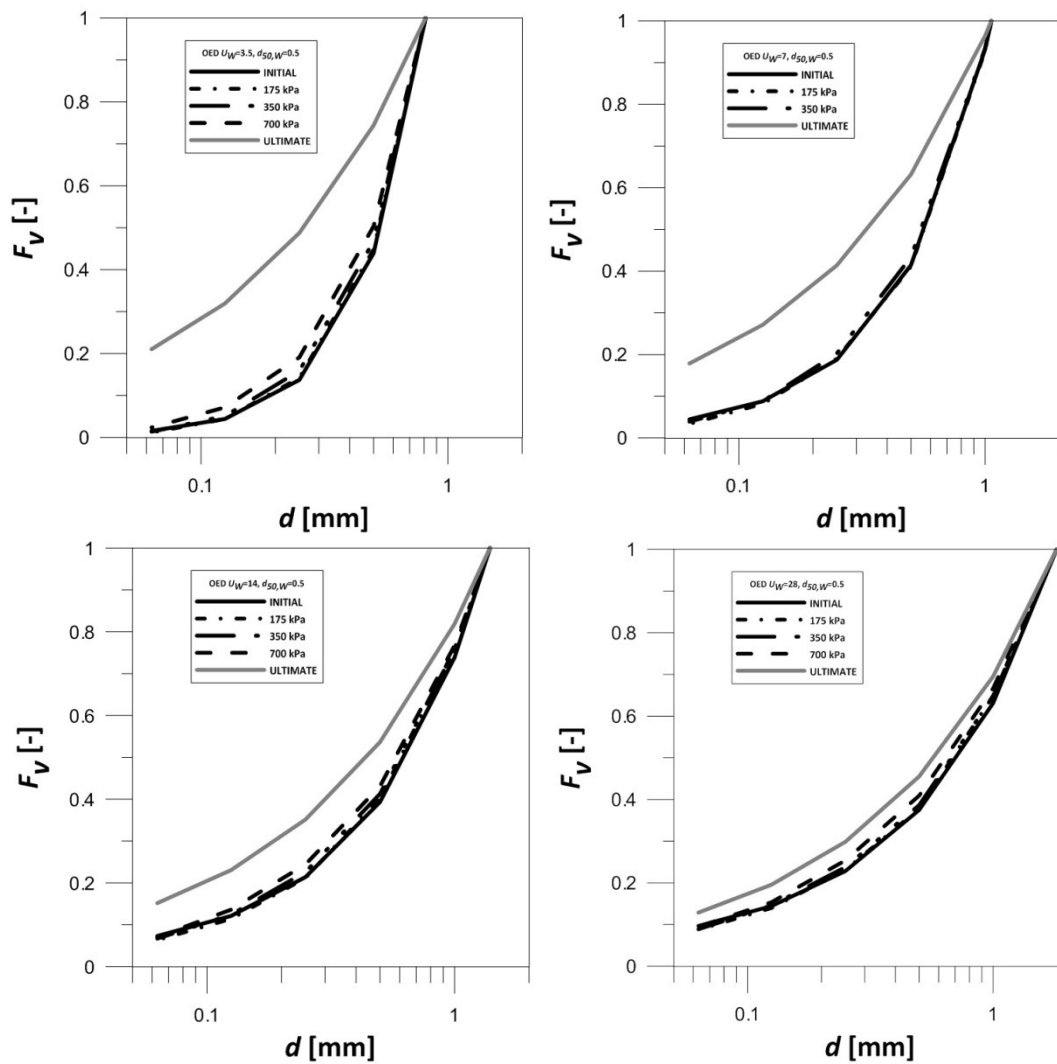


**Slika A.6: Zrnavostne krivulje po opravljenih oedometerskih testih**

**Figure A.6: Grain size distribution curves after the OED tests**

**(iii)     TXC**

• **Stress paths**
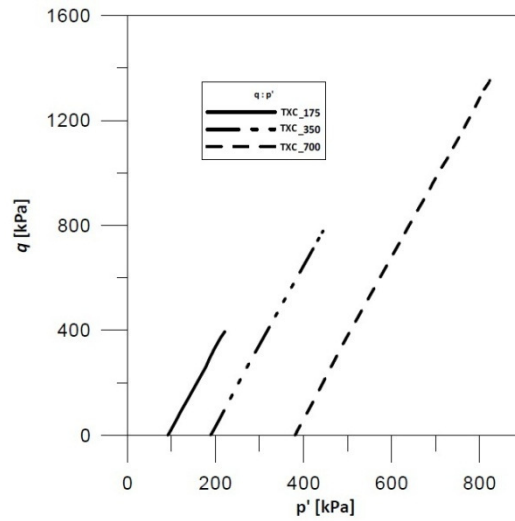


**Slika A.7 : Napetostne poti za opravljene TXC teste**

**Figure A.7 : Stress paths for the TXC tests**

• **Total and relative crushing**
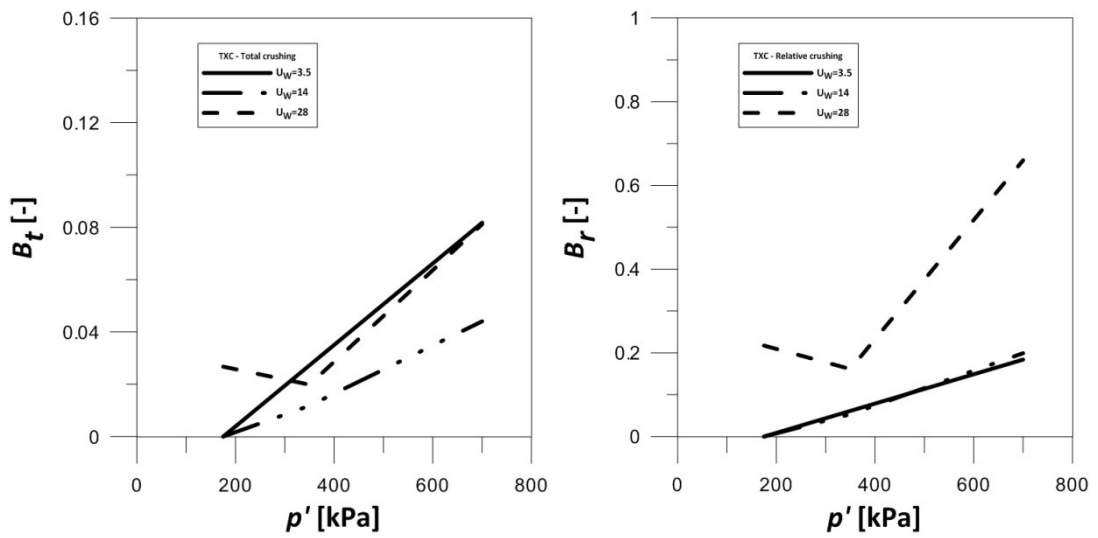


**Slika A.8 : Celotno in relativno drobljenje po opravljenih TXC testih**

**Figure A.8 : Total and relative crushing after the TXC tests**

- **GSD**
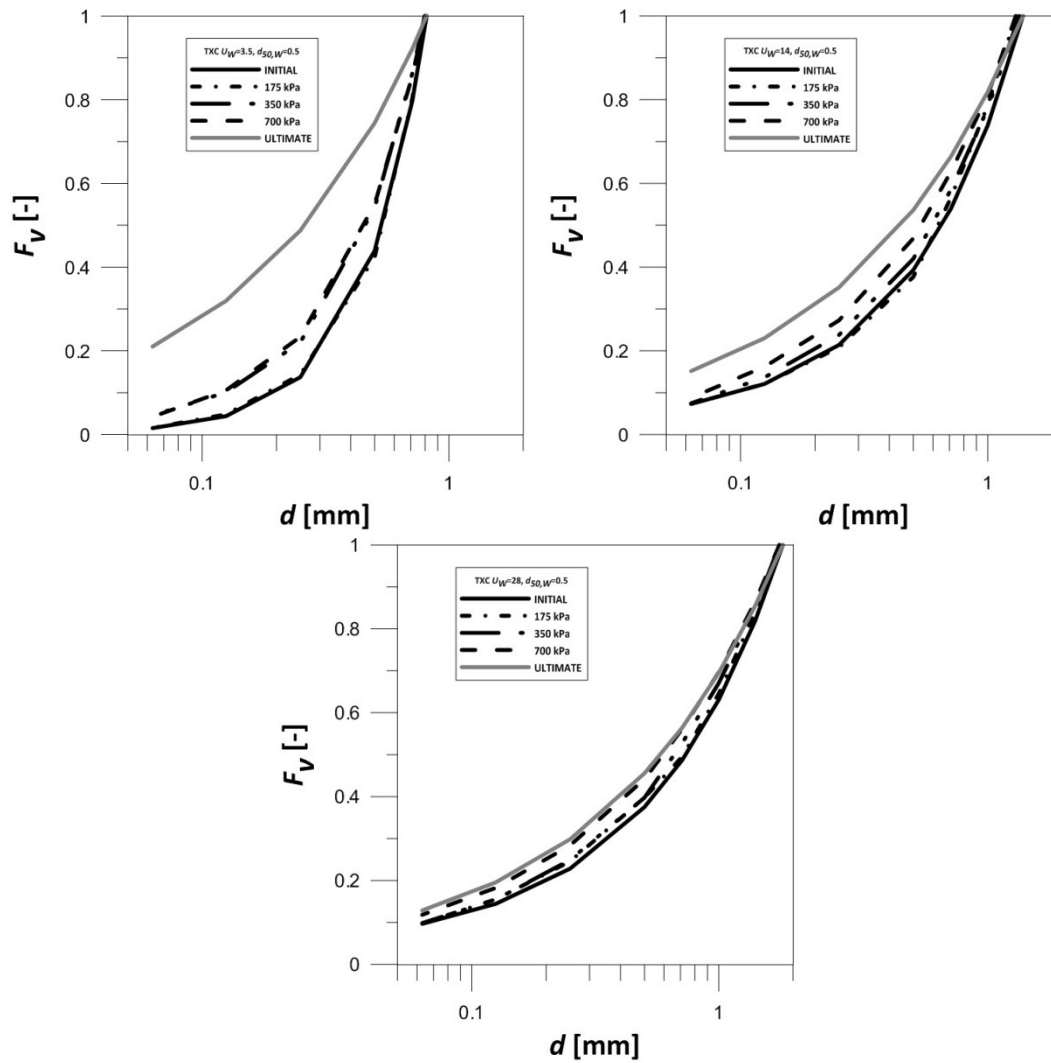


**Slika A.9: Zrnavostne krivulje po opravljenih TXC testih**

**Figure A.9: GSD curves after the TXC tests**

- $q : \varepsilon_s$
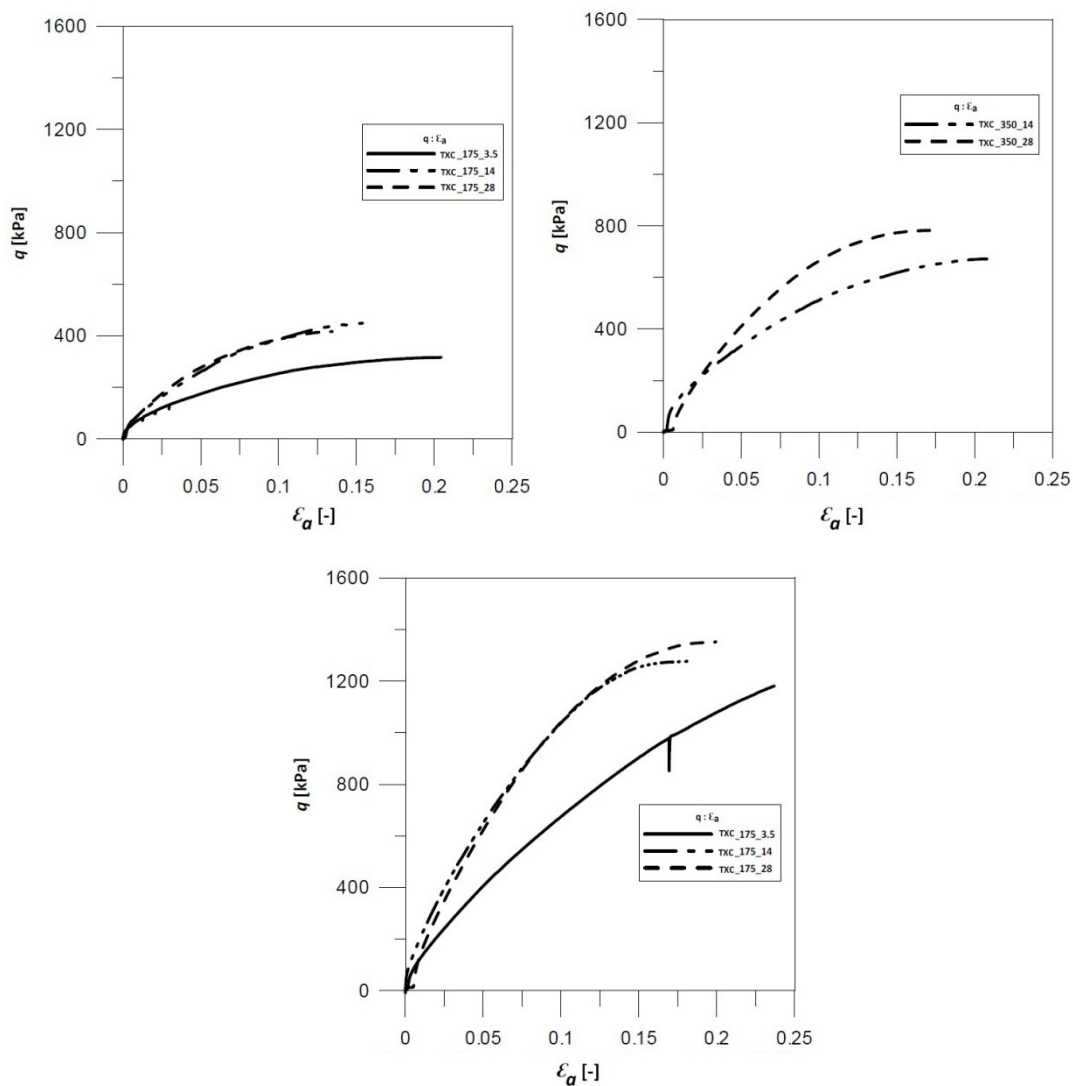


**Slika A.10: Triosni strižni preskus pri konstantnem celičnem tlaku**

**Figure A.10: Triaxial shearing at constant cell pressure**

**(iv)     TXP**

● **Isotropic compression before the triaxial shearing**
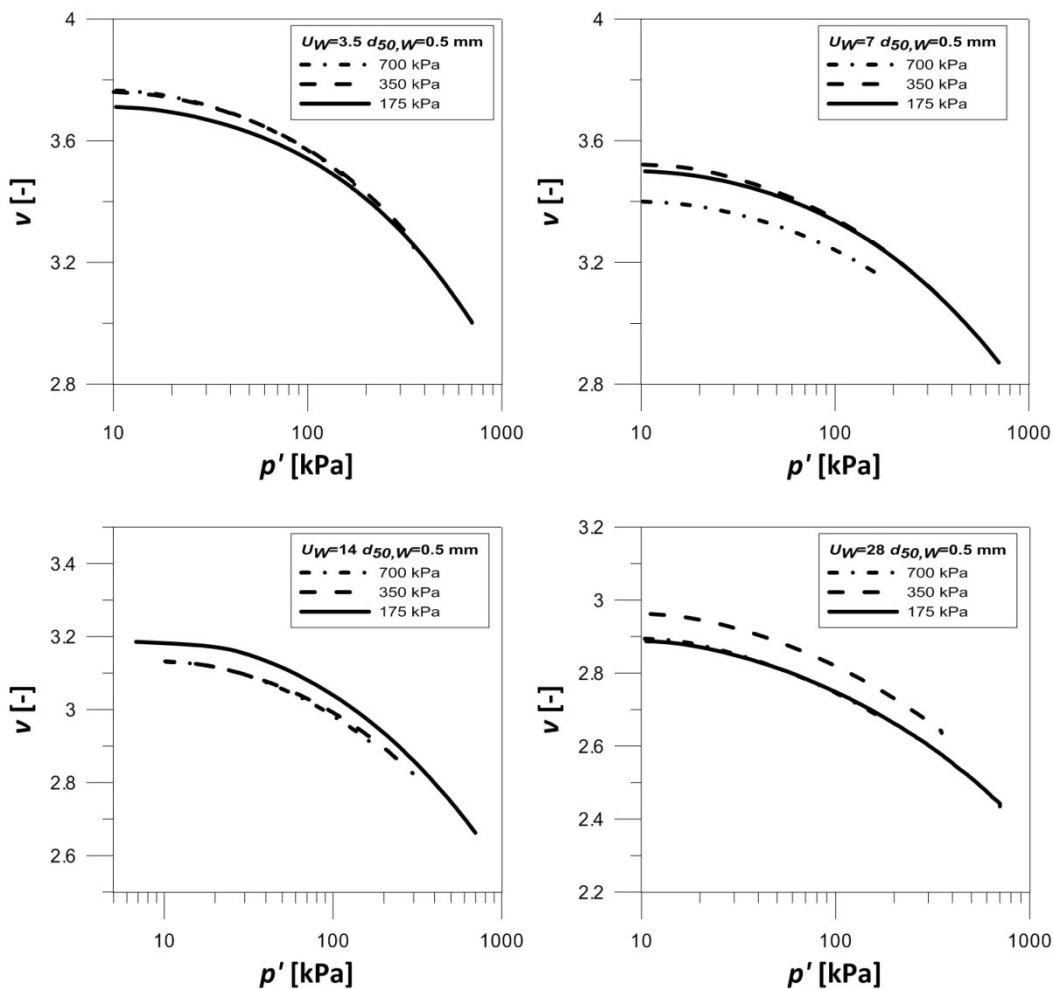


**Slika A.11: Linije izotropne kompresije pred izvajanjem TXP testov**

**Figure A.11: Isotropic compression lines before the TXP test**
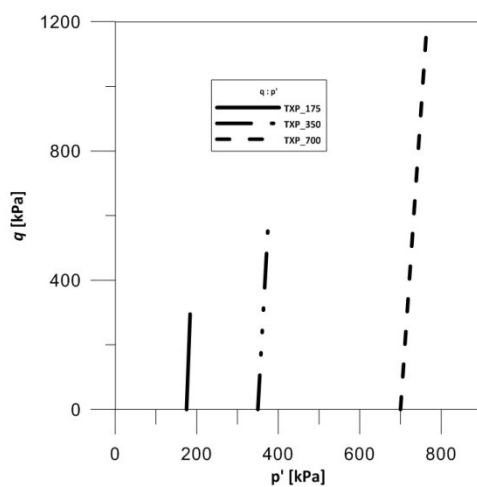


**Slika A.12: Napetostne poti za opravljene TXP teste**

**Figure A.12: Stress paths for TXP tests**

- $q : \varepsilon_s$
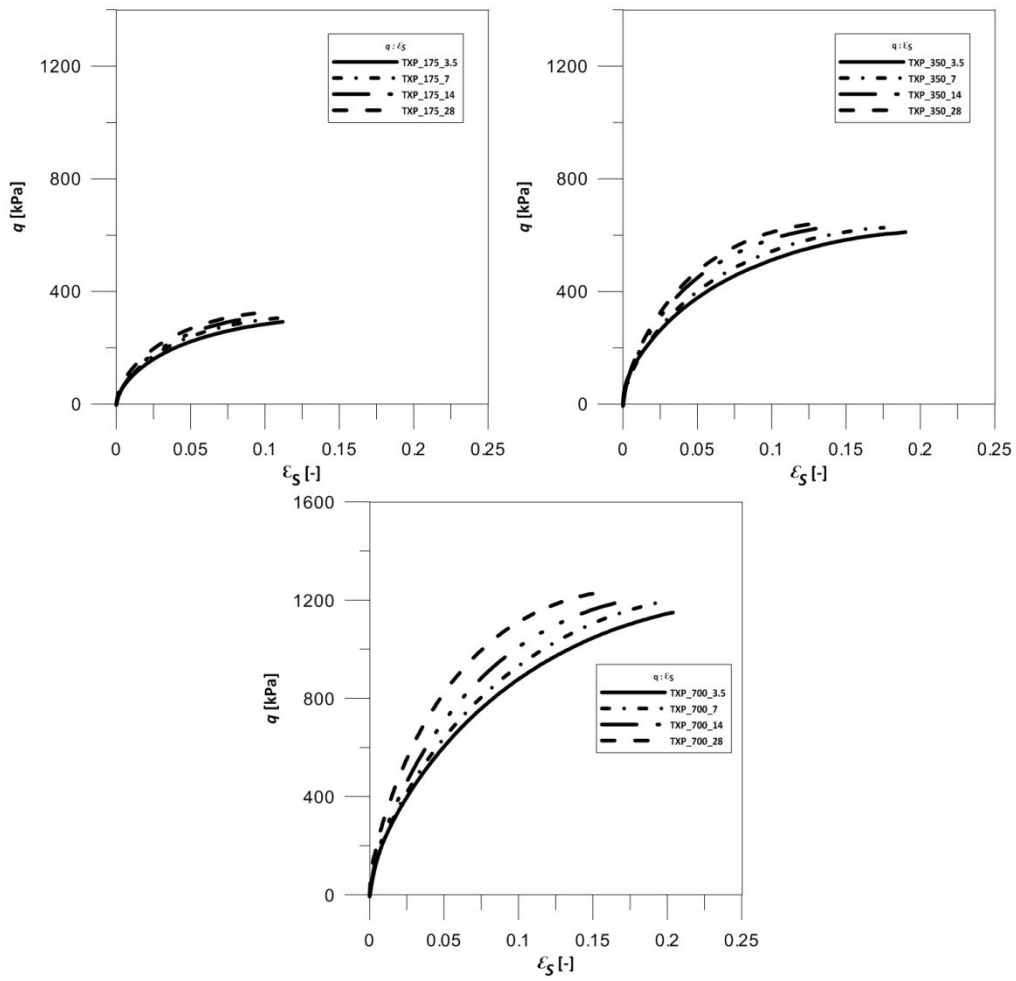


**Slika A.12: Triosni strižni preskus pri konstanti srednji efektivni napetosti**

**Figure A.12: Triaxial shearing at constant mean effective stress**

- **Failure lines**
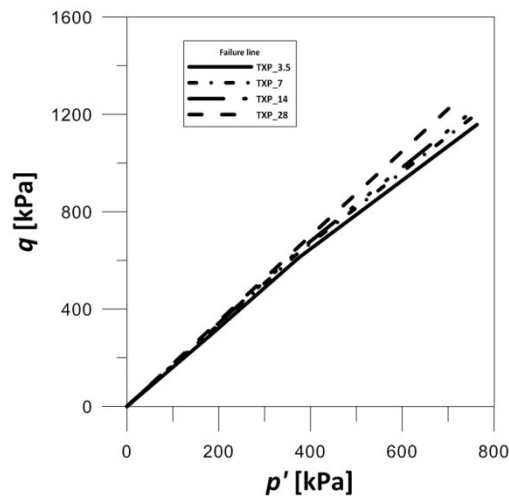


**Slika A.13: Porušne linije za TXP teste**

**Figure A.13: Failure line for TXP tests**

- **Volumetric changes**
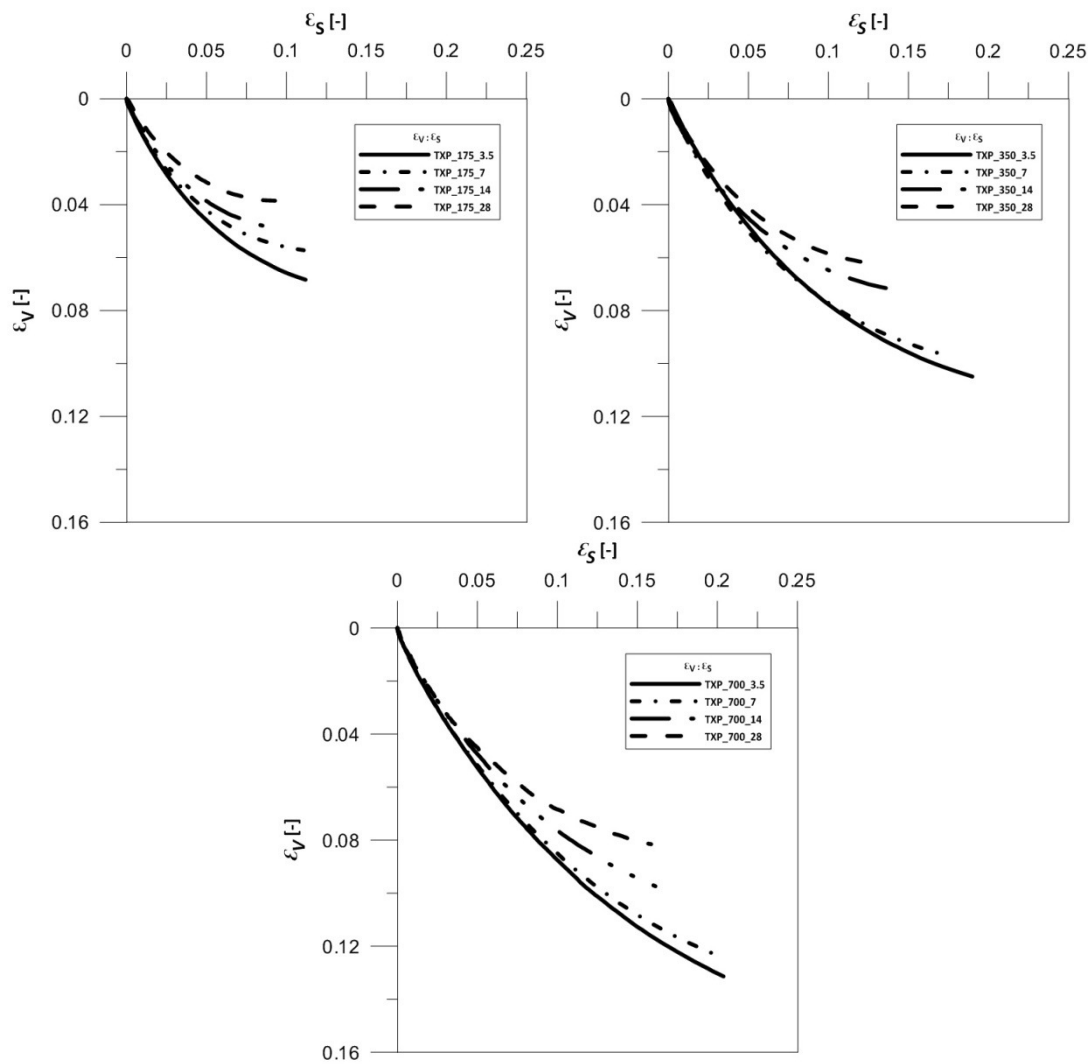


**Slika A.14: Prostorninske deformacije med TXP testi**

**Figure A.14: Volumetric strains during TXP tests**

- **Total and relative crushing**
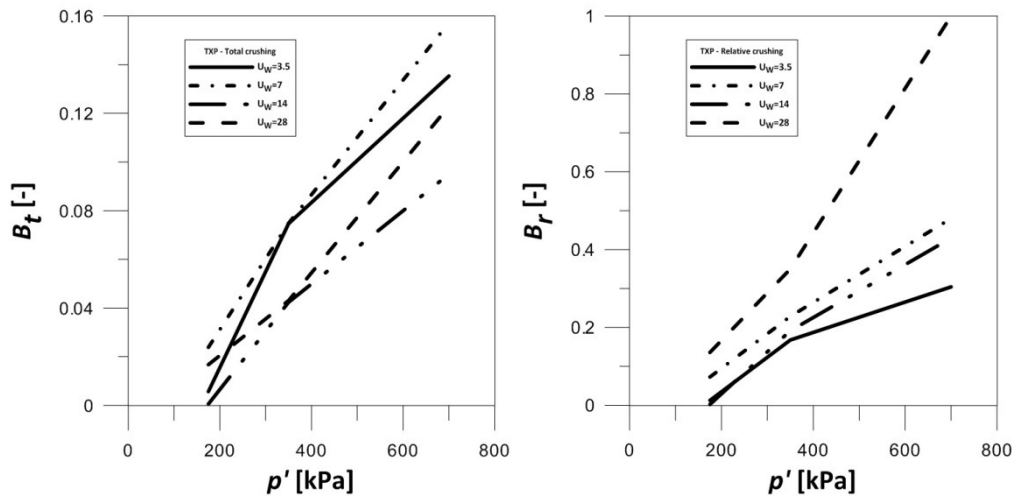


**Slika A.15: Celotno in relativno drobljenje po opravljenih TXP testih**

**Figure A.15: Total and relative crushing after the TXP tests**
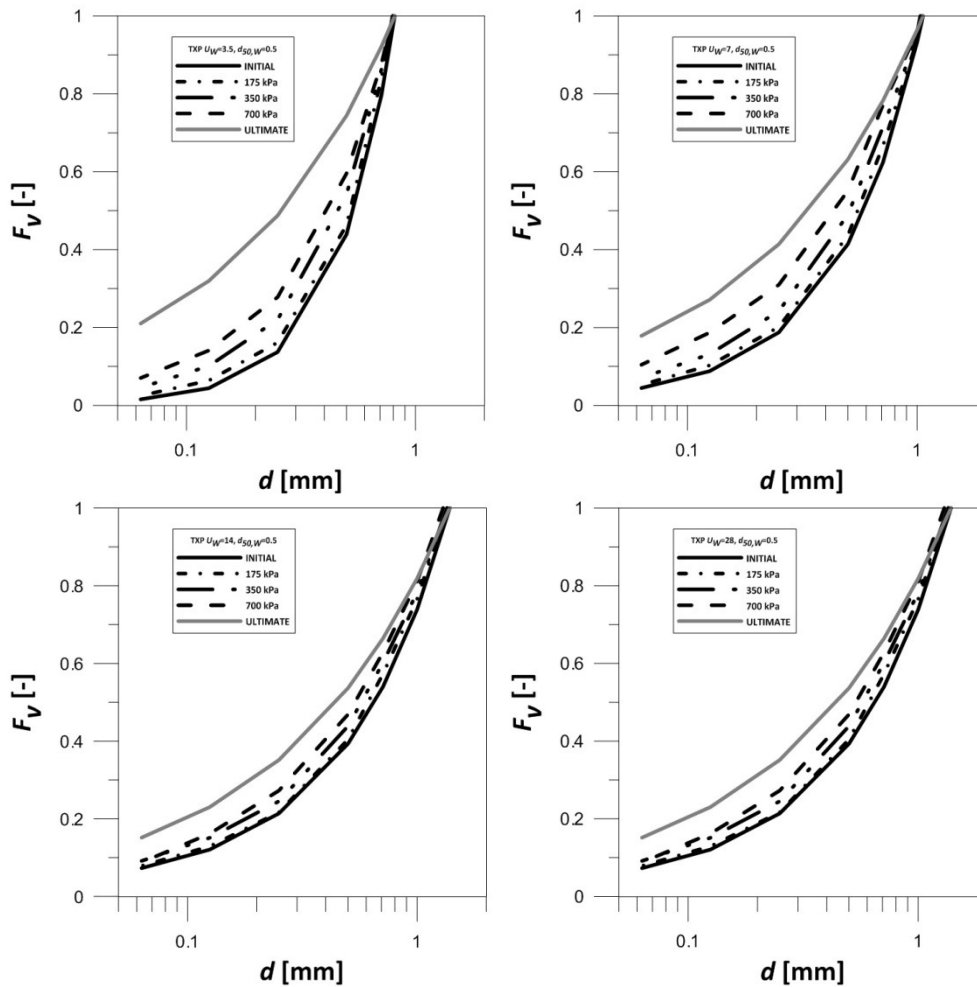


**Slika A.16: Zrnavostne krivulje po opravljenih TXP testih**

**Figure A.16: GSD curves after the TCP tests**

## APPENDIX B: Algorithms

### (i)    Grain size tracking and coordination number

*arr_part* – array with particle identification numbers (ID) for elementary particles within a grain under
           investigation
*arr_cid* – array with clump ID's for each elementary particle
*arr_bid* – array with particle ID's for each elementary particle
*arr_contact* – particle ID's of particles in contact with specific particle. Row number is identical to the
           particle ID

```
def color_2ball
        bp=ball_head
        loop while bp#null
                b_color(bp)=1
                bp=b_next(bp)
        end_loop
end

def GSD_scan
        n_cid=0
        n_arr=0
        bp=ball_head

        loop while bp#null
                n_ball=1
                if b_color(bp)=1
                        n_cid=n_cid+1
                        arr_part(n_ball)=bp
                        n_ball=n_ball+1
                        n_ball_scan=0
                        loop while n_ball_scan#n_ball-1
                                n_ball_scan=n_ball_scan+1
                                n_arr=n_arr+1
                                arr_cid(n_arr)=string(n_cid)
                                n_bid=b_id(arr_part(n_ball_scan))
                                arr_bid(n_arr)=string(n_bid)
                                b_color(arr_part(n_ball_scan))=2
                                cp=b_clist(arr_part(n_ball_scan))

                                bp2=arr_part(n_ball_scan)

                                arr_contact(n_arr)=string(string(n_cid)+' '+string(n_bid))

                                loop while cp#null
                                        if c_ball1(cp)=arr_part(n_ball_scan)
                                                bp_other=c_ball2(cp)
                                        else
                                                bp_other=c_ball1(cp)
                                        end_if
                                        if c_pb(cp)#null
                                                if b_color(bp_other)=1
                                                        arr_part(n_ball)=bp_other
                                                        n_ball=n_ball+1
```

```
                                                        b_color(bp_other)=2
                                        end_if
                        else
                                if pointer_type(bp_other)=100
                                        a=b_id(bp_other)
                                        arr_contact(n_arr)=string(arr_contact(n_arr)+'
'+string(a)) ;BALL
                                else
                                        a=string('w'+string(w_id(bp_other)))
                                        arr_contact(n_arr)=string(arr_contact(n_arr)+'
'+string(a)) ;WALL
                                end_if
                        end_if
                        if c_ball1(cp)=arr_part(n_ball_scan) then
                                cp=c_b1clist(cp)
                        else
                                cp=c_b2clist(cp)
                        end_if
                end_loop

        end_loop
    end_if
    bp=b_next(bp)
    end_loop
end
```

### (ii)      Particle colouring

```
def count_ball
    bp=ball_head
    n_ball=0

    loop while bp#null
            n_ball=n_ball+1
    end_loop
end

count_ball

def meas_gsd
    n_arr_meas=0
    n_gsd=0
    n_cid=1
SECTION
    loop while n_arr_meas#n_arr+1
            n_arr_meas=n_arr_meas+1
            if n_gsd=0
                    nlow=n_arr_meas
            end_if
            if int(arr_cid(n_arr_meas))=n_cid
                    n_gsd=n_gsd+1
            else
                    if n_gsd=1
                            color_b=1
                    end_if
```

```
                        if n_gsd>1
                                if n_gsd<int(n_ball/14.0+1)
                                        color_b=2
                                end_if
                        end_if
                        if n_gsd>int(n_ball/14.0)
                                if n_gsd<int(2*(n_ball/14.0)+1)
                                        color_b=3
                                end_if
                        end_if
                        if n_gsd>int(2*(n_ball/14.0))
                                if n_gsd<int(3*(n_ball/14.0)+1)
                                        color_b=4
                                end_if
                        end_if
                        if n_gsd>int(3*(int(n_ball/14.0)))
                                if n_gsd<int(4*(n_ball/14.0)+1)
                                        color_b=5
                                end_if
                        end_if
                        if n_gsd>int(4*(n_ball/14.0))



                                                    .
                                                    .
                                                    .


                if n_gsd>int(12*(n_ball/14.0))
                                if n_gsd<int(13*(n_ball/14.0)+1)
                                        color_b=14
                                end_if
                        end_if
                        if n_gsd>int(13*(n_ball/14.0))
                                if n_gsd<int(14*(n_ball/14.0)+1)
                                        color_b=15
                                end_if
                        end_if
                        n_cid=n_cid+1
                        n_gsd=0
                        n_arr_meas=n_arr_meas-1
                        loop color_ball(nlow,n_arr_meas)
                                bp1=find_ball(int(arr_bid(color_ball)))
                                b_color(bp1)=color_b

                                if n_arr_meas=n_arr
                                        if color_ball=n_arr_meas
                                                EXIT SECTION
                                        end_if
                                end_if
                        end_loop
                end_if
        end_loop
        ENDSECTION
end
```